Early events of cell autonomous response against *Toxoplasma gondii* in the mouse

Ana Lina Pereira Rodrigues

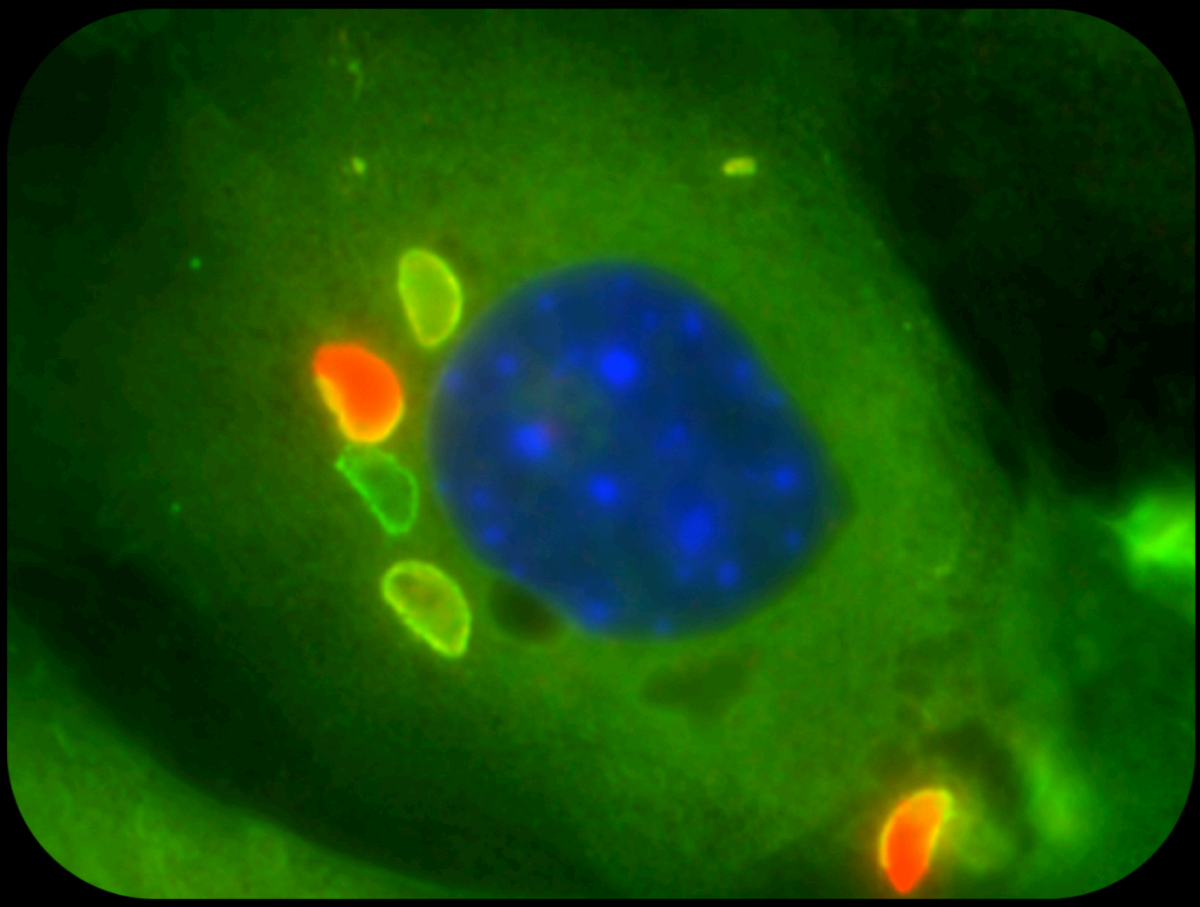

Dissertation presented to obtain the Ph.D degree in Molecular Biosciences

Instituto de Tecnologia Química e Biológica António Xavier | Universidade Nova de Lisboa

Oeiras,
July, 2021

UNIVERSIDADE NOVA DE LISBOA

ITQB-UNL | Av. da República, 2780-157 Oeiras, Portugal
Tel (+351) 214 469 100 | Fax (+351) 214 411 277

www.itqb.unl.pt

Early events of cell autonomous response against *Toxoplasma gondii* in the mouse

Ana Lina Pereira Rodrigues

Dissertation presented to obtain the Ph.D degree in in Molecular Biosciences

Instituto de Tecnologia Química e Biológica António Xavier | Universidade Nova de Lisboa

Research work coordinated by: INSTITUTO GULBENKIAN DE CIÊNCIA

Oeiras, July, 2021

UNIVERSIDADE NOVA DE LISBOA

Cover: IFN gamma-induced murine fibroblast 1,5 hours post-*Toxoplasma gondii* infection. Ubiquitin (red), IRGs (green) and cell nucleus (blue) are marked.

Declaration

This thesis is the result of the work that I developed as a PhD student at the Instituto Gulbenkian de Ciência, supervised by Professor Jonathan Howard under the scope of the Post Graduate Program Science for Development (PGCD) from October 2015 to June 2021.

Author contributions are briefly described in a paragraph after the first page of each chapter. My PhD work is supported by Fundação para a Ciência e Tecnologia, SFR/BD/114402/2016.

Our laboratory was supported by central funds of the Instituto Gulbenkian de Ciência, the Sonderforschungsbereiche 670 and 680 and Schwerpunkt 1399 of the Deutsche Forschungsgemeinschaft.

Summary

Toxoplasma gondii is a widely spread parasite worldwide among warm-blooded organisms thanks to its ability to survive the immune system response and chronically establish itself in its hosts. The success of *T. gondii* depends entirely on the establishment of its intracellular survival niche, called the parasitophorous vacuole (PV). The PV membrane (PVM) is derived from the host plasma membrane at the point of entry. Both at time of entry and from within the vacuole, the parasites release virulence factors into the cytoplasm that restrict the immune response.

The immune response of mice and humans depends on the cytokine IFNγ, which induces the synthesis of hundreds of proteins involved in several modalities of immunity. This thesis focuses on a family of interferon-inducible GTPases, the IRG proteins, that are essential for immunity against *T. gondii* in mice. IRG proteins have three functional subgroups, **effectors**, that bind directly to the PVM, **regulators**, that prevent effectors from activating on endogenous cellular organelle membranes, and **decoys**, that interact directly at the PVM with virulence proteins from type I virulent strains and prevent the inactivation of effector IRGs, thereby attenuating the virulence. In mice, effector IRGs cause destruction of the parasitophorous vacuole leading to elimination of the parasite. In human cells, however, IRG proteins are absent and parasite elimination occurs by other mechanisms, possibly involving a second family of interferon-inducible GTPases, the Guanylate-Binding Proteins, GBPs. Despite this immune response, a small number of parasites escape the action of GTPases, survive, encyst in the brain, and are responsible for subsequent transmission if the current host is predated by a cat. How the parasite can balance how many parasites are eliminated by the host to prevent acute mortality, and at the same time ensure, in the mouse, that at least some vacuoles are not eliminated by IRG proteins, is thus a key factor

in learning how the parasite persists in hosts that exploit the IRG protein resistance mechanism. This major question arises equally in the human case, and in all other warm-blooded host species that become infected by *T. gondii*, how does the parasite find the ideal situation, not killing but also not being fully eliminated by the host?

After *T. gondii* invades a cell, the group of effector IRGs attack the PVM, leading to its destruction. It is not yet known how these proteins recognize and bind to the membrane of these vacuoles. Furthermore, previous work has shown the accumulation of some other proteins in the vacuole region, including ubiquitin, whose function in this context is unknown. In the present study, we focus on the factors that determine the accumulation of IRGs as pioneers in the destruction of specific (susceptible) PVs, avoiding others (resistant) and its relationship with the recruitment of ubiquitin.

We started the study by analyzing how the concentration of IRG proteins available in the cytoplasm determines its recruitment to PVs and how different IRGs accumulate there. We found that regardless of the supply of cytosolic IRG, each one independently binds to different proportions of PVs summing up to ~80%. The destruction of the PV results from the joint action of the IRGs. Irgb6 loads onto the highest proportion of vacuoles but alone is not sufficient to destroy the PVM.

Then we ask if the duration of parasite persistence in the cells before loading of IRGs, which we here call PVM maturation, prevents its targeting by IRGs, thereby accounting for the ~20% of PVMs that do not load with IRG proteins. Using parasites lacking TgIST, a protein that inhibits the interferon response at the level of the chromatin, and thus inhibits the induction of IRG proteins, we demonstrated that the residence time in the cell before IRGs bind does not make the PVMs progressively less likely to bind IRG proteins. Therefore, vacuolar maturation does not explain the elimination-resistant vacuoles.

We then focus on determining the link between ubiquitin accumulation in PV and the presence of IRGs. We found that after IRG recruitment, ubiquitin is present in ~70% of PVs already covered by IRGs, equivalent to those loaded by Irgb6, Irga6 and Irgd, but not those loaded by Irgb6 alone. A detailed analysis allowed us to verify that ubiquitin does not use IRG proteins as a substrate, but needs their action in destroying PVMs to allow ubiquitin accumulation in or on parasites. We show that ubiquitin is present exclusively on the parasite and not on the PVM.

In conclusion, our results suggest that *T.gondii* elimination is initiated by the recruitment of IRGs to PVs. The accumulation of the different effector IRG proteins may be through the recognition of specific molecular targets on the cytosolic face of the PVM that are carried into the PVM from the plasma membrane at the time of parasite entry. Disruption of the PVM needs cooperation between different IRG effectors. Disruption of the PVM allows ubiquitin access to the parasite membrane, and initiates a process leading to death of the parasite and necrosis of the host cell.

Resumo

O *Toxoplasma gondii* é um parasita amplamente disseminado mundialmente entre os organismos de sangue quente, graças à sua capacidade de sobreviver à resposta do sistema imunológico e estabelecer-se de forma crónica nos seus hospedeiros. O sucesso do *T. gondii* depende inteiramente do estabelecimento do seu nicho de sobrevivência intracelular, denominado vacúolo parasitóforo (PV). A membrana do PV (PVM) é derivada da membrana citoplasmática da célula hospedeira no ponto de entrada. Quer no momento da entrada quer desde o interior do vacúolo, os parasitas libertam no citoplasma fatores de virulência que restringem a resposta imunitária.

A resposta imunitária em ratos e humanos depende da citoquina interferão gama ou IFNγ, que induz a síntese de centenas de proteínas envolvidas em diversas modalidades de imunidade. Esta tese tem como foco uma família de GTPases induzíveis por interferão, as "immunity-related GTPases" ou IRGs, essenciais para a imunidade contra *T. gondii* em ratos domésticos. As proteínas IRG têm três subgrupos funcionais: os efetores, que se ligam diretamente à PVM; os reguladores, que impedem a ativação dos efetores nas membranas dos organelos celulares endógenos; e os "decoys", que funcionam como "isco" e interagem diretamente na PVM com proteínas de virulência de estirpes virulentas de *T. gondii* do tipo I e evitam a inativação de IRGs efetoras, atenuando assim a virulência. Em ratos domésticos, as IRGs efetoras causam a destruição do vacúolo parasitóforo levando à eliminação do parasita. Em células humanas, as proteínas IRG estão ausentes e a eliminação do parasita ocorre por outros mecanismos, possivelmente envolvendo uma segunda família de GTPases induzíveis por interferão, as proteínas de ligação ao guanilato ou GBPs. Apesar desta resposta imunitária do ratinho, um pequeno número de parasitas escapa à ação das GTPases, sobrevive,

enquista em órgãos como o cérebro e é responsável pela transmissão subsequente se o hospedeiro atual for predado por um gato. Um fator chave para aprender como o parasita persiste em hospedeiros que exploram o mecanismo de resistência via proteínas IRGs no ratinho é compreender como o parasita pode equilibrar quantos parasitas são eliminados pelo hospedeiro para prevenir a mortalidade aguda e, ao mesmo tempo, garantir que pelo menos alguns vacúolos não sejam eliminados pelas proteínas IRG. Esta questão principal surge igualmente no caso humano, e em todas as outras espécies de hospedeiros de sangue quente que são infectadas pelo *Toxoplasma*: como consegue o parasita encontrar a situação ideal, não matando, mas também não sendo totalmente eliminado pelo hospedeiro?

Depois que o *T. gondii* invade uma célula, o grupo de IRGs efetores ataca a PVM, levando à sua destruição. Ainda não se sabe como as IRGs efetoras reconhecem e se ligam à membrana desses vacúolos. Além das IRGs, também há acumulação de algumas outras proteínas na região do vacúolo, incluindo a ubiquitina, cuja função neste contexto é desconhecida. O presente estudo foca-se nos fatores que determinam a acumulação de IRGs como pioneiros na destruição de PVs específicos (suscetíveis), evitando outros (resistentes) e a sua relação com o recrutamento de ubiquitina. Começamos o estudo analisando como a concentração de IRG disponível no citoplasma determina o seu recrutamento para os PVs e como diferentes IRGs se acumulam (carregam) ali. Descobrimos que, independentemente do fornecimento disponível de IRGs citosólicas, cada uma se liga de forma independente a diferentes proporções de PVs, totalizando ~ 80% dos PVs. A destruição do PV resulta da ação conjunta das IRGs. A Irgb6 carrega na maior proporção de vacúolos, mas por si só não é suficiente para destruir a PVM. Em seguida, perguntamos se a duração da persistência do parasita nas células antes do carregamento de IRGs, que aqui chamamos de maturação da PVM, impede que as

IRGs se direcionem para certos vacúolos, respondendo assim por ~ 20% dos PVMs que não carregam com IRGs. Usando parasitas sem TgIST, uma proteína que inibe a resposta do interferão ao nível da cromatina e, portanto, inibe a indução de proteínas IRG, demonstramos que o tempo de residência na célula antes que os IRGs se liguem não torna as PVMs progressivamente menos propensas à ligação de proteínas IRG, e portanto a maturação vacuolar não explica os vacúolos resistentes à eliminação. Em seguida, concentramo-nos em determinar a ligação entre a acumulação de ubiquitina no PV e a presença de IRGs. Descobrimos que após o recrutamento das IRGs, a ubiquitina está presente em ~ 70% dos PVs já cobertos pelas IRGs, equivalente aos carregados por Irgb6, Irga6 e Irgd, mas não aqueles carregados apenas por Irgb6. Uma análise detalhada permitiu-nos verificar que a ubiquitina não usa proteínas IRG como substrato, mas precisa da sua ação na destruição de PVMs para permitir a acumulação de ubiquitina dentro ou sobre os parasitas. Mostramos claramente que a ubiquitina está presente exclusivamente no parasita e não na PVM.

Em conclusão, os nossos resultados sugerem que a eliminação de *T. gondii* é iniciada pelo recrutamento de IRGs para os PVs. A acumulação de diferentes proteínas IRG efetoras poderá ocorrer através do reconhecimento de alvos moleculares específicos na face citosólica da PVM que são transportados para a PVM a partir da membrana citoplasmática da célula hospedeira no momento da entrada do parasita. A interrupção (ruptura) da PVM precisa da cooperação entre diferentes IRG efetores. A ruptura da PVM permite o acesso da ubiquitina à membrana do parasita e inicia um processo que leva à morte do parasita e à morte necrótica da célula hospedeira.

Acknowledgments

Almost six years ago, I left Cape Verde determined to seize the opportunity to do my PhD in Portugal. I grabbed it, aware that this time away from home would bring many challenges that I would have to face. The PhD is a long scientific and intellectual journey inseparable from family and social life, and requires support at many levels. For my journey, I was able to count on many people that I would like to thank here.

First of all, I would like to especially thank my supervisor Jonathan Howard, who accepted me into his laboratory, even though we were unable to communicate orally at the beginning due to language limitations. Thank you very much for having trusted me and for allowing me to enjoy the excellent conditions afforded by your laboratory, your vast knowledge and experience. I thank you also for the shared moments of learning, anguish, and ultimately overcoming on the path to this joint project of "doing science". Thank you so much for being so supportive, for your criticisms, suggestions, corrections and especially your patience and understanding, which allowed me to progress and complete the challenging process of pursuing a PhD. I would also like to thank Dr Colin Adrain as my second adviser for support and encouragement, critiques and suggestions at the early stages of this work. I would like to thank my thesis committee members Claudia Bank and Carlos Penha Gonçalves for the very productive discussions we had together.

I want to thank all current and former members of the Howard Lab for sharing discussions and suggestions that have integrated and improved my project. Thank you very much, Cláudia Campos, for the reception at the lab, and for the technical and scientific mentoring, especially in the initial phase of my work, which gave me the necessary tools to develop my project. Catalina Alvarez, thank you for sharing this journey with me, for your criticisms, suggestions, and for almost always

solving my computer problems. Joana Loureiro, thank you very much for the welcome, for your kindness, for the mentoring in choosing the laboratory and for all the guidance, especially at the beginning of my project. Thank you very much for the friendship, which won my trust and allowed me to alleviate my anguish when necessary and for the promptness with which you answered all my requests.

I would also like to thank Gabriel Martins, who was much more than the resident scientist responsible for the Advanced Imaging facility and a former teacher, but also a friend, who greatly facilitated and improved my microscopy work.

I must also thank the PGCD directors, especially Joana Gonçalves-Sá, for accepting me into the program, Élio Sucena, whose recommendation was decisive in my being selected for the PGCD program. To the former director of the IGC doctoral program, Ana Aranda, thank you for everything.

And thank you my fellow classmates of the PGCD 2015.

Thank you Ana Regalado for the friendship, understanding and for having been a bench-side psychologist for me so many times. Thank you Mónica Medina for sharing our writing moments.

My biggest thank you also to my family, relatives and friends who, even without understanding the complexity of a PhD, have been by my side and expressed their concern throughout these years.

To my husband Paulo Cabral for his permanent support.

Special thanks to my lovely daughter and companion at all times, away from whom this PhD took a lot of attention. Rihana: thank you for always being present and for the words of encouragement since the beginning of this project. I loved every "you can do it!" and every “is it going well?" that you directed at me.

To the friends that the PGCD gave me, especially Cláudia Gonçalves and Cíntia Horta, for their encouragement and concern over the years.

To all those who wouldn't fit in these pages, who at various moments

asked me the dreaded question “so, how’s that PhD?” and who, with that, encouraged me to proceed: thank you.

List of abbreviations

AF	Alexa fluor
APS	Ammonium peroxydisulfate
BCA	Bicinchoninic acid
BL/6	Mouse strain C57BL/6
BMM	Bone marrow-derived macrophages
BSA	Bovine serum albumin
CAI	Cell Autonomous Immunity
CLRs	C-type lectin receptors
CO2	Carbon dioxide
DAPI	4′,6-diamidino-2-phenylindole
DC	Dendritic cells
DMEM	Dulbecco's modified Eagle's medium
DNA	desoxyribonucleic acid
DUBs	Deubiquitinating enzymes
EDTA	Ethylenediaminetetraacetic acid
ER	endoplasmatic reticulum
FACS	Fluorescence-activated cell sorting
FBS	Fetal bovine serum
FCS	Fetal calf serum
GABARAPs	g-aminobutyric acid receptor-associated protein
GAP	GTPase activating proteins
GAS	IFNγ-activated site
GBP	Guanylate-binding protein
GDP	Guanosine diphosphate
GED	GTPase effector domain
GTP	Guanosine triphosphate
HEK293T	Human Embryonic Kidney 293 cells
HeLa	Henrietta Lacks
HFFs	Human foreskin fibroblasts
HI-FBS	Heat-inactivated fetal bovine serum

HMGB1	High-mobility group box 1
hMSC	Human mesenchymal stromal cells
HUVECs	Human Umbilical Vein Endothelial Cells
IFNGR	Interferon (IFN)-gamma receptor
IFNγ	Interferon (IFN)-gamma
IRG	Immunity-related GTPases
ISGs	Interferon-stimulated gene
ISRE	Interferon-stimulated response element
IVN	Intravacuolar network
JAK	Janus kinase
KO	Knockout
LIR	LC3-interacting region
MEFs	Mouse Embryonic Fibroblasts
MHC	Major Histocompatibility Complex
MIC	Micronemal proteins
MJ	Moving junction
MOI	Multiplicity of infection
MX1	Myxovirus resistance protein 1
NDP52	Nuclear dot protein 52 kDa
NK	Natural killer cells
NLPR	Pyrin domain PYD-containing proteins
NLR	NOD-like receptors
OPTN	Optineurin
PAMPs	Pathogen-associated molecular patterns
PBS	Phosphate-buffered saline
PBS	Phosphate-buffered saline
PBST	Phosphate-buffered saline Tween
PCR	Polymerase chain reaction
PFA	Paraformaldehyde
PRR	Pattern recognition receptors
PV	Parasitophorous vacuole

PVDF	Polyvinylidine difluoride
PVM	Parasitophorous vacuole membrane
RLR	RIG-I-like receptors
RNA	ribonucleic acid
RON	Rhoptry neck protein
ROP	Rhoptry bulb protein
RT	Room temperature
SCV	Salmonella-containing vacuole
	sodium dodecyl sulfate-polyacrylamide gel
SDS-PAGE	electrophoresis
SQSTM	sequestosome 1
STAT1	Signal Transducer And Activator Of Transcription 1
T.gondi, *Tg*	*Toxoplasma gondii*
TLR	Toll-like receptors
TRAF6	TNF receptor-associated factor 6
TRIM21	Tripartite motif containing-21
TVN	Tubulovesicular network
UB	Ubiquitin
UBD	Ubiquitin Binding domain
UV	Ultraviolet
W/d	Without
WT	Wild type

Table of contents

List of figures

List of tables

Chapter 1

---

1. Introduction

1.1. Cell autonomous immune response

Cell-autonomous immunity (CAI) is the intrinsic ability of individual non-immune cells to respond against a pathogenic agent via effector defense mechanisms usually induced by cytokines, and especially interferons (IFNs) [1]. Such cell-autonomous defense mechanisms are dependent on the production and availability of interferon and on both immune and non-immune cells. Host-pathogen interactions comprise scenarios in which the pathogenic agent attempts to maintain itself and multiply in the host and achieve transmission, whilst avoiding elimination by the host. The host, in turn, mobilizes its immune defenses to prevent or resist infection, either eliminating it or keeping the infectious organism in check and minimizing pathology. In host-pathogen scenarios the ultimate fate of the host depends upon the rapidity and efficacy of pathogen transmission to a new host. Following transmission the fate of the host is immaterial for the pathogen.

The key to pathogen elimination or limitation is pathogen recognition and the distinction between invading organisms (non-self) and host cells themselves (self), to trigger the cell innate defense. Different groups of pathogens share similar structures, pathogen-associated molecular patterns (PAMPs), which allow their recognition by several families of so-called pattern recognition receptors (PRRs) expressed by host cells. Some PRRs, such as Toll-like receptors (TLRs) are located on the cell membrane[2]. Other PRRs include C-type lectin receptors (CLRs), NOD-like receptors (NLRs), RIG-I-like receptors (RLRs), and cytosolic DNA sensors [3,4] are located in the cytoplasm. PRRs can recognize very different structures such as oligosaccharides, peptidoglycans and lipopolysaccharides, non-methylated DNA, single-stranded DNA, double-stranded RNA etc.

PRR-mediated recognition of the pathogen can trigger different signalling pathways that result in synthesis of pro-inflammatory

cytokines and interferons [5]. These cytokines are not only involved in the regulation of immune action by specialized immune cells but can also enable cell-autonomous immunity resistance mechanisms in cell types outside the traditional immune cell lineages [6,7] Interferons trigger cell autonomous defense, which may rely on effector mechanisms as distinct as synthesis of antimicrobial peptides and proteins, the orchestration of specialized degradative compartments (via the autophagy and/or the autolysosome pathways), or the stimulation of programmed host cell death; these defense execution mechanisms provide different layers of physical barriers that the pathogen must try to overcome to achieve and sustain infection before transmission.

1.2. Interferon induction of cell autonomous Immunity.

Interferons (IFNs), first discovered and described as substances released from virus-infected cells with an anti-viral action on uninfected cells [8], are employed by vertebrates to activate mechanisms of immunity against intracellular pathogens such as viruses, bacteria and parasites [9,10]. Multiple different genes encode three types of IFN: Type I IFN (IFNα, β, ε, κ, other structurally related subfamilies) [11], type II IFN encoded by a unique gene, IFNγ, and type III IFN (IFNλ1, INFλ2, IFNλ3, and IFNλ4) [9,12,13].

The type I IFNα is the most complex IFN type, encoded by 13 different genes located on the same chromosome, while IFNγ is encoded by a single gene [14].

Unlike type I IFNs which are expressed by most cell types, including hematopoietic cells [8] and fibroblasts, the main source of IFNβ [15], IFNγ secretion is largely limited to immune system cells, mainly natural killer (NK) cells [16] and T lymphocytes (CD4 and CD8) [9], although being produced by other haematopoietic cells under certain conditions[18]. Type III IFNs can also be produced by many different cell types, in

particular pDCs, monocytes, monocyte-derived dendritic cells (MDDC), and epithelial cells [19,20]. While type I and type III are primarily activators of antiviral activities [21], IFNγ is implicated in defense against many other pathogen classes, such as bacteria and parasites [11,21,22]. Interferons, which act in both autocrine and paracrine manner, ensure that the generating cells, as well as others cells participate in the response to infections [16,23].

IFNs activate the transcription of thousands of target genes [8,18] through activation of the signaling cascade, a JAK/STAT pathway (Janus kinase/signal transducer and transcription activator 1), which allows cells to respond in various ways to eliminate pathogens. The IFN dependent pathways are initiated with binding of IFNs to their cognate specific receptors on the plasma membrane, which leads to activation and dimerization of STAT proteins [14,21]. Active, tyrosine-phosphorylated STAT dimers translocate from the cytoplasm to the nucleus [11] where they bind to DNA sequences called IFN-stimulated response elements (ISRE), and gamma-activated sites or sequences (GAS) in the promoter regions of IFN-responsive or IFN-stimulated genes (ISGs), resulting in gene transcription [8,11,24]. Some of these genes are commonly regulated by more than one type of IFN, while others are selectively regulated by one IFN separately [25]. Any interference with STAT binding to these sites can affect the production of ISGs.

So far, about 10000 genes [24,26,27] or ISGs stimulated by human and mouse IFNs have been identified, most of which are not fully functionally characterized [10,27].

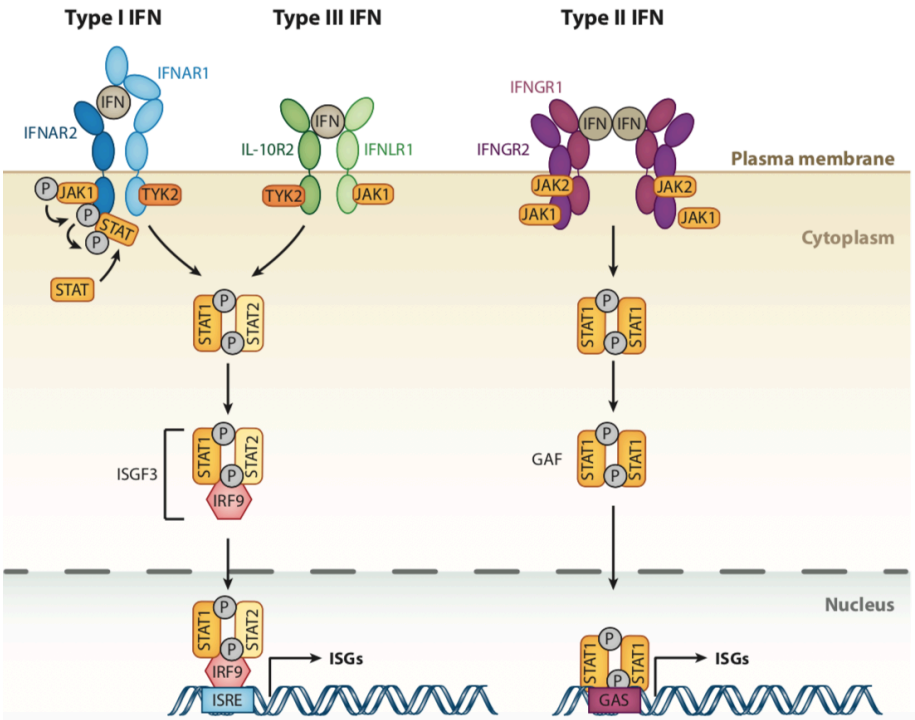

Figure 1. 1. IFN-stimulated gene (ISGs) induction via the JAK/STAT pathway

All types of Interferon (IFN) bind to two-chain receptors on the surface of cells. Type I IFN targets IFN receptor 1 (IFNAR1) and IFN receptor 2 (IFNAR2); type II IFN the IFNγ receptor 1 (IFNGR1) and IFNGR2; and type III IFNλ with IFNλ receptor 1 (IFNLR1); also known as IL28RA) and interleukin 10 receptor 2 (IL10R2; also known as IL10RB). This binding triggers the activation of the receptor-associated Janus kinases (JAK) and tyrosine kinase 2 (TYK2) that leads to tyrosine phosphorylation of signal transducer and activator of transcription (STAT), which then leads to the formation of STAT1–STAT2–IRF9 (IFN-regulatory factor 9) (now termed interferon-stimulated gene factor 3 or ISGF3 complexes) for Type I and III IFN, and STAT1-STAT1 complex (now termed gamma activation factor or GAF) for Type II IFN. Phosphorylated ISGF3 and GAF complexes translocate to the nucleus to bind the promoter elements such as IFN-stimulated response element (ISRE) and IFNγ-activated site (GAS) elements in DNA to initiate the transcription of Interferon-stimulated genes (ISGs) [8,11,14].

The first wave of transcription of these genes occurs within 15-30 min of IFN treatment [28], the so-called primary response genes. Some of those genes encode further transcription factors termed interferon regulatory factors (IRFs), which are capable of promoting subsequent

waves of transcription events modulated indirectly by IFNs, the secondary response genes [24]. ISGs function in systemic resistance and/or autonomous resistance of cells, and those involved in the study performed in this thesis are described below.

1.3. Interferon-inducible GTPases:

Among many other targets, IFNγ-dependent signaling leads to transcription of several families of large guanosine triphosphatases (GTPases), which are among the most prominently IFNγ-induced proteins and play important roles in the immune response of diverse cell types against pathogens ranging from bacteria, to viruses, fungi and parasites [29]. Indeed it was study of interferon-mediated induction of human Guanylate Binding Protein 1 (GBP1) that led to the identification and elucidation of the JAK-STAT pathway [30].
The interferon-inducible GTPases are enzymes with an N-terminal globular GTPase domain (GD) followed by a C-terminal helical domain (CTHD). The ancient conserved domain, the G-domain or GD, is able to bind and hydrolyze guanosine 5'-triphosphate (GTP) to guanosine 5'-diphosphate (GDP) or guanosine 5'-monophosphate (GMP). These proteins work by switching between the two interconvertible bound states, the inactive GDP-bound form and the active GTP-bound form, mediating effector functions. They are able to switch ON and OFF between these two forms.

In contrast with small GTPases, in which the transitions between GDP and GTP are facilitated by guanine nucleotide exchange factors (GEFs) and GTPase-activating proteins (GAPs), large GTPases generally have low affinities for nucleotides and exchange GDP and GTP freely in the cytoplasm. Activation is initiated by dimerization between the nucleotide-binding domains, often with subsequent oligomerization

trapping the GTP-bound state and functioning as “GAP” activity and consequently facilitated hydrolysis [29,31]. Like dynamins, large GTPases generally associate with intracellular lipid membranes and possess the ability to self-assemble and allow protein–protein or protein–lipid interactions through the C-terminal helical domain [31–33].

There are 3 families of GTPases playing a role in IFN-mediated immune resistance: the myxovirus resistance proteins (Mx), the immunity-related GTPases (IRGs), and guanylate-binding proteins (GBPs) [31]. Both IRG and GBP proteins can be transcribed in response to type I, II and III Interferon [29] while the Mx family proteins, are not induced by type II Interferon[31].

1.3.1. Immunity-related GTPases (IRGs)

The IRG proteins are strongly transcribed only in response to IFN, with IFNγ being their major inducer; IFNα / β also triggers IRG expression, although to a lesser extent [31]. These 47kDa unit proteins (former “p47 GTPases”) have been extensively studied since the identification of the first family member, Irgd (as IRG47 in Gilly and Wall 1992), in the early 1990s. In this thesis I will use the widely accepted formal nomenclature for IRG genes and proteins introduced by Bekpen et al (2005).

In the C57BL/6 mouse genome, there are 16 functional and possibly functional genes: 9 functional IRG genes,namely the three IRGM proteins (Irgm1, Irgm2, Irgm3) Irga6, Irgb6, Irgb6*, Irgb10, Irgd, and Irgb2b1, 7 possibly functional (Irga3, Irga4, Irga7, Irga8, Irgb5*b3, Irgb5b4, Irgb9b8), and 3 non-functional pseudogenes (Irga1, Irga2, Irga5 and Irgb7); all 16 are distributed in 3 clusters, two clusters separated by 10Mb on Chromosome 11 and one cluster on chromosome 18. An isolated divergent and highly conserved IRG gene on chromosome 7 (Irgc) has no immune role, is expressed exclusively

in the testis in haploid spermatids and is required for normal spermatogenesis [34] (Howard Lab unpublished results). Characteristically, the 47 kDa open reading frames of IRG proteins are encoded on single exons. Four pairs of IRGB genes (Irgb2-b1, Irgb5*-b3; Irgb5-b4; and Irgb9-b8) on chromosome 11 encode “tandem” IRG proteins built of two exons each encoding the typical 47 kDa IRG protein structure, giving a molecular weight around 94 kDa [34,35]

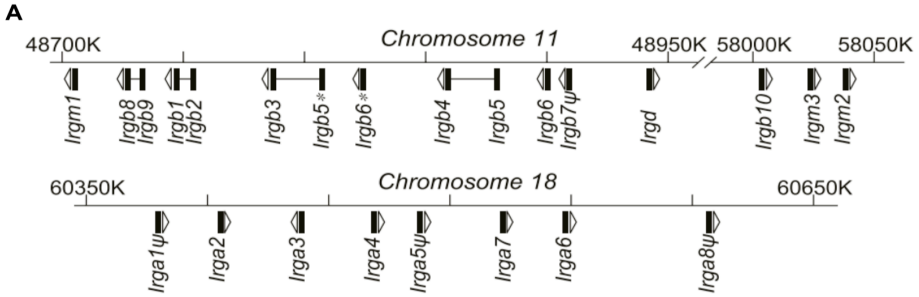

Figure 1. 2. Linear order of IRG gene clusters on Chromossome 11 and Chromossome 18 of C57BL/6 mouse strain

Distribution of IRG genes in chromosomes 11 and 18 including the position of the IRG coding units (black blocks) and the direction of transcription (arrowhead), the position on the chromosome (numbers), and the tandem genes connected with a line. ψ indicates pseudogenes, * marks the second copy of the Irgb6 gene identical at the protein level (modified from Lilue et al. 2013).

In humans and higher primates the p47 GTPase family is greatly reduced and probably non-functional. The human genome has only two IRG genes, IRGC and the greatly truncated IRGM, homologous to mouse IRGM proteins [34,36,37]. The human IRGM fragment is not inducible by interferons [38].

The mouse immune IRG proteins, despite great similarity in sequence and structure can be subdivided into 3 functionally distinct subfamilies: effectors, regulators and decoys (see section 1.3.1.1.). The effectors and decoys were initially called GKS proteins,[31] and the regulators GMS proteins because of a striking sequence feature of the nucleotide

binding site. GKS IRG proteins (effectors and decoys) possess the universally conserved sequence (GX4GKS) of the G1 motif of the GTP binding site and the GMS regulator proteins contain the non-canonical GX4GMS sequence in the G1 motif [31,39]. It is still not yet known whether purified GMS proteins can hydrolyze GTP, although it has been suggested from pull-down experiments that Irgm3 has GTPase activity [40]. However, the G1 methionine would seem to be incompatible with correct positioning of the nucleotide phosphates.

1.3.1.1. Molecular properties of IRG proteins: Biochemistry and structure

Studies of the GTPase activity of the IRGs evidenced hydrolysis of GTP to GDP were extended with the study of the purified Irga6 [41,42].

The Irga6 protein (originally called IIGP1) is the only IRG protein that has its structure and chemical properties characterized in detail so far [43]. Since IRG proteins have high sequence homology, the Irga6 structure determined in 2004 has been used as a model for the other IRG proteins. This protein structure breaks down into three regions: N- and C-terminal helical domains, with a Ras-like G domain between them (Figure 1.3).

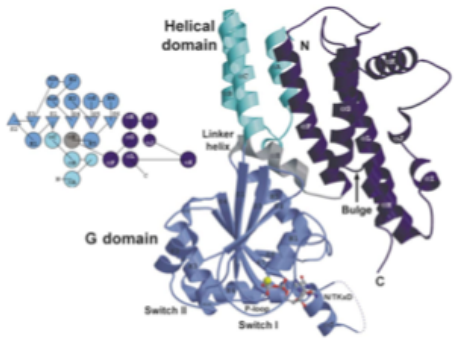

Figure 1. 3. Crystal 3D struture of Irga6 protein

Ribbon presentation of the Irga6 crystal attached to GDP / Mg2 + is showing the helical N-terminal region (αA-C helix) in Cyan, the G domain (helix S1-H5) in light blue, the linker helix (αE) in gray and the helical C-terminal region (αF-αL helix) in dark blue. GDP and Mg^{2+} are shown as atomic stick figure and yellow sphere. The topology is shown schematically using the same color code [43] .

Irga6 binds GDP with greater affinity than GTP. Its basal GTPase activity increases with increasing protein concentration suggesting cooperative interactions. Irga6 can be found *in vitro* in monomers (in the absence of nucleotides) and in GTP-dependent homo-oligomers, accompanied by a conformational change, that are resolved after GTP hydrolysis [44]. The oligomerization of Irga6 and accelerated hydrolysis of the GTP occurs through an interface of Irga6 within the G domain and includes the nucleotide binding site and the exchange regions of the bound GTP substrate. This interface is also responsible for the interaction of Irga6 with others IRGs [42]. The possibility that cooperative hydrolysis between IRG effector proteins normally oocurs between different members of the group has not yet been examined.

The cooperative hydrolysis of GTP by Irga6 has been assumed to be generally true for the GKS IRG proteins. In fact, Pawlowski showed that although purified Irgd and Irgb6 are both slow GTPases, the hydrolysis rates are independent of protein concentration, raising the possibility that the cooperative activity of purified Irga6 is an in vitro artefact[42].

Irga6 carries an amino-terminal myristoylation site [38] at glycine 2, which is active and has been shown to partially favour binding of the protein to membranes [45,46]. The four tandem IRG proteins, Irgb2b1, Irgb9b8 Irgb5b4 and Irgb5*b3 also carry canonical amino-terminal myristoylation sequences, though only Irgb2b1 is known to be significantly expressed in C57BL6 mice.

IRG proteins associate with membranes to varying degrees. Regulatory

proteins bind to membranes through C-terminal helical sequences [47,48] With the exception of the plasma membrane, regulator IRG proteins Irgm1, Irgm2 and Irgm3 are distributed in distinct compartments including all the membrane organelles: Irgm1 is associated with Golgi complex [48,49] endosomes, lysosomes [47,50] mitochondria [47,50,51] and lipid droplets [52,53]; Irgm2 is associated with Golgi [29,54]. Irgm3 localises to the ER [54,55] and lipid droplets [52,53]. In all three cases the different compartmental specificities of the IRGM proteins can be reproduced by short peptides derived from the C-terminal helical regions of the full-length proteins.

In IFN-stimulated cells, effector IRGs (Irga6, Irgb6, Irgb10 and Irgd) are found in GDP-bound form mainly in the cytosol, and only Irga6 can be found associated mainly with the endoplasmic reticulum membrane [49,58]

1.3.1.2. IRG genes in mouse resistance immunity

The first evidence that IRGs have some role in resistance to infections came from a study in Irgm3 (formerly IGTP) knockout (KO) mice, in which there was 100% mortality following infection with an avirulent strain of *T. gondii* [58]. Then, a series of studies involving more genetic deletions of IRG genes in mice have supported the notion of a role for the IRG system in resistance against certain pathogens.

Single knock-out mouse models are available for Irgm1, Irgm3, Irgd, Irga6, Irgb10 and Irgb6, as well as an Irgm1/Irgm3 double knock-out mouse strain. Evidence from *in vivo* and *in vitro* studies indicating susceptibility or resistance to certain organisms in comparison with wild type C57BL/6 mice is summarized in Table 1.

Table 1. 1. Susceptibilities of Irg-deficient mice and cells to intracellular pathogens

M, mouse; C, cells; R, resistant; S, sensitive; Sm, knockout mouse sensitive; Rm, knockout mouse resistant; Sc, knockout cells sensitive; Rc, knockout cells resistant. m, mouse, c, cells. where not specified, the results are from knockout mice. nd, not determined.

Organisms	Wild type	Irgm1-/-	Irgm3-/-	Irgd-/-	Irga6-/-	Irgb10-/-	Irgb6-/-
Toxoplasma gondii	**R**	S	S	Sm, RC	S	Rc	S
Trypanosoma cruzi	**R**	S	R	ND	ND	ND	ND
Leishmania major	**R**	S	S	ND	R	ND	ND
Mycobacterium tuberculosis	**R**	S	R	R	ND	ND	ND
Mycobacterium avium	**R**	S	R	ND	ND	ND	ND
Listeria monocytogenes	**R**	S	R	R	R	ND	ND
Salmonella typhimurium	**R**	S	R	R	ND	ND	ND
Chlamydia trachomatis	**R**	S	S	ND	Rm, Sc	Sc	ND
Francisella novicida	**R**	ND	ND	ND	ND	S	ND
Microsporidia	**R**	Sc	Sc	Rc	Rc	ND	ND

Table 1 is adapted from work in the Howard lab [29] and summarizes various studies on IRGm1[49,56,59–64] on IRGm3 [56,58,60–62,64], on IRGd[59,60,62,64] on Irga6[60], on Irgb10[56,65,66], and on Irgb6[67].

The resistance system linked to the IRG proteins has been demonstrated in the knock-out mouse models for a number of IRG genes, showing greater susceptibility to certain pathogens including protozoa, unicellular fungi and intracellular bacteria, illustrated in Table 1. The loss of pathogen resistance of the Irgm1 -/- mice has been determined for almost all the pathogens enumerated. Loss of Irgm1 results in loss of resistance to every organism that has been tested for which IFNγ-induction plays a role in resistance. The only tested organism where resistance was not lost in Irgm1-deficient mice was the trematode *Schistosoma mansoni* where resistance is completely independent of IFNγ [68]. Mice deficient in Irgm1 infected with a number of different organisms (*Toxoplasma gondii*, *Mycobacterium avium*, *Trypanosoma cruzi* and *Salmonella typhimurium*) suffer an impressive collapse of the lymphoyeloid system [61,63,69]. Despite earlier claims [62], Irgm1 does not seem to colocalize with pathogens [51] and it is clear that

susceptibility of Irgm1-deficient animals is due to the IFN-dependent lymphomyeloid collapse [61] and not to an effector function on these pathogens. Since Irgm1 is a negative regulator of IRG protein activation, the cytotoxic effect of interferon in the Irgm1-deficient mouse may be a consequence of the induction and intracellular activation of IRG effector proteins causing damage to organelles, particularly lysosomes during lymphomyeloid development [51,54].

Regarding the effector IRGs, it is evident that Irgd -/- and Irga6 -/- mice show significant susceptibility to avirulent strains of *T. gondii* [59,70], while the presence of Irgb10 seems to be important in the resistance against the bacteria *Chlamydia trachomatis* [65], *Chlamydia psittaci* and *Fransisella novicida* [66]. The meaning of these different resistance specificities of different effector IRG proteins is completely unknown, and presumably implies unexpectedly different mechanisms of action from different members of this well-defined structural family.

The differential role of IRG proteins in the mouse resistance to pathogens at the level of cell autonomous immunity (CAI) is illustrated in the *T. gondii* system and detailed in 1.6. IFNγ is the main mediator of immunity to toxoplasmosis [67,70]. In mice deficient in regulatory IRGs Irgm1, Irgm3 or Irgm1/Irgm3, infection with *T. gondii* leads to the rapid death of 100% of mice in the acute phase of the disease, about 9-11 days after an intraperitoneal infection, an infection outcome similar to that previously described for IFNγ-deficient mice [58,59,67,71]. However, the susceptibility of Irgm1-deficient mice probably has a different origin, as set out above. Interestingly, the Irgm1/Irgm3 double deficient mouse no longer shows the universal susceptibility of the Irgm1 deficient animal and is susceptible only to T. gondii [72]. The absence of Irga6 and Irgd causes a less severe defect in resistance than loss of the IRGM proteins. About 50% of Irga6- and Irgd-deficient mice die from infection with *T. gondii* in the acute phase and in the chronic phase [59,70].

Recently published data in Irgb6/Irgb6* KO show that 100% of animals succumb to infection with the avirulent *T. gondii* strain, PRU [67]. An independent deletion of Irgb6 and Irgb6* has confirmed the high susceptibility to PRU infection, but also showed that the animals are largely resistant to another avirulent *T. gondii* strain, ME49 at the same level of Irga6 and Irgd resistance (Claudia Campos, unpublished data).

IRG proteins act as effectors against pathogens. Evidence to support this notion includes the fact that IRGs colocalize with different pathogens. Irga6, Irgb6, Irgd, Irgb10 colocalize with the *Toxoplasma gondii* PVM [45,49,73,74], Irga6, Irgb6 and Irgb10 are somewhat recruited to *Chlamydia trachomatis inclusions* [53,75]*. Irgb10 controls growth of Chlamydia in mice* [65]*; the roles of Irga6 and Irgb6 remain unclear. Irgb10 colocalizes with Francisella novicida* [66], and Irga6, Irgb6, Irgd and Irgm2 colocalize with the microsporidian fungus *Encephalitozoon cuniculi* [60]. The nature of the resistance mechanisms is discussed below.

1.3.2. Guanylate-binding proteins (GBPs)

GBP proteins, composed of 65-73 kDa units, are strongly induced by IFNγ, accounting for as much as 20% of IFNγ-stimulated proteins [29,32]. Infections by the protozoan *T. gondii* or the bacterium *Listeria monocytogenes*, that induce strong IFNγ responses, also stimulate expression of GBPs [76].

GBPs are present in most vertebrates, with 11 genes identified in mice in clusters on chromosomes 3 (mGbp1, mGbp2, mGbp3, mGbp5, and mGbp7) and 5 (mGbp4, mGbp6, mGbp8, mGbp9, mGbp10, and mGbp11) [76,77] and seven genes (hGBP1–7) in human chromosome 1 [78] where it was first identified, due to its robust IFNγ induction [79].

1.3.2.1. Biochemical Properties of GBPs

The GTPase-domain of GBPs binds guanine nucleotides with low affinities, and binds both GTP and GDP similarly to other GTPases. Human GBP1 is able to hydrolyze GTP in two steps to GMP[80]. GBPs are able to multimerize and organize into vesicle-like structures (VLS) in the cytoplasm[81], as has been proposed for mGBP2 multimerizing with mGBP1 and mGBP3 [82].

Human and mouse GBP1, GBP2, and GBP5 contain a motif in the C-terminus, the CaaX sequence, that is posttranslationally modified by isoprenylation, which is required for membrane interaction [83,84] eg with the Golgi complex membrane [81,85] while others are predominantly cytosolic [76,83].

1.3.2.2. Role of GBP against pathogens

GBPs play an important role in defense of the organism against a broad array of pathogens such as viruses, bacteria and parasites [86].

The anti-pathogen actions of GBPs [87] are well characterized in bacterial infections of medical significance across the human population, such as *Chlamydia*, *Salmonella*, *Listeria*, *Francisella novicida*, and *Legionella pneumophila* infections [83,88–90].

Recruitment of GBPs to several bacteria have an effect on bacterial survival [86], a good example of which can be seen in the recruitment of hGBP1 and hGBP2 and mGBP1, mGBP2, mGBP3, mGBP6, mGBP7, mGBP9, and mGBP10 in the control of *Chlamydia* [91].

To fulfil their anti-microbial functions, GBPs use multiple mechanisms. Predominantly cytosolic GBPs or GBPs present in vesicle like structures (VLS) act as an effector, by association with membranous compartments [31,33,84] and as a contributor to other mechanisms, such as recruitment of other effector complexes for production of reactive

oxygen species, autophagy, inflammasome activation, and/or cell death [92].

1.3.3. Parasite control by the IRG and GBP resistance systems

1.3.3.1. Toxoplasma gondii

The success of the *T. gondii* requires transmission between a definitive host, a feline, for sexual reproduction and an intermediate host, where asexual multiplication occurs, and which can probably be any warm-blooded animal [93]

In definitive hosts, ingestion of infected intermediate hosts leads to the sexual process of gametogenesis and gametic fusion in the intestinal epithelium and results in release of environmentally resistant sporocysts in the faeces that can infect an intermediate host upon ingestion [94].

The infection of intermediate hosts is ensured by sporozoites, resulting from the disruption of cysts in the digestive tract, that invade the intestinal epithelium and differentiate into the rapidly replicating tachyzoite form that spreads rapidly throughout the host by cycles of intracellular invasion and fast replication, which in vitro is initiated in about 7 hours post-host cell invasion. Following several replication cycles the host cell is actively disrupted and the released tachyzoites spread to neighbouring cells [93]. Later, upon reaction of the host's immune system, the tachyzoites convert to a slowly replicating form (bradyzoite) that persists in slowly growing cysts in brain and muscle for the life of the infected host [95,96].

1.3.3.2. Cell invasion and vacuole formation

The triumph of *T. gondii* in the infected host depends on the efficiency of cell invasion by the parasite, its establishment within the host cell and surviving the immune response, with which it has many crucial interactions. This makes *Toxoplasma* infection a good model for studying molecular mechanisms guiding host-parasite interaction.

The interaction begins with an active cell invasion process that, despite being fast (<30 s), comprises several steps that require a specific complex of proteins secreted by the parasite's secretory organelles, micronemes, (MIC proteins) rhoptries (ROP and RON proteins) and dense granules (GRA proteins). Micronemal proteins guarantee the adhesion between the parasite and the host cell membrane by connecting the parasite's actin-myosin gliding motility machinery to host cell proteins [96,97].

The second wave of protein secretion comes from the rhoptry organelle - the RON proteins that together with AMA1 form a remarkable moving junction (MJ) that connect parasite to the host cytoskeleton [97]. The importance of this highly conserved protein among Apicomplexan parasites for host cell invasion was demonstrated with its inactivation or depletion that severely compromises the invasion by *T. gondii* AMA1 [97,98].

Immediately following the formation of the MJ, anterior secretory organelles, rhoptries, secrete multiple different proteins (ROP proteins) into the cytoplasm of the host cell [99]. As the MJ displaces towards the rear, the parasite progresses actively to invade the host cell, creating an invagination of the plasma membrane that will pinch off to create the parasitophorous vacuole (PV) which is modified to serve as a niche for intracellular survival [93].

The achievement of the non-fusogenic PVM composition, that does not fuse with the host cell machinery, starts with the passage through the

MJ that sieves the host plasma membrane proteins leaving only host glycosylphosphatidylinositol (GPI)-anchored proteins [100,101]. The lipid composition of plasma membrane is preserved in the newly formed PVM [102].

The modification of the PVM further proceeds with the release of effectors by the tachyzoites to facilitate their intracellular lifestyle, such as rhoptry proteins ROP2 and ROP18, ROP5 and dense granule proteins GRA5 and GRA7, GRA17 and GRA23 [99,100]. These effectors such as GRA17 and GRA23 ensure nutrition [103] and others such GRA15 [104], GRA6, GRA16, GRA18, GRA28, TgIST (*T. gondii* inhibitor of STAT1 transcriptional activity), MyR, TgNSM and GRA24 are translocated to the nucleus to modulate host cell signaling [105–109].

In in *vitro* cultured cells the parasite starts replicating after about 7 hours, forming large rosettes, followed by the parasite egress in a potassium-dependent manner[93] after approximately 48 hours, ready to infect neighbour cells [107].

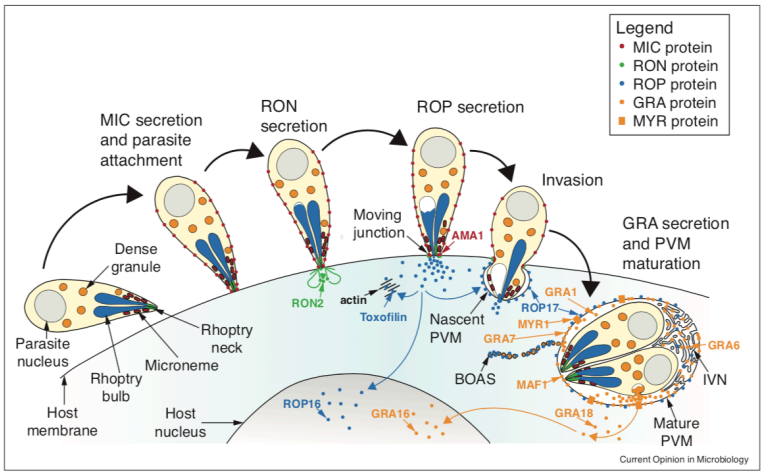

Figure 1. 4. Toxoplasma protein secretion during infection

Micronemal proteins (MICs) are secreted to anchor the parasite to the host cell. While the parasite invades the host cell, the Rhoptry organelle secretes RONs that integrates the MJ and specific ROP as well as dense granule proteins (GRAs) are secreted into the cytosol via a pore formed between parasite and hot membranes. After detachment

of the PVM from the plasma membrane, the maturation of the PVM occurs with the continuous release of GRA proteins into the PV, PVM, or intravacuolar network (IVN). This latter is a tubular-vesicular system of uncertain function. Several parasite effector proteins stay within the vacuole, on PVM, or are translocated by MYR to either host cytosol or host nucleus [97].

1.3.3.3. Cell autonomous resistance against T.gondii by IRG proteins

The loss of resistance against *T. gondii* described above in IRG-deficient mice is reflected in loss of cell-autonomous immunity *in vitro* in cell lines from IRG knockout animals or with defects in IRG expression. IFNγ-stimulated bone marrow-derived macrophages (BMM), astrocytes and fibroblasts from IRG deficient mice fail to control *T. gondii* replication [45,70,108]. *In vivo* mouse deficiency in IRG protein Irgb6, but not Irgb10 deficiency, has been shown to cause a defect in the reduction of *T. gondii* killing activity and an increased infection rate in diferent organs by in vivo imaging and luciferase assay respectively [67].

Although regulatory GMS proteins do not localise at PVs (Irgm1) or localise only residually (Irgm2 and Irgm3), their presence is essential for *T. gondii* resistance. Cells deficient in Irgm1, Irgm3 and cells doubly resistant for Irgm1 and Irgm3 (Irgm1 / m3 double KO cells) are susceptible to *T. gondii* [49,73].

In the presence of IFNγ, regulator IRGs associated with cytoplasmic membrane-bounded organelles maintain the IRG effector proteins in the GDP-bound inactive state in the cytosol of the host cells and prevent their premature activation on cytoplasmic organelles [46,54,71,109,110].

Upon infection, the absence of IRG regulators on the PVM allows effector IRGs to change their distribution and state to accumulate in

high density on the newly formed PVM in the GTP-bound state [45,46,54,74] in a sequential and coordinated manner, with Irgb6 (and possibly also Irgb10) being the first to arrive as 'pioneers', followed by Irga6 and then Irgd [74]. The accumulation of effector proteins creates tension on the surface of the PVM leaving it vesiculated and ruffled, ultimately causing it to rupture [111,112]. This sudden local break in the integrity of the PVM causes its detachment leaving the parasite exposed to the cytosol [111]. Finally, eviction from the PV results in death of the parasite and subsequently to necrosis in fibroblasts [45,73,111] or possibly autophagic elimination in macrophages [73].

In the absence of regulator IRG proteins in cells induced with IFNγ, the effectors activate spontaneously, form probably GTP-bound and possibly denatured aggregates, and are unable to interact with the PVM during *T. gondii* infection. In contrast, effector IRGs may attack cellular endomembranes: indeed, cellular endomembranes may be vulnerable to the attack of effector IRGs, such as lysosomes in Irgm1KO cells, or the ER in Irgm3-deficient cells [110].

In *in vitro* studies, the Irga6 protein can be detected with a specific monoclonal antibody that distinguish between the GDP-bound state in the cytosol and the GTP-bound state. While the inactive GDP-bound Irga6 form in the cytoplasm and in uninfected cells is hardly detected by the 10D7 monoclonal antibody, it is easily detected by the monoclonal antibody 10E7 or the rabbit serum 165 [46]. However the Irga6 active oligomers on the PVM are easily detected by 10D7 [41]. The10D7 epitope is hidden in the crystal structure of Irga6. It is presumed that a conformational change occurs on binding GTP that exposes the epitope. Denaturation of Irga6 (eg on a Western blot from a SDS gel) also allows binding of 10D7, presumably again due to exposure of the epitope [46].

1.3.3.4. Cell autonomous resistance against T. gondii by GBP proteins

Functional studies of GBPs in defense against *T. gondii* are done predominantly in mice, in parallel with studies of *Chlamydia* infection, as previously mentioned [76,91,113]. Initially, in addition to IRGs, several mouse GBPs were shown to accumulate around the PV shortly after *T. gondii* invasion [76].

The deletion of mouse GBP1, GBP2, GBP7 or deletion of the complete chromosome 3H1 region causes increased susceptibility to avirulent *Toxoplasma* strains [83,113,114]. In mouse cells, the resistance mechanisms start with IRG recruitment immediately after infection, then the recruitment of GBPs follows recruitment of other proteins [76,91]. Together with IRGs, GBPs accumulate on the PVM [114] and GBP2 has been supposed to damage the parasite membrane [82], as well as GBP7 [115], after PV disruption.

In human cells, that are devoid of IRGs, GBPs have been proposed to control *T. gondii* through mechanisms that, although not fully characterized, are constantly emerging [32].

GBPs seem to play a cell-type specific role in the resistance to *T. gondii*, of which the best characterized example of *T. gondii* restriction is GBP1, as GBP1 is necessary to restrict the parasite whether it colocalizes with the PV or not. In primary mesenchymal stem cells activated with IFN-γ, GBP1 restricts *T. gondii* [116]. In human A549 epithelial cells, GBP1 is necessary to restrict the growth of the parasite, although it does not target PVs [117], whereas in macrophages GBP1 is co-localized with *T. gondii* PVs [118,119]. It appears that colocalization of GBP1 with the PV is necessary to activate downstream processes, by promoting the exposure of DNA that is sensed by AIM2, a cytoplasmic sensor that recognizes dsDNA of microbial or host origin;

DNA sensing leads to inflammasome activation and host cell death [118,119]. Recent studies [118,120] in the mechanisms of action of GBP proteins in resistance against intracellular bacteria released into the cytosol suggest that binding of GBPs to the pathogen surface via a direct interaction with bacterial surface lipopolysaccharides is essential for the activation of downstream effector mechanisms. It is possible to imagine similar events in the role of GBPs in resistance to *Toxoplasma*.

1.4. Ubiquitination as a mechanism of cellular immunity against intracellular pathogens.

The activation of cellular immune response, from pathogen recognition to pathogen elimination involves complex signaling pathways, including stringenty regulated post translational modification by ubiquitination.

Ubiquitination is the most common, complex, conserved and versatile post-translational modification in eukaryotes[121]. Understanding the roles of ubiquitination in regulating cellular functions requires an understanding of the components of the ubiquitination mechanism.

1.4.1. Structure of ubiquitination process

Ubiquitination is a covalent attachment of the 76 aa protein, ubiquitin (Ub), by an exposed C-terminal tail to lysines from other proteins to modify its activities. Ubiquitin uses seven internal lysines (K6, K11, K27, K29, K33, K48, K63) and methionine at position 1 (Met1), to bind to lysine residues of a protein substrate, including ubiquitin itself to form polyubiquitin chains [122].

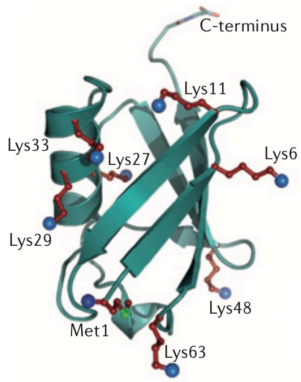

Figure 1. 5. Ubiquitin and its lysine residues

The ubiquitin molecule including its seven lysine residues (K6, K11, K27, K29, K33, K48, and K63), the N-terminus amino group (Met1) and the carboxyl terminus [123].

Ubiquitination is the result of a three-step enzymatic cascade. The reaction starts with the Ub-activating E1 activating a ubiquitin molecule in its C-terminal glycine residue (Gly76), to bind an E1 specific cysteine residue. Then the activated Ub is transferred to form an E2–Ub thioester complex (Figure 8). In the final step of the reaction, one of hundreds of ubiquitin ligase E3 proteins transfers Ub to the amino group of a lysine residue on the substrate protein [121,124,125] (Figure 8). This modification is a continuously reversible process carried out by deubiquitinases (DUBs), which remove ubiquitin from the targeted proteins[126].

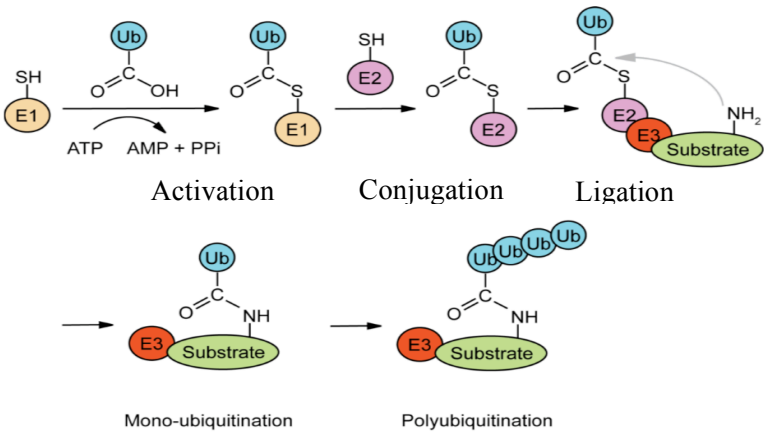

Figure 1. 6. Enzymatic machinery that leads to substrate to assembly of ubiquitin (Ub) chains on a substrate

The coordinated activity of three classes of enzymes is required for ubiquitination. The ubiquitin-activating (E1) conjugates with ubiquitin to transfer it to a ubiquitin-conjugating (E2), that works in concert with E3 ubiquitin-ligase enzyme (E3) to form a bond between ubiquitin and on the substrate protein. The substrate can be the target of single ubiquitin moieties (monoubiquitination) or by multiple ubiquitin molecules, which attach to the previously attached ubiquitin (polyubiquitination)[127].

The different ways that different linkages bind to the substrate, which can be just one ubiquitin molecule or several molecules (polyubiquitination) through the same link (homotypic) or through different linkages (mixed and branched) (Figure 8), allow for a great diversity of ubiquitination topologies that form the "ubiquitin code", which translates into different and generalized repertoire of biological outcomes [128].

1.4.2. Role of ubiquitin in immunity against pathogens

The translation of the "ubiquitin code", defines protein function, protein localization and protein-protein interactions that may be included in pathways used by the cell in the immune response to pathogens [129,130].
Ubiquitination has emerged as an immune defence mechanism against pathogenic organisms [131], not only by regulating key and practical aspects of the autonomous cell response but also of pathways activated by recognition of PAMPs [132,133]. However, the ubiquitin signals in the context of infection are not fully understood.
The translation of the ubiquitin code through recognition of the ubiquitin-binding domain (UBD) drive degradative and non-degradative functions.
The functions of the two most abundant linkages in mammalian cells, K48-linked and K63-linked chains [128] are the best characterized. However, knowledge about the so-called "atypical" chains formed by connections through K6, K11, K27, K29, K33 and Met1, also involved in

the immune response is continuously improving [122]. K48, K11 and K29 poly-Ub chains and all heterotypic Ub chains which include K48 branched Ub chains, can signal for proteasome degradation [122,129], whereas K63 Ub chains are associated with lysosomal degradation [126,128,134], and K11 and M1 are involved in the critical step of NF-κB activation [122,135].

1.4.2.1. Ubiquitin-dependent antimicrobial autophagy

Ubiquitination regulates one of the most relevant cell autonomous mechanisms for the elimination of intracellular pathogens, namely selective autophagy or xenophagy. Ubiquitination is thus both implicated in autophagosome biogenesis, through modification of autophagy-inducing factors which act at different stages [129,132,136,137], as well as in the binding of the pathogen to the autophagosome for lysosomal degradation or for other unknown purpose.

Protein ubiquitination marks a pathogen for xenophagy-dependent degradation via recognition by the autophagy adapters - proteins that possess a ubiquitin binding domain (UBD) as well as an LC3-interacting region (LIR) motif – followed by cargo delivery to autophagy pathways [138].

Ubiquitination is involved in the elimination of many bacteria including *Mycobacterium tuberculosis*, *Listeria monocytogenes* [139,140] and *Chlamydia trachomatis* [141], but the best-studied example of xenophagy-dependent control is in *Salmonella* infection[142], which shares some aspects of the process with other vacuolar bacteria. Exposure of *Salmonella typhimurium* to the cytoplasm allows PAMP recognition, which immediately triggers assembly of different ubiquitin chains on the surface of cytosolic bacteria or within the damaged Salmonella-containing vacuole [93,132,139,142].

Autophagy receptors deliver the bacteria to the autophagy machinery to be ultimately degraded by lysosomes [138]. In addition to inducing autophagy, these associated ubiquitin chains lead to the activation of NF-Kß signalling and cytokine production [132].

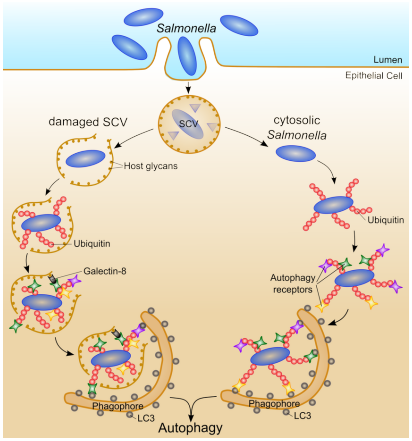

Figure 1. 7. Involvement of ubiquitin in Salmonella clearance

Following damage of *Salmonella*-containing vacuole, several host E3 ligases assemble poly-Ub chains on the surface of Salmonella, which are recognized by the p62, NDP52 and OPTN autophagy adapters that deliver the ubiquitinated *Salmonella* to maturing autophagosomes for degradation[143].

More recently ubiquitin has also been associated with clearance of *Toxoplasma gondii* [141]. Although not as detailed as the studies of ubiquitination in *Salmonella*, some reports have emerged suggesting that ubiquitin and autophagic components, such as LC3, GABARAP family proteins, p62 and NDP52 assemble around *T. gondii* PVs [131]. Notwithstanding the fact that ubiquitin is enriched in the PV of *T. gondii* in IFNγ-activated mouse cells, and the control of parasite infection depends on autophagy-proteins, control of *T. gondii* occurs through a mechanism independent of the formation of autophagosomes [144–146]. There is also the mysterious spontaneous activation and aggregation of effector IRG proteins in IFNγ-induced and infected or uninfected cells deficient in Atg5, Atg16L or Atg12, [75,113,147], behaviour reminiscent of

lack of IRG regulator proteins, but occuring in their presence, suggesting a role for these autophagic proteins in IRG protein function that has not been elucidated [109,113] (Khaminets thesis).

In human cells ubiquitination seems to mediate the elimination of the parasite by different mechanisms, either without the involvement of lysosomal fusion in HeLa cells [148,149], or with ubiquitin- and P62-dependent lysosomal fusion in HUVECs [149,150], and perhaps with recruitment of TRAF6, p62, LC3B and GABARAPs [104]. The different roles of ubiquitin in downstream signaling remain to be clarified. The same is true for the role that ubiquitin recruited to the *T. gondii* PV plays in the control of the parasite.

1.5. Toxoplasma effectors antagonists of host IFNγ- Inducible gene expression.

The success of the obligate intracellular parasite *T. gondii* is guaranteed by its survival of the immune response during acute infection and conversion of tachyzoites to bradyzoites and cysts, thus allowing the chronicity and transmissibility of the disease without killing the host. At the heart of this duality of interests – the parasite interested in being established in the host and the host's interest in elimination of the parasite - is the production of IFNγ. As described in detail earlier, IFNγ signaling leads to the induction of a set of ISGs via the JAK-STAT pathway, that mediate *T. gondii* elimination [151].

For example, IRGs and GBPs colonize and disrupt the PVM, leading to subsequent killing of the released parasite, resulting in the control of the rapid or acute phase of parasite propagation.

However, to counteract the immune system's response, *Toxoplasma* discharges a series of proteins during cell invasion that modulate a variety of host processes, including the expression and activity of GTPases [105,152,153].

Some of these virulence factors, such as ROP kinase family members like ROP5, ROP17, and ROP18 from certain so-called “virulent” strains of *T. gondii*, have been shown to block IRG- and GBP-dependent killing of the parasite in certain strains of mice including C57BL/6. In such strains, *T. gondii* ROP18 associates with the PVM [113,154–156] to phosphorylate conserved threonine residues of at least two effector IRG proteins, Irga6 and Irgb6 [157–160] preventing their oligomerization and interaction with the PVM and thus preventing PVM disruption and killing of the parasite [161]. The complete inactivation of GTPases is guaranteed by the joint action of ROP5/ROP18 proteins and the dense granule protein GRA7 complex [153,157]. Such mouse strains are highly vulnerable to virulent *T. gondii* strains, to the disadvantage of both mouse and parasite, since the early death of the host drastically reduces the probability of transmission of the parasite. The polymorphic virulence factors define different clonal lineages; type I parasites carry a combination of ROP5 and ROP18 alleles that confers high virulence in most laboratory mouse strains, while type II and III parasites carry different ROP allele combinations that allow long-term survival from infection in laboratory mice in laboratory mice [153].

Some wild-derived mouse strains incuding the *Mus musculus castaneus* mouse strain CIM from South India, and *Mus musculus musculus* strains PWD and PWK from the Czech Republic are able to survive infection with highly virulent Type I *Toxoplasma* strains due to the existence of a specific allele of the tandem IRG decoy protein Irgb1-b2, that is highly expressed and interacts directly with the ROP5/ROP18 kinase complex, preventing the phosphorylation of IRG effectors, and thus limiting parasite growth with subsequent survival of the infected animal [35] carrying infectious cysts in the brain favouring parasite transmission.

In addition, *T. gondii* infection has been shown to interfere with IFNγ-STAT1/STAT2 dependent gene expression, when *T. gondii* infects cells prior to encountering IFN [162–164]. The *Toxoplasma* secreted protein TgIST (inhibitor of STAT1-dependent transcription) was shown to block the STAT1 transcription factor in human and mouse cells [116] . The molecular mechanisms at the nucleus level, where STAT1 is affected, have been explored. TgIST is secreted into the host cytoplasm immediately after infection and traffics to the host cell nucleus by MYR [166,167] where it recruits the Mi-2/NuRD complex to the activated STAT1 and STAT2 to block the subsequent transcription of genes that are important for control of *Toxoplasma* infection, such as IRGs and GBPs, IRF1 and iNOS [165,168] and IDO1[169]. In this way, *T. gondii* tachyzoites proliferate freely in the impotent host cell [105]. This is presumably the situation when the parasite first enters a host. Within a day or two, however, IFNγ production will have been initiated. Later rounds of cellular infection by the parasite will therefore confront IFNγ-induced cells, IRG protein mediated resistance, resulting in subsequent differentiation to the non-virulent slow-replicating bradyzoite state and the formation of essentially silent brain and muscle cysts.

1.6. Thesis aims.

The recognition and destruction of the *T. gondii* PV is not well understood. In vitro experiments have demonstrated that the parasite confronts interferon-dependent resistant mechanisms orchestrated by IRGs and GBPs. At the single-cell level immediately after infection IRG proteins accumulate on the PVM and participate in its disruption leading to elimination of the parasite and necrotic death of the host cell [45,73,111,145]. It has been shown that both ubiquitin and components of an autophagic mechanism also assemble at the parasitophorous vacuole

and it has been suggested that GTPases are ubiquitinated on the PVM. Some parasites survive the interferon-dependent response initiated by IRGs and the mechanism behind this phenomenon is unknown.

We therefore aimed to investigate:

1. The factors that determine the dynamics of the IRG protein recruitment process onto the PVM, to understand if the host cell or the parasite itself determines the difference in IRG loading.

2. The role of ubiquitin in the resistance of *T.gondii, i.e.,* whether Ub is part of the IRG-mediated mechanism or not.

Bibliography

1. Howard, J. C. Introduction: cell-autonomous immunity. Microbes Infect. 9, 1633–1635 (2007).
2. Fitzgerald, K. A. & Kagan, J. C. Review Toll-like Receptors and the Control of Immunity. Cell 180, 1044–1066 (2020).
3. Akira, S., Uematsu, S. & Takeuchi, O. Pathogen recognition and innate immunity. Cell 124, 783–801 (2006).
4. Martinon, F. & Tschopp, J. NLRs join TLRs as innate sensors of pathogens. Trends Immunol. 26, 447–454 (2005).
5. Murphy, K., Travers, P. & Walport, M. Imunobiologia de Janeway (Livro Completo) (1). (2008).
6. Bautista-Hernández, L. A., Gómez-Olivares, J. L., Buentello-Volante, B. & Bautista-de Lucio, V. M. Fibroblasts: the unknown sentinels eliciting immune responses against microorganisms. Eur. J. Microbiol. Immunol. 7, 151–157 (2017).
7. Boyle, K. B. & Randow, F. The role of 'eat-me' signals and autophagy cargo receptors in innate immunity. Curr. Opin. Microbiol. 16, 339–348 (2013).
8. Borden, E. C. et al. Interferons at age 50: Past, current and future impact on biomedicine. Nat. Rev. Drug Discov. 6, 975–990 (2007).
9. Kalvakolanu, D. V., Nallar, S. C. & Kalakonda, S. Interferons: Cellular and molecular biology of their actions. Encyclopedia of Cancer (Elsevier Inc., 2018). doi:10.1016/B978-0-12-801238-3.96116-6
10. Macmicking, J. D. Interferon-inducible effector mechanisms in cell-autonomous immunity. Nat Rev Immunol 12, 367–382 (2014).

11. Platanias, L. C. Mechanisms of type-I- and type-II-interferon-mediated signalling. Nat. Rev. Immunol. 5, 375–386 (2005).

12. Vilcek, J. Novel Interferons. Nat. Immunol. 4, 8–9 (2003).

13. Kotenko, S. V. et al. IFN-λs mediate antiviral protection through a distinct class II cytokine receptor complex. Nat. Immunol. 4, 69–77 (2003).

14. Schneider, W. M., Chevillotte, M. D. & Rice, C. M. Interferon-stimulated genes: A complex web of host defenses. Annu. Rev. Immunol. 32, 513–545 (2014).

15. Ali, S. et al. Sources of type I interferons in infectious immunity: Plasmacytoid dendritic cells not always in the driver's seat. Front. Immunol. 10, (2019).

16. Lee, A. J. & Ashkar, A. A. The dual nature of type I and type II interferons. Front. Immunol. 9, 1–10 (2018).

17. Choi, J. et al. The Parasitophorous Vacuole Membrane of Toxoplasma gondii is Targeted for Disruption by Ubiquitin-like Conjugation Systems of Autophagy. Immunity. 40, 924–935 (2014).

18. Schroder, K., Hertzog, P. J., Ravasi, T. & Hume, D. A. Interferon-γ: an overview of signals, mechanisms and functions. J. Leukoc. Biol. 75, 163–189 (2004).

19. Wack, A., Terczyńska-Dyla, E. & Hartmann, R. Guarding the frontiers: The biology of type III interferons. Nat. Immunol. 16, 802–809 (2015).

20. Yin, Z. et al. Type III IFNs Are Produced by and Stimulate Human Plasmacytoid Dendritic Cells. J. Immunol. 189, 2735–2745 (2012).

21. Schoggins, J. W. Recent advances in antiviral interferon-

stimulated gene biology. F1000Research 7, 1–7 (2018).

22. Wells, A. I. & Coyne, C. B. Type III Interferons in Antiviral Defenses at Barrier Surfaces. Trends Immunol. 39, 848–858 (2018).

23. Stanifer, M. L., Pervolaraki, K. & Boulant, S. Differential regulation of type I and type III interferon signaling. Int. J. Mol. Sci. 20, 1–22 (2019).

24. Schoggins, J. W. Interferon-Stimulated Genes: What Do They All Do? Annu. Rev. Virol. 6, 567–584 (2019).

25. Der, S. D., Zhou, A., Williams, B. R. G. & Silverman, R. H. Identification of genes differentially regulated by interferon α, β, or γ using oligonucleotide arrays. Proc. Natl. Acad. Sci. U. S. A. 95, 15623–15628 (1998).

26. Boehm, U., Klamp, T., Groot, M. & Howard, J. C. CELLULAR RESPONSES TO INTERFERON-γ. 245–275 (1997). doi:10.1007/978-3-642-60445-4_9

27. Rusinova, I. et al. INTERFEROME v2.0: An updated database of annotated interferon-regulated genes. Nucleic Acids Res. 41, (2013).

28. Kerr, I. M. & Stark, G. R. The control of interferon-inducible gene expression. FEBS Lett. 285, 194–198 (1991).

29. Martens, S. & Howard, J. The interferon-inducible GTPases. Annu. Rev. Cell Dev. Biol. 22, 559–589 (2006).

30. Au-Yeung, N., Mandhana, R. & Horvath, C. M. Transcriptional regulation by STAT1 and STAT2 in the interferon JAK-STAT pathway. Jak-Stat 2, e23931 (2013).

31. Kim, B. H., Shenoy, A. R., Kumar, P., Bradfield, C. J. & MacMicking, J. D. IFN-inducible GTPases in host cell defense.

Cell Host Microbe 12, 432–444 (2012).

32. Praefcke, G. J. K. Regulation of innate immune functions by guanylate-binding proteins. Int. J. Med. Microbiol. 308, 237–245 (2018).

33. Kim, B. H. et al. Interferon-induced guanylate-binding proteins in inflammasome activation and host defense. Nat. Immunol. 17, 481–489 (2016).

34. Bekpen, C. et al. The interferon-inducible p47 (IRG) GTPases in vertebrates: loss of the cell autonomous resistance mechanism in the human lineage. Genome Biol. 6, R92 (2005).

35. Lilue, J., Müller, U. B., Steinfeldt, T. & Howard, J. C. Reciprocal virulence and resistance polymorphism in the relationship between Toxoplasma gondii and the house mouse. Elife 2013, 1–21 (2013).

36. Könen-Waisman, S. & Howard, J. C. Cell-autonomous immunity to Toxoplasma gondii in mouse and man. Microbes Infect. 9, 1652–1661 (2007).

37. Bekpen, C. et al. Death and resurrection of the human IRGM gene. PLoS Genet. 5, (2009).

38. Bekpen, C. et al. The interferon-inducible p47 (IRG) GTPases in vertebrates: loss of the cell autonomous resistance mechanism in the human lineage. Genome Biol. 6, 1–18 (2005).

39. Lilue, J., Müller, U. B., Steinfeldt, T. & Howard, J. C. Reciprocal virulence and resistance polymorphism in the relationship between Toxoplasma gondii and the house mouse. Elife 2013, 1–21 (2013).

40. Taylor, G. A. et al. The inducibly expressed GTPase localizes to the endoplasmic reticulum, independently of GTP binding. J. Biol. Chem. 272, 10639–10645 (1997).

41. Uthaiah, R. C., Praefcke, G. J. K., Howard, J. C. & Herrmann, C. IIGP1, an interferon-g-inducible 47-kDa GTPase of the mouse, showing cooperative enzymatic activity and GTP-dependent multimerization. J. Biol. Chem. 278, 29336–29343 (2003).

42. Pawlowski, N. et al. The activation mechanism of Irga6, an interferon-inducible GTPase contributing to mouse resistance against Toxoplasma gondii. BMC Biol. 9, (2011).

43. Ghosh, A., Uthaiah, R., Howard, J., Herrmann, C. & Wolf, E. Crystal structure of IIGP1: A paradigm for interferon-inducible p47 resistance GTPases. Mol. Cell 15, 727–739 (2004).

44. Uthaiah, R. C., Praefcke, G. J. K., Howard, J. C. & Herrmann, C. IIGP1, an interferon-γ-inducible 47-kDa GTPase of the mouse, showing cooperative enzymatic activity and GTP-dependent multimerization. J. Biol. Chem. 278, 29336–29343 (2003).

45. Martens, S. et al. Disruption of Toxoplasma gondii parasitophorous vacuoles by the mouse p47-resistance GTPases. PLoS Pathog. 1, 0187–0201 (2005).

46. Papic, N., Hunn, J. P., Pawlowski, N., Zerrahn, J. & Howard, J. C. Inactive and active states of the interferon-inducible resistance GTPase, Irga6, in vivo. J. Biol. Chem. 283, 32143–51 (2008).

47. Zhao, Y. O., Könen-Waisman, S., Taylor, G. A., Martens, S. & Howard, J. C. Localisation and mislocalisation of the interferon-inducible immunity-related GTPase, Irgm1 (LRG-47) in mouse cells. PLoS One 5, (2010).

48. Martens, S. et al. Mechanisms regulating the positioning of mouse p47 resistance GTPases LRG-47 and IIGP1 on cellular membranes: retargeting to plasma membrane induced by phagocytosis. J. Immunol. 173, 2594–2606 (2004).

49. Butcher, B. A. et al. p47 GTPases Regulate Toxoplasma gondii Survival in Activated Macrophages. Infect. Immun. 73, 3278–3286 (2005).

50. Tiwari, S., Choi, H. P., Matsuzawa, T., Pypaert, M. & MacMicking, J. D. Targeting of the GTPase Irgm1 to the phagosomal membrane via PtdIns(3,4)P2 and PtdIns(3,4,5)P3 promotes immunity to mycobacteria. Nat. Immunol. 10, 907–917 (2009).

51. Springer, H. M., Schramm, M., Taylor, G. a & Howard, J. C. Irgm1 (LRG-47), a regulator of cell-autonomous immunity, does not localize to mycobacterial or listerial phagosomes in IFN-γ-induced mouse cells. J. Immunol. 191, 1765–74 (2013).

52. Bougnères, L. et al. A Role for Lipid Bodies in the Cross-presentation of Phagocytosed Antigens by MHC Class I in Dendritic Cells. Immunity 31, 232–244 (2009).

53. Haldar, A. K. et al. IRG and GBP Host Resistance Factors Target Aberrant, 'Non-self' Vacuoles Characterized by the Missing of 'Self' IRGM Proteins. PLoS Pathog. 9, (2013).

54. Hunn, J. P. et al. Regulatory interactions between IRG resistance GTPases in the cellular response to Toxoplasma gondii. EMBO J. 27, 2495–2509 (2008).

55. Taylor, G. a. et al. The inducibly expressed GTPase localizes to the endoplasmic reticulum, independently of GTP binding. J. Biol. Chem. 272, 10639–10645 (1997).

56. Coers, J. et al. Chlamydia muridarum Evades Growth Restriction by the IFN-γ-Inducible Host Resistance Factor Irgb10 . J. Immunol. 180, 6237–6245 (2008).

57. Zerrahn, J., Schaible, U. E., Brinkmann, V., Guhlich, U. & Kaufmann, S. H. E. The IFN-Inducible Golgi- and Endoplasmic

Reticulum- Associated 47-kDa GTPase IIGP Is Transiently Expressed During Listeriosis. J. Immunol. 168, 3428–3436 (2002).

58. Taylor, G. A. et al. Pathogen-specific loss of host resistance in mice lacking the IFN-gamma-inducible gene IGTP. Proc. Natl. Acad. Sci. U. S. A. 97, 751–755 (2000).

59. Collazo, C. M. et al. Inactivation of LRG-47 and IRG-47 reveals a family of interferon gamma-inducible genes with essential, pathogen-specific roles in resistance to infection. J. Exp. Med. 194, 181–188 (2001).

60. da Fonseca Ferreira-da-Silva, M., Springer-Frauenhoff, H. M., Bohne, W. & Howard, J. C. Identification of the Microsporidian Encephalitozoon cuniculi as a New Target of the IFN??-Inducible IRG Resistance System. PLoS Pathog. 10, (2014).

61. Feng, C. G. et al. Mice Deficient in LRG-47 Display Increased Susceptibility to Mycobacterial Infection Associated with the Induction of Lymphopenia. J. Immunol. 172, 1163–1168 (2004).

62. MacMicking, J. D., Taylor, G. A. & McKinney, J. D. Immune Control of Tuberculosis by IFN-γ-inducible LRG-47. Science (80-.). 302, 654–659 (2003).

63. Santiago, H. C. et al. Mice Deficient in LRG-47 Display Enhanced Susceptibility to Trypanosoma cruzi Infection Associated with Defective Hemopoiesis and Intracellular Control of Parasite Growth . J. Immunol. 175, 8165–8172 (2005).

64. Taylor, G. A., Feng, C. G. & Sher, A. p47 GTPases: regulators of immunity to intracellular pathogens. Nat. Rev. Immunol. 4, 100–109 (2004).

65. Bernstein-Hanley, I. et al. The p47 GTPases Igtp and Irgb10 map to the Chlamydia trachomatis susceptibility locus Ctrq-3 and

mediate cellular resistance in mice. Proc. Natl. Acad. Sci. U. S. A. 103, 14092–14097 (2006).

66. Man, S. M. et al. IRGB10 Liberates Bacterial Ligands for Sensing by the AIM2 and Caspase-11-NLRP3 Inflammasomes. Cell 167, 382-396.e17 (2016).

67. Lee, Y. et al. Initial phospholipid-dependent Irgb6 targeting to Toxoplasma gondii vacuoles mediates host defense. Life Sci. alliance 3, 1–16 (2020).

68. Feng, C. G. et al. The immunity-related GTPase Irgm1 promotes the expansion of activated CD4 + T cell populations by preventing interferon- c -induced cell death. 9, 1279–1287 (2008).

69. Henry, S. C. et al. Impaired Macrophage Function Underscores Susceptibility to Salmonella in Mice Lacking Irgm1 (LRG-47) . J. Immunol. 179, 6963–6972 (2007).

70. Liesenfeld, O. et al. The IFN-γ-inducible GTPase, irga6, protects mice against toxoplasma gondii but not against plasmodium berghei and some other intracellular pathogens. PLoS One 6, (2011).

71. Henry, S. C. et al. Balance of Irgm protein activities determines IFN-gamma-induced host defense. J. Leukoc. Biol. 85, (2009).

72. Coers, J. et al. Compensatory T cell responses in IRG-deficient mice prevent sustained Chlamydia trachomatis infections. PLoS Pathog. 7, (2011).

73. Ling, Y. M. et al. Vacuolar and plasma membrane stripping and autophagic elimination of Toxoplasma gondii in primed effector macrophages. J. Exp. Med. 203, 2063–2071 (2006).

74. Khaminets, A. et al. Coordinated loading of IRG resistance GTPases on to the Toxoplasma gondii parasitophorous vacuole.

Cell. Microbiol. 12, 939–961 (2010).

75. Haldar, A. K., Piro, A. S., Pilla, D. M., Yamamoto, M. & Coers, J. The E2-like conjugation enzyme Atg3 promotes binding of IRG and Gbp proteins to Chlamydia- and Toxoplasma- containing vacuoles and host resistance. PLoS One 9, (2014).

76. Degrandi, D. et al. Extensive Characterization of IFN-Induced GTPases mGBP1 to mGBP10 Involved in Host Defense. J. Immunol. 179, 7729–7740 (2007).

77. Kresse, A. et al. Analyses of murine GBP homology clusters based on in silico, in vitro and in vivo studies. BMC Genomics 9, 1–12 (2008).

78. Olszewski, M. A., Gray, J. & Vestal, D. J. In silico genomic analysis of the human and murine guanylate-binding protein (gbp) gene clusters. J. Interf. Cytokine Res. 26, 328–352 (2006).

79. Cheng, Y. S. E., Colonno, R. J. & Yin, F. H. Interferon induction of fibroblast proteins with guanylate binding activity. J. Biol. Chem. 258, 7746–7750 (1983).

80. Ghosh, A., Praefcke, G. J. K., Renault, L., Wittinghofer, A. & Herrmann, C. How guanylate-binding proteins achieve assembly-stimulated processive cleavage of GTP to GMP. Nature 440, 101–104 (2006).

81. Britzen-Laurent, N. et al. Intracellular trafficking of guanylate-binding proteins is regulated by heterodimerization in a hierarchical manner. PLoS One 5, (2010).

82. Kravets, E. et al. Guanylate binding proteins directly attack Toxoplasma gondii via supramolecular complexes. Elife 5, (2016).

83. Degrandi, D. et al. Murine Guanylate Binding Protein 2 (mGBP2) controls Toxoplasma gondii replication. Proc. Natl. Acad. Sci. U.

S. A. 110, 294–299 (2013).

84. Vestal, D. J., Gorbacheva, V. Y. & Sen, G. C. Different subcellular localizations for the related interferon-induced GTPases, MuGBP-1 and MuGBP-2: Implications for different functions? J. Interf. Cytokine Res. 20, 991–1000 (2000).

85. Modiano, N., Lu, Y. E. & Cresswell, P. Golgi targeting of human guanylate-binding protein-1 requires nucleotide binding, isoprenylation, and an IFN-γ-inducible cofactor. Proc. Natl. Acad. Sci. U. S. A. 102, 8680–8685 (2005).

86. Tretina, K., Park, E. S., Maminska, A. & MacMicking, J. D. Interferon-induced guanylate-binding proteins: Guardians of host defense in health and disease. J. Exp. Med. 216, 482–500 (2019).

87. Pilla-Moffett, D., Barber, M. F., Taylor, G. A. & Coers, J. Interferon-Inducible GTPases in Host Resistance, Inflammation and Disease. Journal of Molecular Biology 428, 3495–3513 (2016).

88. Shenoy, A. R. et al. GBP5 Promotes NLRP3 inflammasome assembly and immunity in mammals. Science (80-.). 336, 481–485 (2012).

89. Wallet, P. et al. IFN-γ extends the immune functions of Guanylate Binding Proteins to inflammasome-independent antibacterial activities during Francisella novicida infection. PLoS Pathog. 13, 1–26 (2017).

90. Kim, B. H. et al. A family of IFN-γ-inducible 65-kD GTPases protects against bacterial infection. ERS Monogr. 332, 717–721 (2011).

91. Lindenberg, V. et al. Broad recruitment of mGBP family members to Chlamydia trachomatis inclusions. PLoS One 12, 1–

14 (2017).

92. Meunier, E. & Broz, P. Interferon-inducible GTPases in cell autonomous and innate immunity. Cell. Microbiol. 18, 168–180 (2016).

93. Blader, I. J., Coleman, B. I., Chen, C.-T. & Gubbels, M.-J. Lytic Cycle of Toxoplasma gondii : 15 Years Later . Annu. Rev. Microbiol. 69, (2015).

94. Keats Shwab, E. et al. Human impact on the diversity and virulence of the ubiquitous zoonotic parasite Toxoplasma gondii. Proc. Natl. Acad. Sci. U. S. A. 115, E6956–E6963 (2018).

95. Dubey, J. P. History of the discovery of the life cycle of Toxoplasma gondii. Int. J. Parasitol. 39, 877–882 (2009).

96. Attias, M. et al. The life-cycle of Toxoplasma gondii reviewed using animations. Parasites and Vectors 13, 1–13 (2020).

97. Rastogi, S., Cygan, A. M. & Boothroyd, J. C. ScienceDirect Translocation of effector proteins into host cells by Toxoplasma gondii. Curr. Opin. Microbiol. 52, 130–138 (2019).

98. Drew, D. R. et al. Functional Conservation of the AMA1 Host-Cell Invasion Ligand between P. falciparum and P. vivax: A Novel Platform to Accelerate Vaccine and Drug Development. J. Infect. Dis. 217, 498–503 (2018).

99. Panas, M. W. & Boothroyd, J. C. Seizing control: How dense granule effector proteins enable Toxoplasma to take charge. Mol. Microbiol. 115, 466–477 (2021).

100. Mordue, D. G., Desai, N., Dustin, M. & Sibley, L. D. Proteins on the Basis of Their Membrane Anchoring. J. Exp. Med 190, 1783–1792 (1999).

101. Charron, A. J. & Sibley, L. D. Molecular Partitioning during Host

Cell Penetration by Toxoplasma gondii. Traffic (2004).

102. Suss-Toby, E., Zimmerberg, J. & Ward, G. E. Toxoplasma invasion: The parasitophorous vacuole is formed from host cell plasma membrane and pinches off via a fission pore. Proc. Natl. Acad. Sci. U. S. A. 93, 8413–8418 (1996).

103. Gold, D. A. et al. The Toxoplasma dense granule proteins GRA17 and GRA23 mediate the movement of small molecules between the host and the parasitophorous vacuole. Cell Host Microbe 17, 642–652 (2015).

104. Mukhopadhyay, D., Sangaré, L. O., Braun, L., Hakimi, M. & Saeij, J. P. Toxoplasma GRA 15 limits parasite growth in IFN γ activated fibroblasts through TRAF ubiquitin ligases . EMBO J. (2020). doi:10.15252/embj.2019103758

105. Hakimi, M. A., Olias, P. & Sibley, L. D. Toxoplasma effectors targeting host signaling and transcription. Clinical Microbiology Reviews 30, (2017).

106. Rosenberg, A. & Sibley, L. D. Toxoplasma gondii secreted effectors co-opt host repressor complexes to inhibit necroptosis. Cell Host Microbe 1–13 (2021). doi:10.1016/j.chom.2021.04.016

107. Black, M. W. & Boothroyd, J. C. Lytic Cycle of Toxoplasma gondii . Microbiol. Mol. Biol. Rev. 64, 607–623 (2000).

108. Halonen, S. K. et al. Gamma Interferon-Induced Inhibition of. Society 69, 5573–5576 (2001).

109. Traver, M. K. et al. Immunity-related GTPase M (IRGM) proteins influence the localization of guanylate-binding protein 2 (GBP2) by modulating macroautophagy. J. Biol. Chem. 286, (2011).

110. Maric-Biresev, J. et al. Loss of the interferon-γ-inducible regulatory immunity-related GTPase (IRG), Irgm1, causes activation of effector IRG proteins on lysosomes, damaging

lysosomal function and predicting the dramatic susceptibility of Irgm1-deficient mice to infection. BMC Biol. 14, 1–20 (2016).

111. Zhao, Y. O., Khaminets, A., Hunn, J. P. & Howard, J. C. Disruption of the Toxoplasma gondii parasitophorous vacuole by IFNg-inducible immunity-related GTPases (IRG proteins) triggers necrotic cell death. PLoS Pathog. 5, (2009).

112. Howard, J. C., Hunn, J. P. & Steinfeldt, T. The IRG protein-based resistance mechanism in mice and its relation to virulence in Toxoplasma gondii. Curr. Opin. Microbiol. 14, 414–421 (2011).

113. Selleck, E. M. et al. Guanylate-binding Protein 1 (Gbp1) Contributes to Cell-autonomous Immunity against Toxoplasma gondii. PLoS Pathog. 9, (2013).

114. Yamamoto, M. et al. A cluster of interferon-γ-inducible p65 gtpases plays a critical role in host defense against toxoplasma gondii. Immunity 37, 302–313 (2012).

115. Steffens, N. et al. Essential Role of mGBP7 for Survival of Toxoplasma gondii Infection. Biol. Host-microbe 11, 1–14 (2020).

116. Darnell, J. E., Kerr, I. M. & Stark, G. R. Jak-STAT Pathways and Transcriptional Activation in Response to IFNs and Other Extracellular Signaling Proteins. Adv. Sci. 264, 1415–1421 (1994).

117. Johnston, A. C. et al. Human GBP1 does not localize to pathogen vacuoles but restricts Toxoplasma gondii. Cell. Microbiol. 18, 1056–1064 (2016).

118. Fisch, D. et al. Human GBP1 Differentially Targets Salmonella and Toxoplasma to License Recognition of Microbial Ligands and Caspase-Mediated Death. SSRN Electron. J. 1–28 (2020). doi:10.2139/ssrn.3593524

119. Fisch, D. et al. Human GBP 1 is a microbe□specific gatekeeper

of macrophage apoptosis and pyroptosis . EMBO J. 38, 1–19 (2019).

120. Kutsch, M. et al. Direct binding of polymeric GBP 1 to LPS disrupts bacterial cell envelope functions. 1–22 (2020). doi:10.15252/embj.2020104926

121. Swatek, K. N. & Komander, D. Ubiquitin modifications. Cell Res. 26, 399–422 (2016).

122. Vozandychova, V., Stojkova, P., Hercik, K., Rehulka, P. & Stulik, J. The ubiquitination system within bacterial host-pathogen interactions. Microorganisms 9, 1–22 (2021).

123. Kulathu, Y. & Komander, D. Atypical ubiquitylation-the unexplored world of polyubiquitin beyond Lys48 and Lys63 linkages. Nat. Rev. Mol. Cell Biol. 13, 508–523 (2012).

124. Ye, Y. & Rape, M. Building ubiquitin chains: E2 enzymes at work. Nat. Rev. Mol. Cell Biol. 10, 755–764 (2009).

125. Buetow, L. & Huang, D. T. Structural insights into the catalysis and regulation of E3 ubiquitin ligases. Nat. Rev. Mol. Cell Biol. 17, 626–642 (2016).

126. Husnjak, K. & Dikic, I. Ubiquitin-binding proteins: Decoders of ubiquitin-mediated cellular functions. Annu. Rev. Biochem. 81, 291–322 (2012).

127. Jiang, X. Mechanism of Ubiquitin Induced Activation of Rig-I Like Receptors in Antiviral Innate Immunity Approved By Supervisory Committee. (2012).

128. Komander, D. & Rape, M. The ubiquitin code. Annu. Rev. Biochem. 81, 203–229 (2012).

129. Li, J., Chai, Q. Y. & Liu, C. H. The ubiquitin system: A critical regulator of innate immunity and pathogen-host interactions.

Cell. Mol. Immunol. 13, 560–576 (2016).

130. Yau, R. & Rape, M. The increasing complexity of the ubiquitin code. Nat. Cell Biol. 18, 579–586 (2016).

131. Haldar, A. K. et al. Ubiquitin systems mark pathogen-containing vacuoles as targets for host defense by guanylate binding proteins. Proc. Natl. Acad. Sci. U. S. A. 112, E5628–E5637 (2015).

132. Grumati, P. & Dikic, I. Ubiquitin signaling and autophagy. J. Biol. Chem. 293, 5404–5413 (2018).

133. Hu, H. & Sun, S. C. Ubiquitin signaling in immune responses. Cell Res. 26, 457–483 (2016).

134. Duncan, L. M. et al. Lysine-63-linked ubiquitination is required for endolysosomal degradation of class I molecules. EMBO J. 25, 1635–1645 (2006).

135. Wijk, S. J. L. Van et al. Linear ubiquitination of cytosolic Salmonella bacterial proliferation. 17066, (2017).

136. Chen, R. H., Chen, Y. H. & Huang, T. Y. Ubiquitin-mediated regulation of autophagy. J. Biomed. Sci. 26, 1–12 (2019).

137. Morishita, H. & Mizushima, N. Diverse cellular roles of autophagy. Annu. Rev. Cell Dev. Biol. 35, 453–475 (2019).

138. Gomes, L. C. & Dikic, I. Autophagy in antimicrobial immunity. Mol. Cell 54, 224–233 (2014).

139. Wang, L., Yan, J., Niu, H., Huang, R. & Wu, S. Autophagy and ubiquitination in Salmonella infection and the related inflammatory responses. Front. Cell. Infect. Microbiol. 8, 1–14 (2018).

140. Sharma, V., Verma, S., Seranova, E., Sarkar, S. & Kumar, D. Selective autophagy and xenophagy in infection and disease.

Front. Cell Dev. Biol. 6, 1–17 (2018).

141. Haldar, A. K. et al. Chlamydia trachomatis is resistant to inclusion ubiquitination and associated host defense in gamma interferon-primed human epithelial cells. MBio 7, 1–12 (2016).

142. Thurston, T. L. M. The tbk1 adaptor and autophagy receptor ndp52 restricts the proliferation of ubiquitin-coated bacteria. Nat. Immunol. 10, 1215–1222 (2009).

143. Scheidel, J., Amstein, L., Ackermann, J., Dikic, I. & Koch, I. In Silico Knockout Studies of Xenophagic Capturing of Salmonella. PLoS Comput. Biol. 12, 1–18 (2016).

144. Ohshima, J. et al. Role of Mouse and Human Autophagy Proteins in IFN-γ–Induced Cell-Autonomous Responses against Toxoplasma gondii . J. Immunol. 192, 3328–3335 (2014).

145. Zhao, Z. et al. Autophagosome-Independent Essential Function for the Autophagy Protein Atg5 in Cellular Immunity to Intracellular Pathogens. Cell Host Microbe 4, 458–469 (2008).

146. Park, S. et al. Targeting by AutophaGy proteins (TAG): Targeting of IFNG-inducible GTPases to membranes by the LC3 conjugation system of autophagy. Autophagy 12, 1153–1167 (2016).

147. Choi, J. et al. The parasitophorous vacuole membrane of toxoplasma gondii is targeted for disruption by ubiquitin-like conjugation systems of autophagy. Immunity 40, 924–935 (2014).

148. Selleck, E. M. et al. A Noncanonical Autophagy Pathway Restricts. MBio 6, 1–14 (2015).

149. Clough, B. et al. K63-Linked Ubiquitination Targets Toxoplasma gondii for Endo-lysosomal Destruction in IFNγ-Stimulated Human Cells. PLoS Pathog. 12, (2016).

150. Subauste, C. S. Interplay between toxoplasma gondii, autophagy, and autophagy proteins. Front. Cell. Infect. Microbiol. 9, 1–11 (2019).

151. MacMicking, J. D. Interferon-inducible effector mechanisms in cell-autonomous immunity. Nat. Rev. Immunol. 12, 367–382 (2012).

152. Zhu, W., Li, J., Pappoe, F., Shen, J. & Yu, L. Strategies developed by toxoplasma gondii to survive in the host. Front. Microbiol. 10, (2019).

153. Ihara, F. & Nishikawa, Y. Toxoplasma gondii manipulates host cell signaling pathways via its secreted effector molecules. Parasitol. Int. 83, 102368 (2021).

154. Etheridge, R. D. et al. The Toxoplasma pseudokinase ROP5 forms complexes with ROP18 and ROP17 kinases that synergize to control acute virulence in mice. Cell Host Microbe 15, 537–550 (2014).

155. Taylor, S. et al. A secreted serine-threonine kinase determines virulence in the eukaryotic pathogen Toxoplasma gondii. Science (80-.). 314, 1776–1780 (2006).

156. Kim, E. W. et al. The Rhoptry Pseudokinase ROP54 Modulates Toxoplasma gondii Virulence and Host GBP2 Loading . mSphere 1, (2016).

157. Hermanns, T., Müller, U. B., Könen-Waisman, S., Howard, J. C. & Steinfeldt, T. The Toxoplasma gondii rhoptry protein ROP18 is an Irga6-specific kinase and regulated by the dense granule protein GRA7. Cell. Microbiol. 18, 244–259 (2016).

158. Fentress, S. J. et al. Phosphorylation of immunity-related GTPases by a toxoplasma gondii-secreted kinase promotes macrophage survival and virulence. Cell Host Microbe 8, 484–

495 (2010).

159. Niedelman, W. et al. The rhoptry proteins ROP18 and ROP5 mediate Toxoplasma gondii evasion of the murine, but not the human, interferon-gamma response. PLoS Pathog. 8, (2012).

160. Steinfeldt, T. et al. Phosphorylation of mouse immunity-related gtpase (IRG) resistance proteins is an evasion strategy for virulent Toxoplasma gondii. PLoS Biol. 8, (2010).

161. Steinfeldt, T. et al. Phosphorylation of mouse immunity-related gtpase (IRG) resistance proteins is an evasion strategy for virulent Toxoplasma gondii. PLoS Biol. 8, (2010).

162. Matta, S. K. et al. Toxoplasma gondii effector TgIST blocks type I interferon signaling to promote infection. Proc. Natl. Acad. Sci. U. S. A. 116, 17480–17491 (2019).

163. Rosowski, E. E., Nguyen, Q. P., Camejo, A., Spooner, E. & Saeija, J. P. J. Toxoplasma gondii inhibits gamma interferon (IFN-γ)-and IFN-β-induced host cell STAT1 transcriptional activity by increasing the association of STAT1 with DNA. Infect. Immun. 82, 706–719 (2014).

164. Kim, S.-K., Fouts, A. E. & Boothroyd, J. C. Toxoplasma gondii Dysregulates IFNy Inducible Gene Expression in Human Fibroblasts. J. Immunol. (2007).

165. Gay, G. et al. Toxoplasma gondii TgIST co-opts host chromatin repressors dampening STAT1-dependent gene regulation and IFN-γ-mediated host defenses. J. Exp. Med. 213, 1779–1798 (2016).

166. Wang, Y., Sangaré, L. O., Paredes-Santos, T. C. & Saeij, J. P. J. Toxoplasma Mechanisms for Delivery of Proteins and Uptake of Nutrients across the Host-Pathogen Interface. Annu. Rev. Microbiol. 74, 567–586 (2020).

167. Panas, M. W. & Boothroyd, J. C. Seizing control: How dense granule effector proteins enable Toxoplasma to take charge. Molecular Microbiology 115, 466–477 (2021).

168. Olias, P., Etheridge, R. D., Zhang, Y., Holtzman, M. J. & Sibley, L. D. Toxoplasma Effector Recruits the Mi-2/NuRD Complex to Repress STAT1 Transcription and Block IFN-γ-Dependent Gene Expression. Cell Host Microbe 20, 72–82 (2016).

169. Bando, H. et al. Toxoplasma effector TgIST targets host IDO1 to antagonize the IFN-γ-induced anti-parasitic response in human cells. Front. Immunol. 9, 1–14 (2018).

Chapter 2

---

2. Mechanisms of IFNγ-inducible GTPases in the cell-autonomous early response against *Toxoplasma gondii*.

Ana Rodrigues[1] Claudia Campos[1] and Jonathan C. Howard[1, 2]

[1]Fundação Calouste Gulbenkian, Instituto Gulbenkian de Ciência, 2780- 156 Oeiras, Portugal,

[2] Institute for Genetics, University of Cologne, 50674 Cologne, Germany

Author contributions

AR - Study concept and design; Cell culture; Infection experiments; Microscopy and image analyses; Protein quantification; Flow cytometry experiments Statistical analysis; Drafting and editing the manuscript.
CC - Parasite propagation; Irgb6 deletion, Infection experiments;
JCH - Study concept and design; Supervision of execution; Editing of the manuscript.

2.1. Abstract

The first events of control of the *Toxoplasma gondii* parasite in mice are characterized by the confrontation of parasite-containing vacuoles by the IFNγ-dependent resistance mechanism based on a family of large GTPases, the IRG proteins.

IRG proteins, expressed via the STAT1 pathway, assemble on the Parasitophorous Vacuole Membrane (PVM) in a cooperative manner, and by an unknown mechanism induce rupture of the vacuolar membrane. The parasite, now exposed to the cytosol, dies shortly afterwards. A small proportion of infecting parasites are not targeted by IRG proteins and survive immune attack. What determines whether PVs are covered by IRGs or not is completely unknown.

We show that the attack on the PVM by IRGs starts early after the invasion of the parasite and reaches a plateau at 1 h, leaving about 10 to 20% uncovered PVs. The accumulation of IRGs is quantitatively very heterogeneous. The heterogeneity of IRG recruitment is only partially dependent on availability in the cytoplasm, but also probably dependent on other unknown factor(s) associated with individual vacuoles. TgIST is not the only parasite-derived factor that can inhibit the IFNg and STAT1-induced expression of IRG. Such factors reduce the cytosolic availability of IRG, which impacts on their recruitment to the PVM.

The absence of Irgb6 does not affect generally the loading of the other IRG members, throwing doubt on the definition of Irgb6 as a “pioneer”. The behavior of the IRG protein complex in cell autonomous resistance to *T. gondii* remains unclear.

Keywords: Parasitophorous Vacuole Membrane (PVM), IRG loading, *toxoplasma*

2.2. Introduction

IFNγ is the main cytokine orchestrating resistance to the obligate intracellular parasite *Toxoplasma gondii*. During toxoplasmosis, IFNγ is produced by lymphocytes and natural killer cells (NK) and regulates more than 10000 known genes [1–4]. IFNγ uses the JAK / STAT1 signalling pathway through phosphorylation and translocation of STAT1 to the nucleus to initiate transcription of IFNγ responsive genes [5,6] to which belong the IFN-inducible GTPases[7], such as p47 immunity-related GTPases (IRGs) [8] and the guanylate-binding proteins (GBPs) [9].
In mice, IRGs and GBPs are the main early cell-autonomous resistance mechanism to *T. gondii* [10,11] and to some other pathogens [12] such as *Chlamydia trachomatis* [13,14], Encephalitozoon *cuniculi*[15] and murine norovirus [16].
The IRG protein family in mice is composed of the catalytically active, GKS GTPase subfamily which possesses the conserved GX4GKS sequence in the P-loop of the first nucleotide-binding motif (G1) and the GMS regulator subfamily which instead contain a non-canonical P-loop sequence GX4GMS [7,17]. The catalytic activity of the GMS sub-family is not definitely known.

In IFNγ induced cells the GKS proteins are diffused in the cytoplasm and maintained in GDP-bound state while the GMS proteins are bound to specific endomembrane systems (Irgm1, Golgi and endolysosomal system, lipid droplets; Irgm2, Golgi; Irgm3, ER and lipid droplets), [18–22]. The GKS proteins or effectors transition from GDP-bound to GTP to target the PVM [23], while the GMS or IRGM proteins (Irgm1, Irgm2 and Irgm3) negatively regulate the GKS proteins to maintain the GDP-bound state and prevent their activation on normal intracellular membranes[17,24]. GBPs can form multimers and some are modified by

C-terminal isoprenylation of the CaaX-box motif that facilitates interaction with endomembranes and *T. gondii* PVs and parasite membranes [9,25–30].

In IFNγ-induced, *Toxoplasma*-infected murine cells the effector IRG proteins (Irga6, Irgb6, Irgb10 and Irgd) accumulate on the PVM [18,26,31,32] and so do proteins involved in autophagy [33], ubiquitin machinery components [34,35] and GBPs [26,28,36], leading to its "ruffling and vesiculation" followed by disruption, then culminating in damage of the parasite's intracellular niche [37–39]. Exposed to the cytoplasm, the parasite dies and eventually, the host cell undergoes necrotic cell death [39]. The mechanisms by which parasite and host cell death occur are not well understood.

The virulent strains of *T. gondii* use ROP5 and ROP18 to block the deposition of GKS proteins on their PVMs, through targeted phosphorylation of the nucleotide-binding domain [40,41].

T. gondii has the ability to interfere with the expression of IFN-responsive genes. If *T. gondii* enters a cell that is not induced with IFNγ, subsequent induction of resistance by IFNγ is inhibited [42,43].

Although IRGs have been intensively studied and much data has established the importance of GTPase recruitment to PVs in the control of *T.gondii*, it is not known how the IRGs select PVs for destruction and elimination. Here we explore IRG recruitment to the PVM to understand what factors determine the selection of particular PVs to be covered by the IRGs and thus eliminated, or not covered by the IRG and to persist in the cell. We ask whether these are parasite-derived or cell intrinsic factors.

2.3. Material and Methods

2.3.1. Material

2.3.1.1. Mammalian cells and media

Mouse embryonic fibroblasts (MEFs) and diaphragm-derived cells DDCs from C57/BL6 were cultured in Dulbecco's modified Eagle's medium (DMEM), high glucose w/o L-glutamine w/o sodium pyruvate (DMEM) supplemented with 10% heat-inactivated fetal bovine serum or HI-FBS, 2mM L-glutamine, 1mM sodium pyruvate, 1x non-essential amino acids, and 1x penicillin/streptomycin. Human Foreskin fibroblasts (Hs27) obtained from ATCC were maintained in Iscove's Modified Dulbecco's medium, high glucose (IMDM) supplemented with 5% heat-inactivated fetal bovine serum, 2mM L-glutamine, 1mM sodium pyruvate and 1x non-essential amino acids without antibiotic.

For experiments with immortalized MEFs, MEFs were prepared from mice at day 12-14 post coitum and immortalized with DNA: pSV3-neo plasmid using FuGENE 6 [44] or Screenfect A.

Immortalized MEFs were also prepared from a new C57BL/6 mouse strain in which both isomorphs of Irgb6 were removed by CrispR-Cas9 (Claudia Campos, unpublished results)

MEFs were used in the following conditions:

1. For microscopy experiments:

- 20000 cells/well plated on 13mm coverglass into 24 well plates
- 20000 cells/well plated on Lab-TekII chamber slide 4 well
- 10000 cells/well plated on Lab-TekII chamber slide 8 well

2. For Western blot experiments:

- 250000 cells/well plated on i6 well plates

For *T. gondii* maintenance Hs27 (ATCC (CRL-1634)) were used.

2.3.1.2. Toxoplasma gondii strains

All the experiments were performed using the type II Me49[45], PRUku80, PRUku80ΔIST, PRUku80ΔIST+IST-HA [46] (kind gifts from Dr. Hakimi) and type I RH [47] *T. gondii* strains.

2.3.1.3. Primary Imunoreagents:

Rat monoclonal anti-GRA7 (2.1.2) used at 1/500, rabbit serum anti-Irga6 (165/4) used at 1/4000, rabbit serum anti-Irgb6 (141/3) used at 1/2000, rabbit serum anti-Irgb10 (940/6) used at 1/2000, rabbit serum anti-Irgd (081/3) used at 1/3000, rabbit serum anti-Irgb1 (954/1) used at 1/4000, mouse monoclonals anti-Irga6 (10D7 /1000)) used at 1/1000, mouse monoclonal anti-Irgb6 (B34)[48] used at 1/2000, rabbit serum anti-GBP1[49] (kindly provided by Dr. Eva Frickel) used at 1/500. Antibody references followed by slash-number indicate the number of the rabbit bleed.

2.3.1.4. Secondary antibodies

Goat anti-rabbit Alexa 488, donkey anti-rabbit Alexa 488, goat anti-rat Alexa 647, donkey anti-mouse Alexa 555 and donkey anti-mouse Alexa 488, (Molecular Probes) were used at 1:1000 for immunofluorescence.

2.3.2. Cell-biological methods

2.3.2.1. Passaging, freezing and thawing of mammalian cells

The C57/BL6 MEFs were maintained in culture by regular passages of 48 hours, not exceeding a maximum of 15 passages. Regularly the cells went through the thawing and freezing processes. Aliquots of cells from earlier passages were frozen, to allow storage of lower passaged cells.

Passaging:

Cells were washed with sterile PBS 1X at RT and then detached with 3ml of a solution of 1X trypsin-EDTA for 3-5 min at 37ºC, 10%CO2. Trypsin action was stopped by adding 7ml of warm complete DMEM (DMEM supplemented with 10% heat-inactivated fetal bovine serum or HI-FBS, 2mM L-glutamine, 1mM sodium pyruvate, 1x non-essential amino acids, and 1x penicillin/streptomycin). Cells were centrifuged at 20-25ºC at 290g for 5 min and the pellet was resuspended in DMEM and split to a new flask.

Freezing:

Cells were washed with sterile PBS1X, detached with 1X trypsin-EDTA for 3-5 min at 37ºC, 10%CO2, then centrifuged at 290g for 5 min at 4ºC. The pellet was resuspended in cold sterile FBS-10%DMSO and then transferred into cryotubes in the cold (Mr. Frosty) to -80º C.

Thawing:

Cells were rapidly resuspended in 15ml of complete DMEM at 37ºC then placed in a T75 flask. After attachment, the medium was replaced.

2.3.2.2. Propagation of T. gondii

Tachyzoites were maintained by serial passages of 48-72 hours in 25 cm^2 flasks containing confluent monolayers of Hs27 cultured in complete IMDM without antibiotic. For collection of tachyzoites, the suspension from lysed and scraped HFFs was harvested and passed through a 25G syringe needle several times. The parasite suspension was exposed to two rounds of differential centrifugation to remove cell debris, the first at 100 g for 5 min RT, followed by centrifugation of the supernatant at 700g for 15 min RT. Tachyzoites were resuspended in 2ml of medium, and viable parasites were counted in a Neubauer chamber using trypan blue, and immediately used for infection experiments and for propagation.

2.3.2.3. Cell induction with IFN-γ and Infection with T.gondii

After 24 hours of growth either on UV-sterilized 13mm diameter cover glass or other culture surfaces, for the regular experiments, murine fibroblasts were induced with mouse IFNγ (Cat. 315-05 Peprotech) at 40 ng/ml (200 U/ml) for 18 to 24 hours or were left untreated. The cultures were then inoculated with a small volume of a fresh suspension of *T. gondii* ME49 tachyzoites at a required multiplicity of infection (MOI) of 1,5 to 10 and kept at 37°C, 10% CO2 for the required time of the essay.

For the experiments to study parasite interference with the expression and recruitment of IRG proteins in the PVM, cells were exposed to IFN-γ for decreasing time periods (24, 12, 10.5, 6, 4.5, 3, 2, 1 and 0 hours before infection) until they reached time 0 when they were inoculated with tachyzoites at a required multiplicity of infection (MOI) of 1,5 to 10 and kept at 37°C, 10% of CO2 for the required time of the assay.

2.3.3. Immunofluorescence

For visualization of the loading of IRG proteins and GBP1 onto the PVM by immunofluorescence, MEFs were allowed to adhere on a UV sterilized coverslip or in sterile Lab-Tek chambers for 24 hours. 24, 12, 6, and 0 hrs IFNγ induced and uninduced cells infected with Me49 tachyzoites were washed twice with PBS1X supplemented with 1,8mM of $CaCl_2$ and 0,8mM of $MgSO_4$ and fixed in 4% paraformaldehyde (PFA) for 30 min at room temperature (RT). Before
immunostaining, the cells were washed twice with PBS, permeabilized in 0.1% saponin for 10min and blocked in blocking buffer (3% bovine serum albumin (BSA) and 0,1% saponin) for 1h at room temperature (RT). These cells were then stained with indicated antibody reagents specific for *T. gondii* GRA7, for one or more IRG proteins (165, 141, 940, 81) and for GBP1, all diluted in blocking buffer, for at least 1 hour at RT.

Subsequently, after three washes with blocking buffer, the cells were stained with Alexa Fluor-conjugated secondary antibodies: AF488 donkey anti-rabbit, AF647 goat anti-rat, and AF555 donkey anti-mouse diluted in blocking buffer, for at least 45 min at RT. Cell nuclei/DNA were labelled by 4',6-diamidino-2-phenylindole (DAPI D3571— 889 Life Technologies) The stained cells were washed and mounted on glass microscope slides with Prolong gold antifade reagent. For Lab-Tek chambers the whole immunofluorescence procedure took place in the small chambers where the cells grow on a standard microscope slide. When the procedures were completed, the upper structure was removed, and the samples were covered with cover slips in presence of Prolong gold antifade reagent.

2.3.4. Analyses of cellular proteins

2.3.4.1. Western blot analysis

Lysate preparation from infected cells.

$2x10^5$ MEFs were seeded on day -2, stimulated with 200U/ml of IFNγ during day-1 for 24 hours (control) and other required times (12, 6, 3, 2, 1 and 0 hours) before infection, and then infected with Me49 tachyzoites for the required times. From these and control non-infected cells the supernatant was removed and the cells washed twice with PBS 1X, then lysed in 500µl of cold lysis buffer (20 mM Tris/HCl (pH 7.6), 140 mM NaCl, 5 mM MgCl2, 0.5% NP-40, supplemented with Complete Protease Inhibitors tablets (Roche)) for 30min on ice. The lysate supernatant was collected after 30 minutes of 14000rpm (>16000rcf) centrifugation at 4ºC. The concentration of the lysate was determined by BCA assay (below) then diluted with lysis buffer to equalize sample concentration.

BCA assay

The protein concentrations of the samples were determined based on colorimetric detection using the Thermo Scientific™ Pierce™ BCA Protein Assay, according to the manufacturer's instructions.

The concentration was determined in comparison with a bovine serum albumin (BSA) Standard. A serial dilution of BSA and BCA working Reagent was prepared. The samples (BSA standards and unknown) were mixed with BCA in a 1:20 ratio and after 30 minutes incubation at 37ºC, the absorbance was measured at 562nm.

Immunoblotting Analysis

Samples in 1X protein sample buffer (375 mM Tris.HCl, 9% SDS, 50% Glycerol, 0.03% Bromophenol blue and 20% β-mercaptoethanol) were

denatured at 90ºC for 3min. 10 to 20 µg of protein were separated on 10% Sodium dodecyl sulphate polyacrylamide gel electrophoresis (SDS-PAGE) with a PageRulerTM Prestained Protein Ladder. The SDS-PAGE was run in running buffer (250mMTris, 192mM glycine, 1%SDS in water) at 120V to 150V until the desired protein separation had been achieved.

The proteins were electrophoretically transferred in membrane electrophoresis buffer (25mM Tris base, 193,7mM Glycine and 20% MeOH in water) in a semi-dry transfer apparatus (Bio-Rad Trans-Blot SD Cell) at 5,5mA/cm2 at a maximum of 25V. Gel and membrane were between four sheets of wet Whatman paper.

Immunoblot staining

The membrane was blocked in milk (powder, commercial supermarket brand) (5% milk, 0.1% Tween20 in PBS1X, PBST) for 1 hour at RT then incubated with primary antibody against Irga6 (165, 1:25000) and Irgb6 (141, 1:8000) diluted in 0,1% PBST for 1 hour. The unbound primary antibodies were washed three times with 0,1% PBS/T and the membranes then incubated with anti-rabbit 680 or 800 DyLight™ (Rockland) (1:10000) in the dark for 1 hour. Membranes were washed 3x in PBS/T and 1x in water and then scanned in an Odyssey CLx Imaging System.

2.3.5. Microscopy and image analyses

2.3.5.1. Fluorescence microscopy

Widefield images were acquired on a Zeiss Axio Observer Z1 fluorescence microscope, using either a 40x 0.94NA or 63x 1.3NA objective, equipped with a Hamamatsu FlashLT camera, a Zeiss Colibri

fluorescence illuminator, and appropriate fluorescence filters all controlled by the Zen 2011 software.

2.3.5.2. Blind and unbiased analysis

To ensure reliable analysis of visual images, the microscope slides prepared and labelled were blinded with adhesive tape before imaging. When this was not possible, another person encoded the files with acquired images before quantification. To minimize bias in the semiautomatic quantification, by applying the macro (described in detail below), the IRG and GBP1 proteins were evaluated only in vacuoles first selected based on GRA7 expression, showing that the organism is intracellular.

2.3.6. Quantification of IRG proteins and GBP1 on the PVM

2.3.6.1. Proportion of coated vacuoles

For each condition at least 100 GRA7 labelled vacuoles were scored. The frequency and intensity of different IRG proteins and GBP1 on the PVM on IFNγ-stimulated and unstimulated cells was determined and rated as a positive or negative. The visual estimate of "positive" or "negative" was further refined by quantification as below.

Macro design

An ImageJ macro was created to automate the quantification of protein intensity at the PVM, by measurement of fluorescence in defined areas, based in GRA7 identification.

The macro assumes a composite image in czi format and based on scripts, divides it into 3 distinct regions: PV, PVM and cytoplasm from which the fluorescence intensity is quantified.

The Macro and its uses are described in full in [50].

2.3.6.2. Quantification of protein intensity.

The amount of IRG or GBP1 proteins present on the PVM in IFNγ-stimulated and non-stimulated MEFs was determined by measuring the fluorescence intensity of the fluorochrome corresponding to each protein using a semi-automated system on the Fiji 2.0.0- rc69/1,52i software [51].

Pixel intensities of the fluorochromes that labelled defined individual target antigens, usually with a secondary anti-Ig reagent excited at 488 nm, were measured in GRA7-positive vacuoles, detected with fluorescent secondary anti- rat Ig reagent excited at 647 nm, by using the created macro on ImageJ.

The czi composite fluorescent images were loaded in the Fiji software, then the macro was run. The GRA7 channel was used to detect intracellular PVs without bias. The tolerance was adjusted for each case as necessary. The wand tool through the tolerance allows the adjustment of the PV line to include some out of focus and scattered light associated with the vacuole.

The background signal in the cytosol is an important variable. Very often, IRG proteins and GBP1 were detected using rabbit first-stage anti-IRG antisera that recognise cytosolic and inactive IRG proteins, as well as activated proteins on the PVM (See Figure 2.1). In these cases, when the cytosolic background was markedly too bright and others when the cytsosol was not very bright, the cytosolic fluorescence intensity was determined and subtracted. The pixel intensity at the PVM was defined as the total excess pixel intensity on the PVM after background subtraction.

The value was used as a readout for the amount of protein recruited to each PVM.

Corrected brightness of PVM = x-Ay/B

where x = total light from PVM ROI, y = total light from cytosol ROI, A = area of PVM ROI and B = area of cytosol ROI.

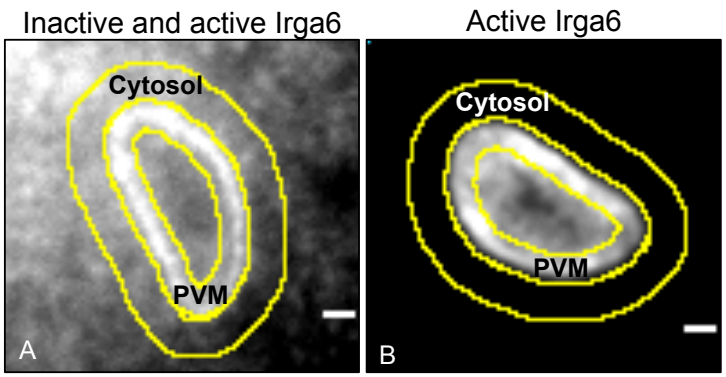

Figure 2.1. Quantification of Irg proteins present on the PVM of avirulent T. gondii in IFNg stimulated MEFs

Fluorescence intensity of Irga6 at the PVM was quantified in intracellular (GRA7-positive) vacuoles using the 165 rabbit antibody against Irga6, simultaneously detected with a fluorescent secondary anti-rabbit Ig reagent (A); and the mouse monoclonal antibody 10D7 against vacuolar Irga6 detected with a fluorescent secondary anti-mouse Ig reagent (B). The scale bar represents 1 µm. To measure the intensity of IRG signal on *T. gondii* PVs, we employed Fiji 2.0.0- rc69/1,52i software and a MACRO designed to allow parasite segmentation from the cytosol and rapid analysis of numerous PVs (see main text for details). A) Irga6 was detected using rabbit antisera that detect cytosolic, inactive Irga6 as well vacuolar, activated proteins. B) Irga6 was detected using the mouse monoclonal antibody, 10D7, which detects only activated Irga6 at the vacuolar membrane [23].

For measuring the fluorescence intensity in the cytoplasm, an oval ROI 8 times bigger than the parasite was created and applied to an area of the cytoplasm that excludes the nucleus and the parasite.

2.3.7. Statistical analysis

The analyses were performed using GraphPad Prism 6.0 and 7.0. Differences between proportion, protein intensity and correlation were

determined using the Q-square (Fisher exact's) t test, Mann-Whitney-test and Pearson correlation coefficient respectively.

2.4. Results

2.4.1. IRG proteins target type II *T. gondii* PVs in an Interferon-γ dependent manner.

The unquestionable importance of IRG proteins in immunity of mice against the protozoan parasite *T. gondii* has already been demonstrated by many authors [32,44,48,52]. In IFNγ stimulated murine cells IRG proteins are responsible for a critical first step in the process of parasite elimination, by recruitment to the PVM, rupture of the PVM, followed by death of the parasite [37,39,53,54]. Despite some quantitative analysis of the IRG protein recruitment process [31,32] much is not yet understood.

To continue exploring the mechanisms and dynamics of IRG recruitment to the parasite vacuoles, we started by repeating previously published experiments [31] about how IFNγ and virulence impact on IRG recruitment, with a view to confirming the main observations from that study and establishing a baseline for the present work. MEFs and DDCs from C56BL/6 mice were stimulated with IFNγ for 24 hours to allow IRG proteins to be expressed, or kept untreated as a control, and then infected with avirulent Me49 or virulent RH *T. gondii* strains for 90 minutes. Immunostaining was performed using a rat anti-GRA7 monoclonal antibody detected with a secondary antibody carrying one fluorochrome to identify intracellular parasites, and rabbit antisera against Irga6, Irgb6, Irgb10, and Irgd, all detected simultaneously with a secondary antibody coupled to another fluorochrome, to detect vacuoles carrying any of the set of effector IRGs respectively. The nuclei were labelled with DAPI. It is important to be clear that this

approach was not directly concerned with the loading hierarchy of the different IRG effectors documented by Khaminets et al. A PVM carrying any or all or a subset of all the effectors would be scored as positive in this analysis. Simultaneously staining the whole set of effectors maximizes brightness and therefore provides our best estimate for the sum of IRG protein-loaded vacuoles. For quantitation, immunofluorescence images were taken.

The loading of IRG proteins onto *T. gondii* ME49 and RH PVs was analyzed as a proportion of the total intracellular parasites (detected by staining for GRA7 protein) and plotted as a percentage of maximum (GRA7 positive PVs=100%) (Figure 2.2. B and D). The pixel intensity of IRG protein loading was determined for each PV as described in Material and Methods (Figure 2.2. C and E). Confirming previous data [31], IRG effector proteins were notably heterogeneously expressed in the cytosol and highly on almost 85% of PVs under IFNγ stimulation (Figure 2.2. A, B and C). Persistently, 10-15% of the vacuoles carried no detectable IRG proteins. The loading of effector IRG proteins onto PVs containing type I virulent parasites (RH) was also heterogeneous, and greatly reduced, reflected both in the proportions of PVs loaded and in the intensity of the IRG signal (Figure 2.2. D and E) as previously reported [31].

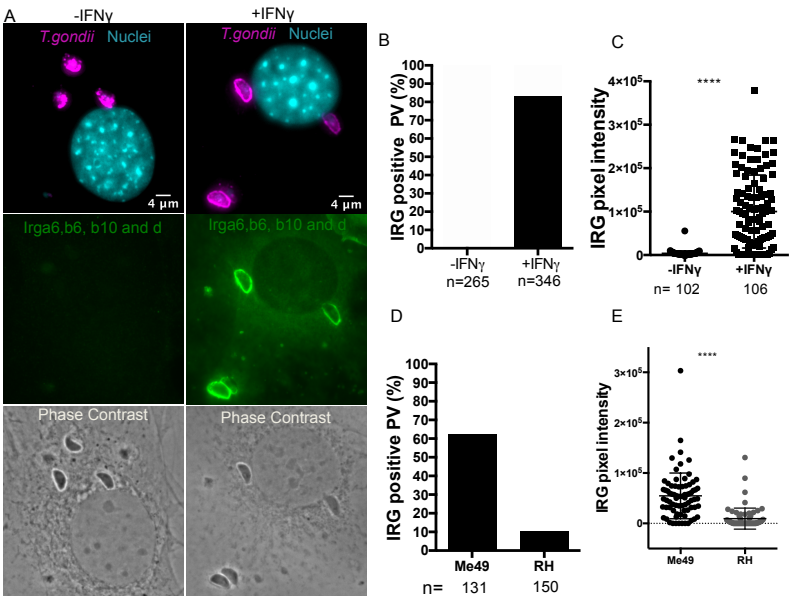

Figure 2.2. IRG proteins preferentially target type II T. gondii PVs in a Interferon-γ dependent manner

WT C56BL/6 MEFs and diaphragm-derived cells (DDCs) treated with IFNγ (200 U/ml) or left untreated were infected with Me49 **(A, B, C)** or Me49 and RH **(D, E)** for 90 min. Cells were washed, fixed and stained for rat monoclonal antibody GRA7 (JH 2.1.2 mAb) with Alexa Fluor647-conjugated goat anti rat IgG (magenta), and for IRG proteins with a pool of the following rabbit antisera: 165/4 for Irga6, 141/1 for Irgb6, 940/6 for Irgb10 and 81/3 for Irgd, followed by Alexa Fluor488-conjugated donkey anti-rabbit IgG (green). The nuclei were labelled with DAPI (cyan). Images taken in a fluorescence microscope are shown of the individual channels for merged GRA7 and DAPI (top), IRG proteins (middle) and phase contrast (bottom). **B)** PVs from non-stimulated and stimulated cells respectively were classified as labelled or not by the anti-IRG antiserum pool and the percentage labelled was obtained based on the presence of GRA7 as 100%. **C** and **E)** The pixel intensity of the IRG signal in each GRA7-labelled PVM was quantified using Image J Fiji software as described in materials and methods.****, P<0,0001

2.4.2. The accumulation of IRG proteins occurs in characteristic proportions but does not cover 100% of PVs.

The IRG effector proteins (Irgb6, Irgb10, Irga6, Irgd) were shown earlier to accumulate on avirulent *T. gondii* PVM [31,37]. As earlier demonstrated, the pool of IRG effector proteins are recruited to about 85% of avirulent *T. gondii* PVs. To discriminate the proportion of PVs covered by each of the IRG proteins, interferon γ-stimulated C56BL/6 MEFs were infected with avirulent Me49 for 90min. The samples were fixed and processed for intracellular immunostaining for Irga6, Irgb6, Irgb10 and Irgd separately with serum against each IRG protein individually (Figure 2.3. A) or against Irga6 and Irgb6 (Figure 2.3. B), or against Irga6, Irgb6, Irgb10 and Irgd with secondary antibody coupled to the same fluorochrome (Figure 2.3. C).

More than a hundred intracellular parasites (GRA7 labelled) were scored blind to define the proportion of PVs covered by each of the IRG proteins. From the most-loaded representative, Irgb6 (about 82% positive) to the least loaded, Irgd (about 45% positive), the order was Irgb6, Irgb10, Irga6 and Irgd in agreement with the previous report [31].

(Figure 2.3. A). Irgb6 and Irga6 and also the pool of effector IRGs cover a maximum of 82% of PVs. About 20% of PVs were not loaded by any IRG, consistent with the previous report (Figure 2.3. A). Irgb6 and Irga6 and also the pool of effector IRGs cover a maximum of 82% of PVs. About 20% of PVs were not loaded by any IRG, consistent with the previous report [31] (Figure 2.3. B and C). Notably, the proportion of vacuoles loaded with Irgb6 alone is similar to the proportion of these covered by the set of effector IRGs, which indicates that the four effector IRGs load onto the same vacuoles.

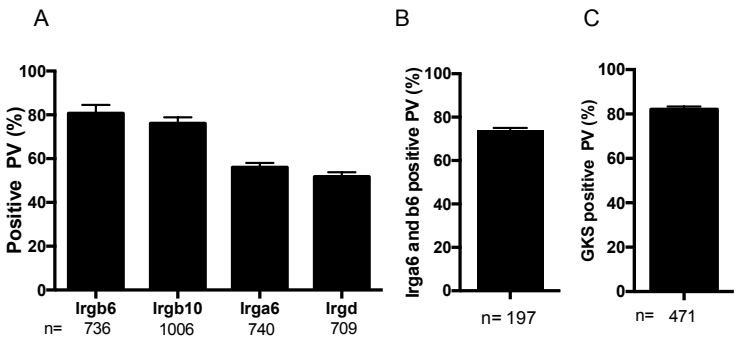

Figure 2.3. The accumulation of IRG proteins occurs in a characteristic proportion that does not cover 100% of PVs.

WT C56BL/6 MEFs were treated with IFNγ (200 U/ml) for 24 hours and infected with *T. gondii* Me49 for 90 minutes. Cells were washed, fixed and stained for GRA7 (JH 2.1.2 mAB) with Alexa Fluor 647-conjugated secondary antibody (magenta): **A)** Individually labelled IRGs: Irga6 (serum 165/4 and 10D7), Irgb6 (serum 141/1), Irgb10 (serum 940/6), Irgd (serum 81/3) and **C)** all IRGs detected with the same secondary: **B)** Irga6 (serum 165/4) and Irgb6 (serum 141/1) with Alexa Fluor488-conjugated secondary antibody (green). The nuclei were labelled with DAPI (cyan). Images were taken in a fluorescent microscope (Fig.2.1-A). **A-C)** The GRA7 positive vacuoles were scored and classified as IRG positive or not, and the proportion was obtained based on GRA7 labelled PVs. The image depicts the percentage of GRA7 labelled PVs that were IRG positive. The range between **A)** four and **B, C)** two independent experiments were shown.

In agreement with Kaminets, the data above (Figure 2.3) suggest that different effector IRGs accumulate on the same vacuoles, suggesting some kind of coperative process. They are distributed over about 80% of PVs in different proportions. To dissect the proportions of the different IRG proteins on the PVs, the samples were co-stained for several combinations of two different IRG proteins at different positions within the loading hierarchy at a time. Intracellular parasites were identified with GRA7 staining. The quantification includes single IRG loaded vacuoles, double-loaded and non-loaded vacuoles. The data revealed a pair of IRG proteins with a hierarchy distribution. The top members of the hierarchy, Irgb6 and Irgb10, covered 88% of PVs,

followed by the combination of Irgb6 with Irga6 (85%), Irga6 with Irgb10 (80%). Normally about 10% of PVs were not covered by any IRG proteins (Figure 2.4. A).

These results largely confirmed the conclusion of Khaminets et al, in which the set of Irga6-positive vacuoles is included in the larger set of Irgb6-positive vacuoles, and the set of Irgd-positive vacuoles is in turn included in the larger set of Irga6-positive vacuoles, like “Russian Dolls”. Khaminets et al noted that Irgb10 is loaded onto almost as many vacuoles as Irgb6 and assumed that these two sets were effectively the same. PVs covered with IRG proteins lower in the hierarchy were essentially completely included in PVs loaded with the IRG proteins higher in the hierarchy: 97% and 98% of PVs with Irga6 were included in Irgb6 and Irgb10 respectively, and 94% of Irgb10 positive PVs were included in Irgb6 covered PVs (Figure 2.4. B). The exception is Irgb10, where the proportions of vacuoles covered by Irgb6 and Irgb10 are consistent with independence.

The most abundantly represented IRG proteins of the hierarchy of PV loading include almost completely the less abundantly represented Irga6 and Irgd [31]. This results in a heterogeneity in vacuoles, some covered by 3 IRGs (b6+a6+d), others by 2 (b6+a6) and 1 (b6 only) and no IRGs, which may result in different outcomes for the parasite. We show in Chapter 3 that the subset of vacuoles with Irgb6 alone is less likely to be disrupted that those with 2 or 3 IRG proteins. The position of Irgb10 in this distribution is not entirely clear. It is, however, a well-represented IRG protein on vacuoles, perhaps very slightly lower than Irgb6, and is therefore present on most vacuoles carrying IRG proteins lower in the hierarchy, but seems to load independently of Irgb6, suggesting there may be a small number of vacuoles loaded with Irgb10 alone.

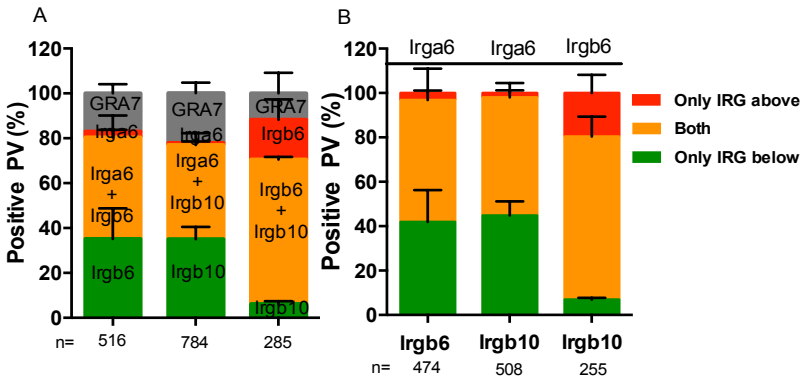

Figure 2.4. Different effector IRG co-localize to the same PVM.

WT C56BL/6 MEFs were treated or not with IFNγ (200 U/ml) for 24 hours and infected with *T. gondii* Me49 for 90 minutes. Cells were washed, fixed and stained for GRA7 (JH 2.1.2 mAb) with Alexa Fluor 647-conjugated secondary antibody (magenta) to define intravacuolar organisms, and for the following pairs of individual IRGs: Irga6 (serum 165) and Irgb6 (serum 141/1); Irga6 (10D7) and Irgb10 (serum 940/6); Irgb6 (B34) and Irgb10 (serum 940/6) in each case with anti-rabbit Alexa Fluor488-conjugated secondary antibody (green) or anti-mouse Alexa Fluor555-conjugated secondary antibody (red). The nuclei were labelled with DAPI (cyan). The quantification of fluorescent images shows **A)** the percentage of GRA7+ PVs without IRG protein labeling (in gray) and PVs labelled for one (in red and green) or both (in orange) IRG proteins; **B)** the percentage of the total PVs labelled for one or both IRG proteins. **A)** and **B)** the range between three (1st and 2nd columns) and two (third columm) independent experiments was shown.

2.4.3. The recruitment of Irga6 to PVs is independent of the recruitment of Irgb6

Previous work [31] showed that Irgb6 loads earlier onto the PVM than Irga6 and Irgd. This has been interpreted to mean that Irgb6 acts as a "pioneer", coming first to the PVM and facilitating the subsequent arrival of Irga6 and Irgd. One possible view of this "pioneer" action could be that the interaction of Irga6 with the PVM also requires affinity between Irga6 and bound Irgb6, and likewise for Irga6 providing assistance for the subsequent binding of Irgd.

If such a model is correct, the number of binding sites for Irga6 should be positively correlated with the number of Irgb6 molecules bound to the PVM. To determine if the pioneer Irgb6 serves as a platform to anchor Irga6, the individual loading of the Irga6 and Irgb6 intensities in the PVM area were measured and the data were subjected to correlation analysis. The surprising result was that the loading intensities of Irga6 and Irgb6 are not correlated (Figure 2.5. A). About 20% of vacuoles were loaded with neither Irgb6 nor Irga6 (the IRG-negative subset). The presence of these double-negative vacuoles contributed somewhat to the correlation coefficient, and as expected, removal of double negatives reduces the correlation coefficient even further.

Many vacuoles showed Irgb6 and Irga6 with opposite intensities (Figure 2.5. B), contrary to expectation if Irgb6 is acting as a form of an anchor or binding site for Irga6. This result was so unexpected that we sought to validate the approach in correlation experiments by assaying as a positive control two antibody reagents, the rabbit anti Irga6 serum 165 and the mouse anti Irga6-specific monoclonal antibody 10E7 against a single IRG protein, Irga6. The intensities of these two reagents on individual vacuoles were strongly positively correlated as expected (Figure 2.5. C).

The results revealed no dependence between recruitment of Irgb6 and Irga6, although all Irga6-positive vacuoles are included in the set of Irgb6 positive vacuoles, suggesting that Irga6 may bind to a different target in the PVM and not to Irgb6 directly. Nevertheless, the loading hierarchy would suggest that, qualitatively but not quantitatively, the presence of targets for Irga6 binding is correlated with the presence of targets for Irgb6 binding.

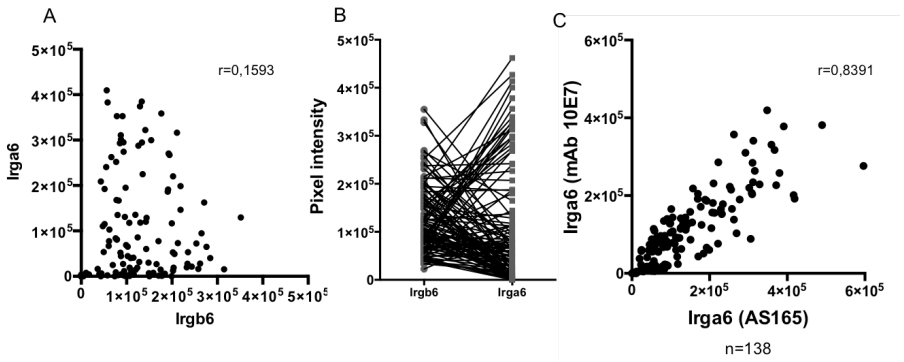

Figure 2.5. Irgb6 and Irga6 on PVM are not correlated.

WT C56BL/6 MEFs were treated with IFNγ (200 U/ml) for 24 hours and infected with *T. gondii* Me49 for 90 minutes. Cells were washed, fixed and stained for GRA7 (JH 2.1.2 mAb) with Alexa Fluor 647-conjugated secondary antibody, and for the following pairs of individual IRGs: Irga6 (10D7) and Irgb6 (serum 141/1); Irga6 (serum 165) and (monoclonal ab 10E7), with anti-rabbit Alexa Fluor488-conjugated secondary antibody (green) and anti-mouse Alexa Fluor 555-conjugated secondary antibody (red). The nuclei were labelled with DAPI (cyan). The quantification of fluorescent images shows the intensity of Irga6 and Irgb6 on the PVM area of every GRA7 positive PVs. **A)** Pearson correlation analysis was performed P value > 0,05. **B)** The intensity of the IRGs is organized on two Y-axes representing Irgb6 and Irga6 intensity, with each line representing a PVM and the symbols at the ends Irgb6 (left) and Irga6 (right). **C)** The intensity of Irga6 labelled with rabbit (165) and mouse (10E7) anti-Irga6 antibodies was measured and submitted to Pearson correlation analysis P value < 0,0001.

2.4.4. The binding of Irgb6 is also not crucial for recruitment of other GTPases to the PVs.

Khaminets suggested that the recruitment of GKS proteins to the PVM occurs in a consistent hierarchy, with Irgb6 arriving earlier and later stabilizing with the arrival of Irga6 and Irgd. According to this model, loading of Irgb6 would be essential for the loading of Irga6 and Irgd. We therefore analyzed whether the absence of Irgb6 affects the loading of the other GTPases onto the PVM in WT and Irgb6 KO (Claudia Campos, unpublished) DDCs after 24 hours of IFNγ induction and 90 min of infection with Me49. The samples were stained for Irgb6 with a

mAb B34, for Irgb10 with serum 940, for Irga6 with serum 165 and for GBP1 with serum anti-GBP1 [55] and for GRA7 with JH 2.1.2 mAb.

The data confirmed the absence of Irgb6 in Irgb6KO cells, while the recruitment of Irgb6 on PVM in WT cells occurred normally with 80% of PVs positive (Figure 2.6. A). The presence of Irgb10 on PVM (many with an unusual vacuolar morphology (Supplemental Figure 2.1.) is slightly affected (intensity and proportion) in Irgb6KO cells with approximately 50% of positive vacuoles loaded with Irgb10 against approximately 75% in WT cells (Figure 2.6. B). The recruitment of Irga6 was barely affected by the absence of Irgb6 (Figure 2.6. C), supporting the supposition above from the lack of a quantitative correlation between Irgb6 and Irga6 loading that the two effector proteins bind essentially independently to different targets on the PVM. The recruitment of GBP1 is also barely affected by the absence of Irgb6 (Figure 2.6. D).

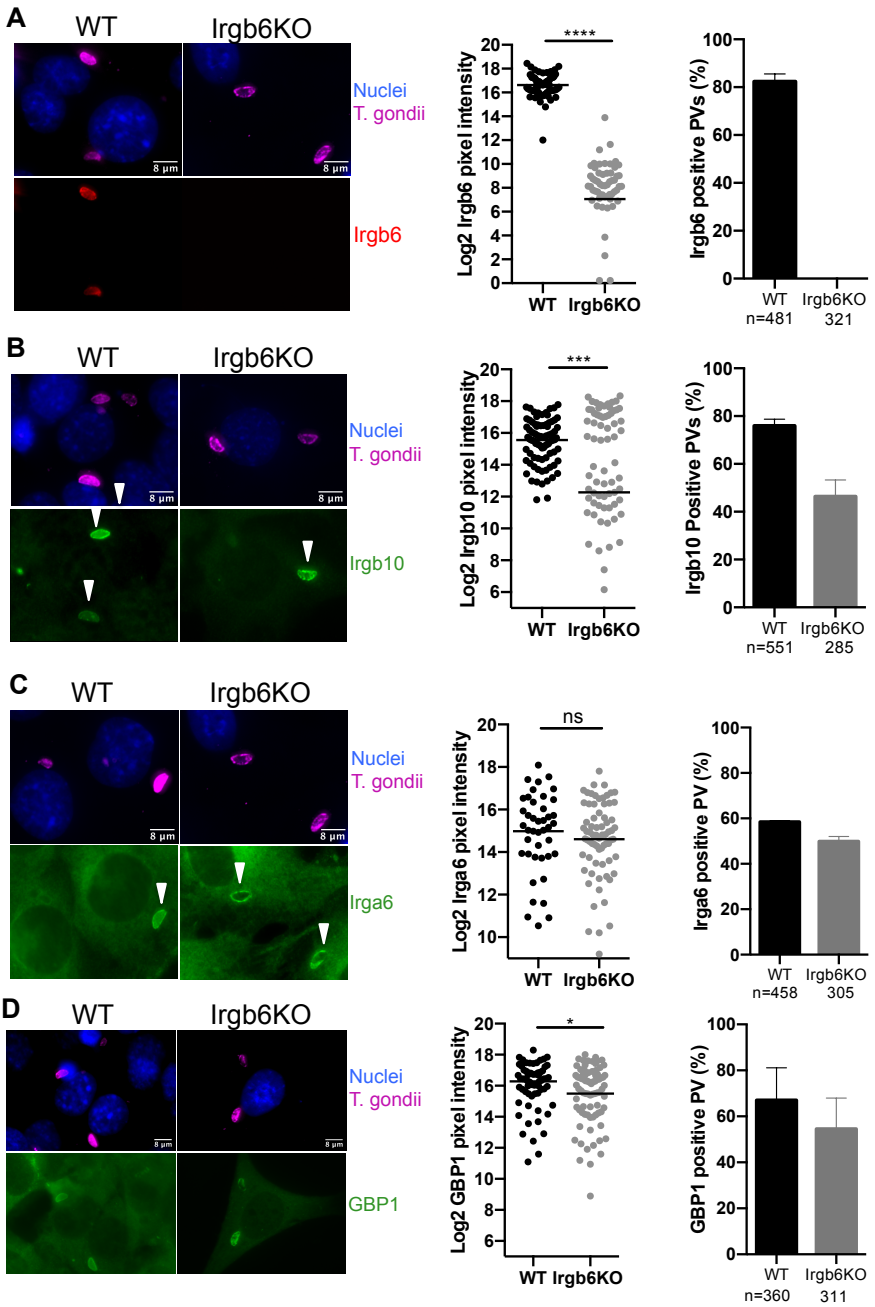

Figure 2.6. The recruitment of others GTPases is not greatly affected by the absence of Irgb6.

WT and Irgb6KO DDCs were treated or not with IFNγ (200 U/ml) for 24 hours and infected with *T. gondii* Me49 for 90 minutes. Cells were washed, fixed and stained for GRA7 (JH 2.1.2 mAb) with Alexa Fluor 647-conjugated secondary antibody (magenta)

to define intravacuolar organisms, and for the following pairs of individual IRGs: Irgb6 (mAb B34), Irga6 (serum 165), Irgb10 (serum 940/6) and GBP1 serum in each case with Alexa Fluor488-conjugated secondary antibody (green) or Alexa Fluor 555-conjugated secondary antibody (red). The nuclei were labelled with DAPI (cyan). Representative Images, are shown. Quantification of fluorescent images shows the intensity of IRG on the PVM and percentage of GRA7+ PVs with **A)** Irgb6 **B)** Irgb10 **C)** Irga6 and GBP1 labeling **B)** the range between two **(D)** and three independent experiments was shown (**A, B** and **C**). ****, P<0,0001;*** P<0,001; n.s., nonsignificant.

These data show that the presence of Irgb6 may predict the presence of other GTPases, but is not required for it. The somewhat reduced binding of both Irga6 and Irgb10 to the Irgb6-deficient vacuoles is reminiscent of the reduced binding of Irgb6 to ME49 PVM in the absence of Irga6 (Khaminets 2010, Figure 6.F) [31] a result interpreted at that time in terms of some kind of interaction between the two effector GTPases resulting in stabilization on the PVM, and this may still be valid. Nevertheless, it is abundantly clear that the binding of at least Irga6 is not qualitatively dependent on bound Irgb6 as a “pioneer”.

2.4.5. IRG protein accumulation on PVs starts early and increases over time.

It has been shown that IFNγ-induced IRG proteins begin to accumulate and activate on at least some vacuoles immediately after *T. gondii* entry[31]. It was previously shown that at 90 min post infection 80% to 90% of PVs were covered by effector IRG proteins (Figure 2.3). To understand the timing of IRG protein recruitment onto *T. gondii* PVs IFNγ stimulated MEFs were infected with Me49 for 15, 30, 60 and 120 minutes. After every time point the samples were fixed and kept in blocking buffer until the last time point infection. Samples were immunostained for GRA7 detected with secondary antibody coupled to the fluorochrome 647, and for Irga6, Irgb6, Irgb10 and Irgd, by using antiserum 165/4, 141/1, 940/6 and 81/3 respectively detected with

secondary antibodies coupled to the same fluorochrome. Subsequently, IRG protein loading intensity was counted from over 100 GRA7 labelled PVs (Materials and Methods, chapter 2.3.4.3).

The results of this experiment indicate that IRG protein accumulation at the PVM starts soon after infection. After 15 minutes of infection a major proportion of PVs was already covered by IRGs (about 60%), suggesting, as Khaminets showed, that the loading of IRG proteins onto the PV begins immediately after infection. The proportions increased over time from 60% to about 75% then 81% at 60 minutes. At 120 minutes post infection fewer apparently intact PVs (67%) were covered by IRG proteins, and more IRG-positive aggregates were present, probably resulting from PVM disruption (Figure 2.7. A. and B).

The increase in the proportion of PVs loaded by IRG proteins was accompanied by an increase in the protein loading as measured by fluorescence intensity. It was clear that much of the loading is already complete 15 minutes after infection. Subsequently, the greatest increase was registered between 15 to 30 minutes, after which slight increases in intensity were recorded. Also, the heterogeneity of intensity increased significantly in this first 30 minutes of infection (Figure 2.7. C). The data all suggested that the first minutes post infection are critical for IRG recruitment to the PVM and its disruption, and confirm the earlier results of Khaminets, who concluded that loading of IRG proteins onto the vacuole may begin at the point and time of entry.

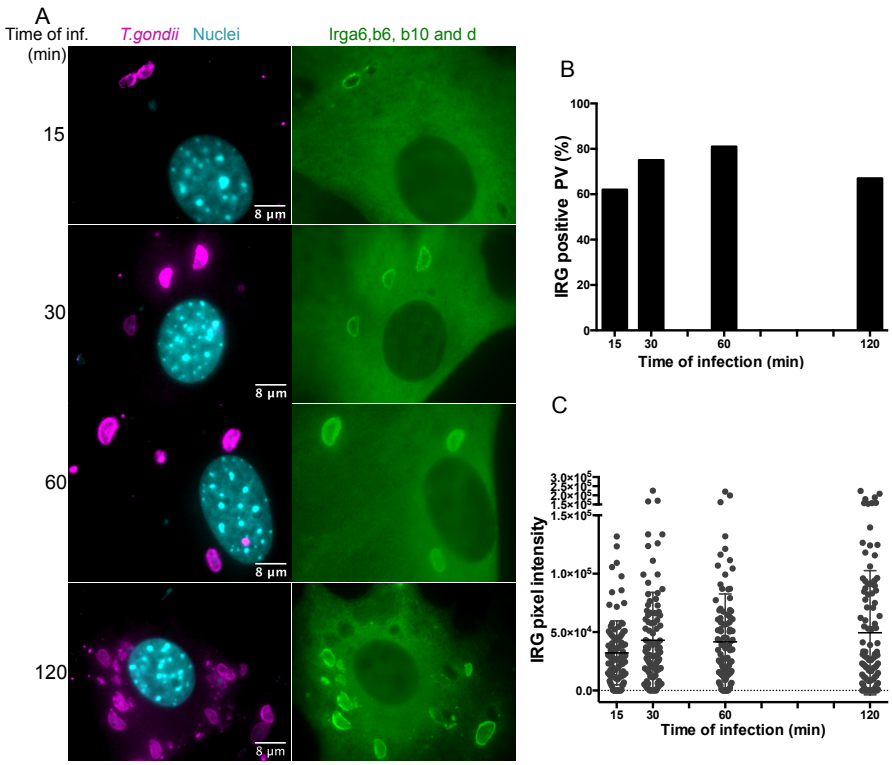

Figure 2.7. Accumulation of IRG proteins on PVs starts early and increases over time.

WT C56BL/6 MEFs induced with IFNγ (200 U/mL) for 24 hours and infected with *T. gondii* Me49 for 15, 30, 60 and 120 minutes. Cells were washed, fixed and stained simultaneously for Irga6 (antiserum 165/4, Irgb6 (antiserum 141/1), Irgb10 (940/6 pAS) and Irgd (antiserum 81/3) with the same secondary antibody coupled with Alexa Fluor 488-conjugated secondary antibody (green) and for GRA7 (JH 2.1.2 mAB) with Alexa Fluor 647-conjugated secondary antibody (magenta). The nuclei were labelled with DAPI (cyan). **A)** Images taken in a fluorescent microscope show merged GRA7 and DAPI channels and IRG channels. **B)** 117, 131, 188 and 222 GRA7 labelled PVs, for time point 15 min to 120min respectively, were classified as IRG positive (with visible accumulations of IRG proteins) or negative (without visible accumulations of IRG proteins) and presented in a graphic as a percentage of GRA7 positive vacuoles. **C)** The pixel intensity corresponding to the IRG channel of each GRA7-labelled PVM at each time point was quantified using Image J Fiji software as described in materials and methods.

2.4.6. The cellular concentration of IRGs is not a limiting factor in its recruitment to vacuoles.

In agreement with Khaminets data[31] it was demonstrated here that 10% to 20% of the PVs are never covered by any IRG proteins. The finding opened the intriguing question of what determines whether PVs are covered by IRGs or not. Are factors intrinsic to parasites or to cells making this determination? To find out whether an obvious potential cellular component, namely the cytosolic concentration of IRG proteins, is a key factor in IRG recruitment to PVs, MEFs were stimulated with IFNγ and infected with Me49 at low MOI. The cells were fixed and stained simultaneously with antisera against Irga6 and Irgb6 and detected together with AF488 and for GRA7 detected with AF555. The nuclei were labelled with DAPI. Only cells infected with a single parasite were selected for classification of the PVs as a positive or negative. If the cytosolic IRG concentration determines the intensity of IRG loading, there should be a clear correlation between these two variables. The immunofluorescence data revealed the level of IRGs expressed within the cytoplasm, but contrary to expectation the coverage of PVs by IRGs was not universal. Only about 75% of the PVs were loaded by Irga6 and Irgb6. The remaining 25% were not covered by either of these two proteins even in the case of high IRG intensities in the cytoplasm, meaning that IRG protein concentrations are, within broad limits not a limiting factor for PV loading (Figure 2.8. A and B). To determine whether the provision of cytoplasmic IRGs is correlated with the amount of IRG present at the PVM, the protein intensities in the PVM and cytoplasm were measured, and the data submitted to Pearson correlation and presented in (Figure 2.8. C). Most surprisingly, the quantitative loading of IRG protein onto the PVM was essentially uncorrelated with the IRG concentration measured in the cytoplasm.

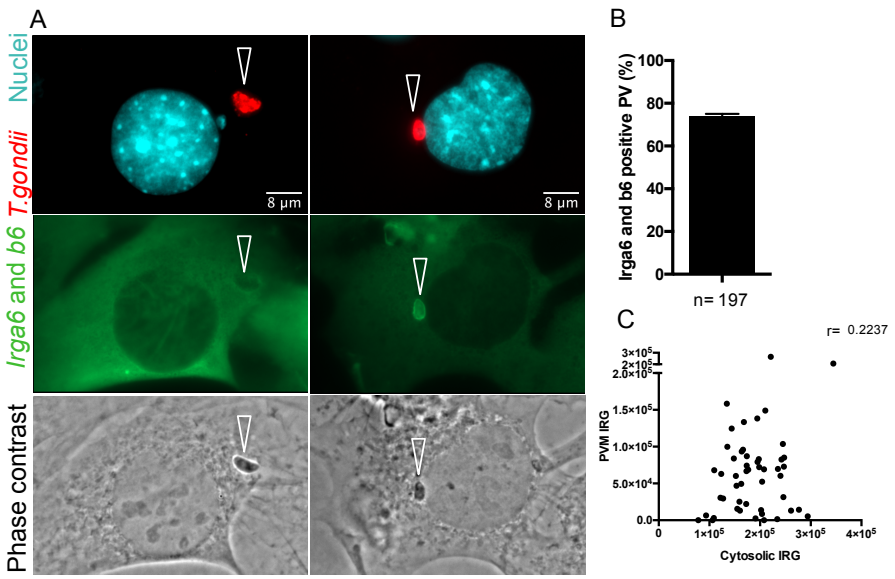

Figure 2.8. The cytosolic concentration of IRG proteins is not normally a limiting factor in their recruitment to vacuoles.

IFNγ induced WT C56BL/6 MEFs were infected with *T. gondii* Me49 for 90 minutes. Cells were washed, fixed and stained simultaneously for Irga6 (165/4 pAS), Irgb6 (141/1 pAS) with the same secondary antibody coupled with Alexa Fluor488 (green) and GRA7 (JH 2.1.2 mAB) with Alexa Fluor 555-conjugated secondary antibody (red). The nuclei were labelled with DAPI (cyan). **A)** Images taken in a fluorescent microscope shows the merged GRA7 and DAPI channels, the individual channel for IRGs, and phase contrast of two different scenarios. White arrows heads pointed to the PVs. **B)** 100 GRA7 positive PVs from cells infected with a single parasite were scored, classified as a positive or not for Irga6 and b6 and presented as a percentage of GRA7 labelled vacuoles. The range between two independent experiments is shown. **C)** The intensity of Irga6 and b6 was measured from all the GRA7 positive vacuoles and Pearson correlation analysis was performed. P Value > 0,1.

Together with the previous data, these data suggest that the propensity to load with an IRG protein is a variable property of the vacuole itself. Only in the limit, with very low cytosolic IRG concentrations, is loading of the PVM quantitatively reduced, showing that the capture of IRG proteins by the vacuolar membrane is highly efficient. The nature of this variable property of the individual PVM is unknown but of considerable interest. It could be a property due to the host events involved in the

formation of the PVM, for example because of stochastic variation in the action and composition of the moving junction, or due to rapid post-entry modification of the PVM, as a result of rhoptry or dense granule secretions. The data so far do not distinguish between a variation between vacuoles that is established at or within minutes after cell entry, or one that develops more slowly after infection in some form of "maturation" process. In view of the probable implications for parasite survival it is possible that the phenomenon is adaptively regulated to allow a proportion of infecting parasites to survive immune attack. Although IRG loading of some vacuoles begins almost immediately after infection, this is not apparent for all vacuoles. Khaminets showed that the initiation of IRG loading has a stochastic time dependence, starting essentially on entry for one vacuole and nearly half an hour later in another. We have argued that this variability is due to a time-dependent probability function arising from the biochemical requirements for cooperative IRG activation [56,57]. In the extreme case one could argue that this alone could account for the constant percentage of unloaded vacuoles, but more plausibly a stochastic delay in loading may provide the time necessary for "maturation" of the vacuole to a resistant state. If the probability of IRG activation due to rate of accumulation is important, IRG loading should show dependence on the cytosolic concentration of IRG protein, but the presence of unloaded vacuoles in cells with high concentrations of IRG shown in Figure 2.8 A and C argue strongly against this.

We then explored IRG recruitment to two PVMs in the same cytoplasm, thus cancelling any effect from cytosolic concentration. Irgb6 was detected with serum 141 in IFNγ stimulated MEFs infected with Me49 for 1 hour. Immunofluorescence images were taken (Figure 2.9. A) and Irgb6 signal intensity on individual PVs was quantified from cells infected with 2 intracellular vacuoles defined by GRA7 labelling:

arbitrarily Left PVM (PVML) and Right PVM (PVMR) as described in Materials and Methods.

The pair of PVs in single cells displayed heterogeneous combinations of IRG intensity on PVM, from very similar intensities (horizontal lines) to very different intensities (oblique lines) (Figure 2.9. B).
The frequency distributions of IRG intensity on the two PVM were similar and the weak correlation in loading values close to insignificant meaning the IRG loading on the (arbitrarily defined) second PV is scarcely dependent on or correlated with the loading of the (arbitrarily defined) primary (Figure 2.9. C and D), so the two distributions are essentially independent of each other, and the host cell plays little if any role in determining the IRG loading intensity of the PVM.

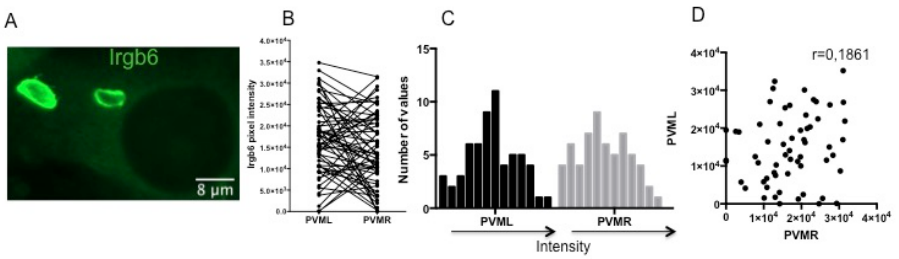

Figure 2.9. Loading of individual PVs in a cell by IRG proteins are not correlated.
A-D) C57BL/6 MEFs were induced with 200U IFN/ml of IFNγ for 24 hours and infected with *T. gondii* Me49 for 1 hour. Cells were fixed, washed and stained for Irgb6 (141/1 pAS), with Alexa Fluor488-conjugated secondary antibody (green) and for GRA7 (JH 2.1.2 mAB) with Alexa Fluor 647-conjugated secondary. **A)** Fluorescent microscope image shows the IRG channel. Cells infected with 2 vacuoles GRA7 labelled: Left PVM (PVML) and Right PVM (PVMR) were selected, the fluorescent signal intensity correspondent to Irgb6 on individual vacuoles was measured, using Image J Fiji as described in materials and methods. **B)** In the graph the dots on the Y-axes correspond to individual PVMs and the joining line link the two vacuoles in each host cell. **C)** The intensities of PVML and PVMR were plotted as frequency distributions and **D)** analyzed by Pearson correlation. P-value> 0,1

2.4.7. *Toxoplasma gondii* infection interferes with IFNγ–induced IRG expression.

The recruitment of IRG proteins to the *T. gondii* vacuoles is a critical step towards elimination of the parasite by PVM disruption[37,53]. It has already been demonstrated and reproduced here, that this recruitment is not completely effective, some vacuoles do not seem to be loaded by any IRG. These IRG-deficient vacuoles may explain the residual portion of parasites capable of surviving the host immune response that can establish themselves chronically at the organism level. How the parasite can ensure that at least some vacuoles are not eliminated by IRG proteins is thus a key factor in learning how the parasite persists in hosts that use the IRG protein resistance mechanism. A similar consideration applies, and similar mechanistic issues arise, in the human infection in which IRG proteins play no role, but where the parasite is also restrained by immunity but never eliminated.

It has been shown that IFNγ regulated gene expression is inhibited in multiple cell types, such as murine bone-marrow-derived macrophages, and RAW264.7, astrocytes and microglia, as well human fibroblasts and HEK293, if infection is allowed to proceed before IFNγ stimulation [58–60]. At least two secreted proteins are known to be necessary for the inhibition of the response, 1) the dense granule proteins TgIST [46,61] responsible for direct inhibition of the IFNγ-induced transcription factor, STAT1, and 2) MYR1 [62], a protein operating further upstream, required for the release of TgIST into the host cell cytoplasm.

The following experiments examined the timing of *T. gondii*-mediated inhibition of IRG protein induction by IFNγ. We first determined the timing of increase of Irga6 and Irgb6 protein levels during IFNγ stimulation of MEFs. Cell lysates were resolved by SDS-PAGE followed by Western Blots that were probed with anti-Irga6 and anti-Irgb6

antibodies. The detection of Irga6 and Irgb6 proteins occurs at an early time of 3 hours after IFNγ induction, increasing until 11 hours after induction (Figure 2.10. A).

To document inhibition of IRG induction by *T. gondii* infection, MEFs were stimulated with IFNγ for 13 h and infected with *T. gondii* either at t=0 (condition I), t=6h (condition II) t=12h (Condition III), and a positive control group was stimulated for 24 h with IFN-γ before infection for 1 h (Condition IV). Samples analyzed by SDS PAGE followed by western blot, probed with Irga6 and Irgb6 antibodies revealed a decrease of the cellular levels of Irga6 and Irgb6 in conditions I and II, when the infection occurred simultaneously with or shortly after IFNγ induction (Figure 2.10. B).

Samples were fixed and stained with sera anti-Irga6 and anti-Irgb6. Representative fluorescent images show intracellular parasite, nuclei and Irgb6 from Conditions I, II, III and IV (Figure 2.10. C).

The blind count of Irga6 and Irgb6 positive vacuoles revealed that cells pre-induced both at 12 and 24 hours (conditions III and IV) can load IRGs to the same number of PVs, although the intensity is somewhat lower with the shorter incubation time (Figure 2.10. D). Consistent with the reduced Western blot signals, the recruitment of IRG proteins was reduced when *T. gondii* infection occurred together with addition of IFNγ (Condition I) or after 6 hours of induction (Condition II). Although there was a reduction in the frequency of PVs covered by IRGs in condition II the greatest impact was recorded in Condition I where the parasite invades the cell at the same time as IFNγ stimulation but before IRG induction (Figure 2.10. E).

Equally, the quantification of Irga6 and Irgb6 intensity data depicted on Figure 2.10. D and 2.10. F shows the impact of *T. gondii* on IRG expression when infection occurs simultaneously with IFNγ induction.

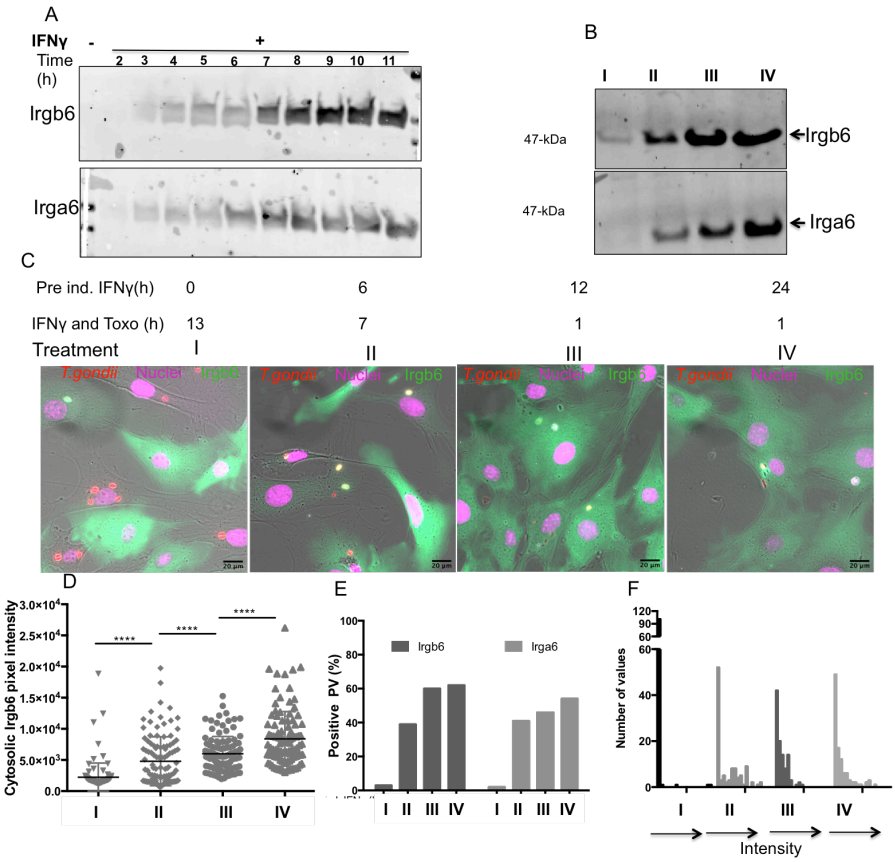

Figure 2.10. The duration of host cell prestimulation with IFNγ interferes with IRG proteins mediated response to T.gondii.

C56BL/6 MEFs stimulated with IFNγ for the indicated periods (2 to 11 hours), or unstimulated, were analyzed by Western Blot as described in Materials and Methods, using the serum 141 (Irgb6) and serum 165 (Irga6) antibodies. **B-F)** MEFs were prestimulated with 200U/ml IFNγ for different periods (0, 6, 12 and 24 hours) corresponding to Treatment I, II, III, and IV respectively and infected with *T. gondii* Me49. Cells were infected for 13, 7,1 hours in the treatment I, II, III and IV respectively. **B)** The expression levels of Irgb6 and Irga6 were analyzed by Western blot of cell lysates, using the 141 or 165 antisera respectively. **C)** The cells were then washed and stained with immunoreagents against Irgb6 (141) or Irga6 (165/3) using secondary antibodies coupled to AlexaFluor488 (green) and against GRA7 (JH 2.1.2 mAB) coupled to AlexaFluorF555 (red). Nuclei were labelled with DAPI (magenta). Immunofluorescence images are shown with merged IRG, GRA7, DAPI and Phase contrast channels for each treatment. **D)** The fluorescent signal intensity of Irgb6 on individual vacuoles was quantified, using ImageJ Fiji as described in materials and methods. For each treatment, the intensity of Irgb6 in an area of cytosol immediately

adjacent to individual PVs was measured. **E)** More than a hundred PVs labelled with GRA7 were evaluated and the proportion of Irgb6 and Irga6 positive PVs are shown. **F)** After background intensity subtraction, the data was shown as 4 mini-histograms showing the frequency distribution of PVM Irgb6 intensity under the 4 conditions. ****, P<0,0001

Further, to determine the minimum duration of IFNγ stimulation prior to infection, to allow an IFNγ dependent response against *T. gondii*, MEFs were pretreated with IFNγ for 3, 2 or 1 hours before infection, simultaneously with infection and 1 hour after infection. Cells were infected with the avirulent Me49 *T. gondii* parasites or left uninfected for 9 hours. Cell lysates were collected and analyzed by SDS-PAGE, followed by Western blotting probed with Irgb6 and vinculin antibodies, as described previously in Materials and Methods. This procedure showed a decline of Irgb6 expression level with the reduction of IFNγ pre-stimulation duration in cells with Me49 (Figure 2.11. A).

The examination of fluorescent images showed that when cells were infected simultaneously with IFNγ stimulation fewer than 30% of cells express either Irga6 or Irgb6 (Figure 2.11. B and C).

The results showed a specific impairment of IRG protein expression in parasite-infected cells. About 65% of the cells that do not express IRG within the cytoplasm contain dividing parasites in their cytoplasm while fewer than 20% of cells that express IRGs contain parasites (Figure 2.11. B) (Figure 2.11. B and D). Taken together, these results demonstrated that, in the absence of a sufficiently long IFNγ pre-induction, *T. gondii* interferes with subsequent IRG expression.

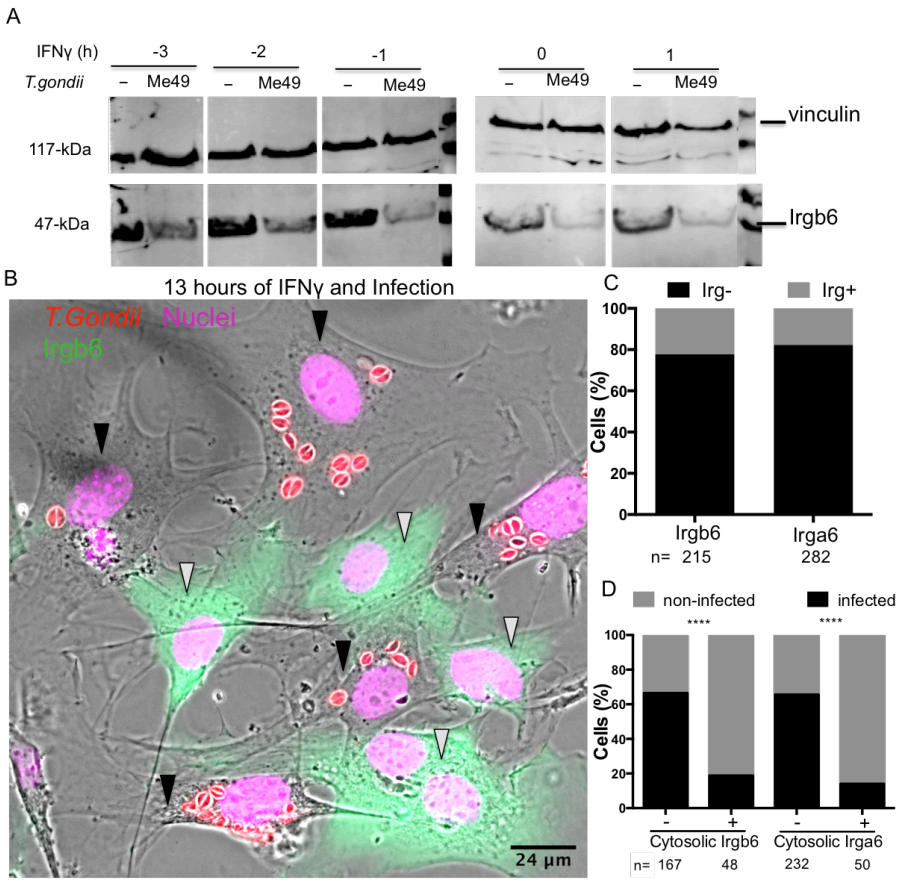

Figure 2.11. Short time prestimulation with IFN-γ allow T. gondii to reduce and suppress IRG expression.

A) C56BL/6 MEFs were stimulated with IFNγ for indicated periods (3, 2, 1, hours prior infection), simultaneously with infection and 1 hour post infection then infected with *T,gondii* Me49 or left uninfected for 9 hours. Total Irgb6 expression was detected from cell lysates with 141 antiserum as described in materials and methods. Vinculin levels are shown as a loading control. **B)** C56BL/6 MEFs simultaneously infected with Me49 and stimulated with IFNγ for 13 hours were washed and stained with immunoreagents against Irgb6 (141) or Irga6 (165/3) using secondary antibodies coupled to AlexaFluor488 (green) and against GRA7 (JH 2.1.2 mAB) using secondary antibodies coupled to AlexaFluorF555 (red). Nuclei were labelled with DAPI (blue). **C)** The proportion of the two populations of cells: Irgb6 or Irga6 positive (grey) and Irgb6 or Irga6 negative (black) were obtained of a total of 167 and 232 cells respectively. **D)** The Irgb6 and Irga6 positive (+) and negative (-) populations of the cells in C were classified as infected (black) or non-infected (grey) with *T. gondii* based on GRA7 labelled PVs. ****, P<0,0001

2.4.8. *Toxoplasma gondii* reduces IRG protein expression and loading in the absence of TgIST

Khaminets [31] showed that the initiation of IRG loading onto PVs has a stochastic time dependence: some vacuoles are loaded by IRGs within a couple of minutes after entry and PV formation, whereas other vacuoles are loaded nearly half an hour later.

We hypothesized that an extended stochastic delay in IRG loading may provide the necessary time for modification of the PVM induced by the enclosed parasite, enabling some kind of “maturation” of the vacuole that might ultimately completely prevent its loading by IRGs, and thereby perhaps provide some explanation for the persistent observation of about 20% of vacuoles carrying no IRG proteins.

Previous studies showed that when *T. gondii* invade cells that are not primed with IFNγ,the parasites block signaling downstream of IFNγ via TgIST [46,61] which, as shown above, in turn blocks expression of IRG proteins [46] .

However the presence of TgIST prevents a direct experiment on any - hypothetical vacuole maturation due to pathogen residence, since even a short preincubation of wild-type parasites suppresses IRG expression. We therefore exploited a TgIST mutant strain, TgΔIST generously provided by Dr Ali Hakimi. With this strain we expected to be able to vary intracellular residence times at will in relation to IFNγ exposure without inhibiting IRG protein induction and expression via TgIST. In this way, we were able to explore whether extended residence of the parasite in a vacuole could reduce the ability of the vacuolar membrane to accumulate IRG proteins.

2.4.8.1. TgIST is not the only parasite-derived factor limiting expression of IRG proteins

In the following experiment, we were unable to show a systematic, time-dependent maturation effect, but we did reveal that infection with TgIST-deficient parasites also imposes a limitation on IRG protein loading, albeit weaker than the effect due to TgIST. In the experiment we consider “standard conditions”, ie cells were infected for 1,5hrs only after IFNγ pre-induction for either 4,5hrs (4,5+1,5) or 10,5hrs (10,5+1,5), or cells were infected at the time of IFNγ induction, ie 0 hr preinduction, 6 or 12 hrs co-incubation (0+6, 0+12). Infection was with wild-type PRUku80, PRUku80TgΔIST and by PRUku80TgΔIST complemented with TgIST.

In both 0+6 and 0+12 protocols the infection with mutant PRUku80ΔIST showed significantly higher cytosolic Irgb6 intensities and more Irgb6 positive cells than infection with the wild-type or TgIST-complemented mutant parasites (Figure 2.12. A-D). The numerical results are summarized in (E). As expected, no similar effect was apparent in the 4,5+1,5 or 10,5+1,5 infection protocols. However, it was apparent that in all cases cells infected with the TgΔIST parasites in the 0+6 or 0+12 protocols failed to develop the frequencies of Irgb6-positive cells or the cytosolic Irgb6 intensities associated with the 4,5+1,5 or 10,5+1,5 protocols, though significantly more than the wild-type or complemented strains. Thus there is indeed a further factor in the parasite that can control the IFNγ-mediated induction of IRG proteins, albeit to a lesser extent than TgIST.

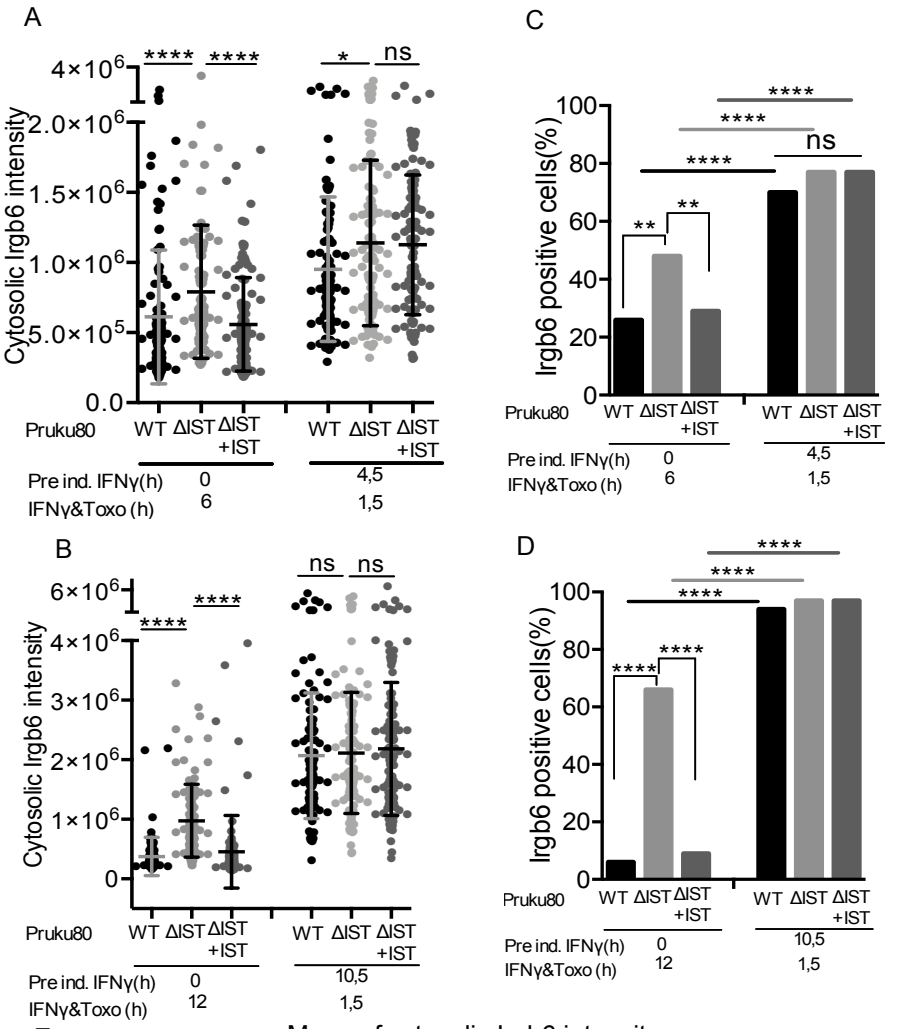

E

Mean of cytosolic Irgb6 intensity

Pre-Ind. IFNγ(h)	0			4,5			0			10,5		
IFNγ&toxo(h)	6			1,5			12			1,5		
PRUku80	Wt	ΔIST	ΔIST+IST	Wt	ΔIST	ΔIST+IST	Wt	ΔIST	ΔIST+IST	Wt	ΔIST	ΔIST+IST
Mean	611974	790923	558549	952020	1139000	1127000	376043	976172	454457	2067000	2114000	2182000

Figure 2.12. *T. gondii* impact the cytosolic Irgb6 via TgIST and TgIST independent factor, independently of time.

DDCs were seeded and pre induced with IFNγ (200 U/ml) for 4,5, 10,5 (control) and 0 hours. The cells were then infected with Pru ku80 (WT), Pruku80ΔIST or Pru ku80ΔIST + HA-IST at a MOI=10 for 1,5 hours or simultaneously induced with IFNγ and infected with the mentioned *T. gondii* strains for 6 and 12 hours.

The samples were processed for Immunofluorescence for GRA7 and for Irgb6 (conditions as in Figure 2.12). Quantification of cytosolic Irgb6 intensity in infected cells was measured and plotted in the graphics and the mean was presented in the table. **A)**

and **B)** Fluorescence intensities were ploted compare each experimental time point with its control. **C)** and **D)** compare the frequency of Irgb6 positive cytosols with detectable Irgb6 protein (more than 650000au).. **E)** The Irgb6 mean intensity of each condition was listed in the table. *, P < 0.05; **, P<0,01, **** P<0,0001; n.s., nonsignificant.

These experiments were designed to search for an effect on vacuole maturation, not an additional parasite-specific inhibitor of Irgb6 expression. The next experiments examined the levels of Irgb6 expression on individual vacuoles within the same experimental protocols.

After observing the effect of TgIST in the expression of cytosolic Irgb6, we further analysed this protein level on the PVM, under the same infection conditions depicted on Figure 2.12. The results (Figure 2.13) generally followed the same trend previously seen for the cytosolic levels.

In both the 0+6 and 0+12 groups the TgΔIST showed more Irgb6-positive vacuoles than either the wild type strain or the TgΔIST strain complemented with TgIST, and in both cases the levels were markedly lower than the vacuoles in the 4.5+1.5 or 10.5+1.5 groups, both in terms of percentage of positive vacuoles (Figure 2.13. A, B) observed and the intensity levels of Irgb6 on the vacuoles (Figure 2.13. C, D, F and G).

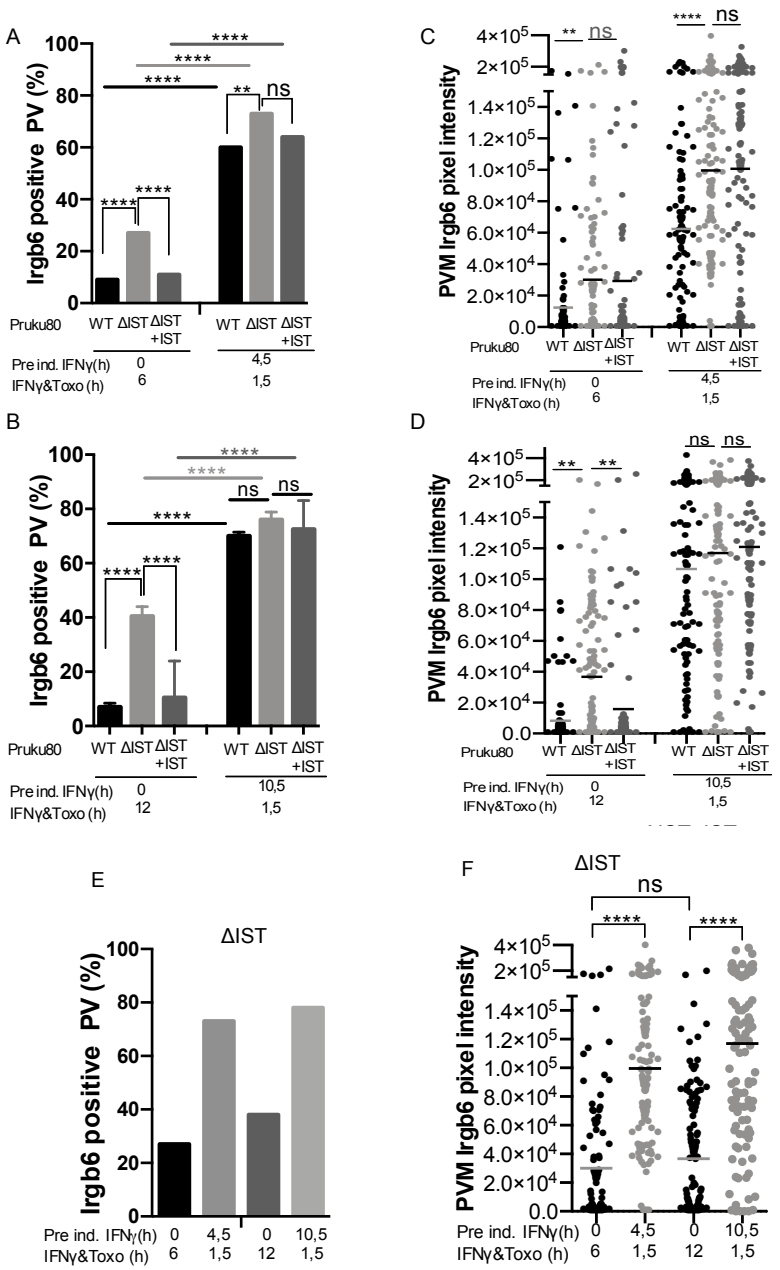

G

Mean of cytosolic Irgb6 intensity

Pre-Ind. IFNγ(h)	0			4,5			0			10,5		
IFNγ&toxo(h)	6			1,5			12			1,5		
PRUku80	Wt	ΔIST	ΔIST+IST	Wt	ΔIST	ΔIST+IST	Wt	ΔIST	ΔIST+IST	Wt	ΔIST	ΔIST+IST
Mean	12345	30081	29266	62430	99657	100732	8271	36687	15864	106700	117025	120892

Figure 2.13. *T. gondii* affect the Irgb6 recruitment to the PVM partially via TgIST.

DDCs were pre-treated with IFNγ and infected following the same condition described in Figure 2.13. The samples were processed for Immunofluorescence for GRA7 and for

Irgb6 (details in Figure 2.12). **A)** and **B)** Quantification of Irgb6 loading onto different *T. gondii* strains PVs was scored for more than 100 intracellular parasites and results were plotted as a proportion of positive PV (in relation to the Gra7 positive PVs). **C)**, **D) F)** and **G)** Fluorescence intensities of Irgb6 were measured in at least 100 PVM as described in Material and Methods; **C)** and **D)** the mean of intensity compare each experimental time point with it's control **E)** The frequency of Irgb6 positive PVs of TgΔIST and **F)** the fluorescence intensities were ploted, comparing different time points. **G)** The Irgb6 mean intensity of each condition was listed in the table. *, P < 0.05; **, P<0,01, **** P<0,0001; n.s., nonsignificant.

While this result seems obvious, it is important to remember that when individual vacuoles from wild-type *T. gondii* were scored for intensity of loading and cytosolic levels there was virtually no correlation. It is not immediately obvious how these discordant results are to be reconciled. One possibility to be explored is that the induction of IRG proteins is delayed by residence of the TgIST mutant parasites in the cytoplasm. Nevertheless, it is clear that there is no additional effect of vacuole-specific maturation beyond a generalised reduction in IRG loading level that is convincingly correlated with the reduced cytosolic levels (Figure 2.13. E and F).

2.4.9. GBP1 is recruited to *T. gondii* PVs and colocalizes to some extent with IRG proteins.

Murine GBP proteins belong to a second large family of IFNγ-inducible GTPases, some members of which target *T. gondii* PVs [26,29,63]. To analyze the reported association of GBP1 with the presence of IRG proteins at PVs, C56BL/6 MEFs and DDCs were stimulated with IFNγ or kept unstimulated for 24 hours, and then infected with a type II *T. gondii* strain for 90 min. Samples were processed by immunofluorescence as described in Materials and Methods. Intracellular parasites were identified with anti-GRA7 Ab, Irga6 with 10 D7 mAb and GBP1 with a rabbit anti-GBP1 antiserum.

As previously shown, GBP1 shows a cytoplasmic distribution strongly enhanced in IFNγ stimulated cells (Figure 2.14. A, middle column). In these cells, GBP1 is robustly expressed and associated with *T. gondii* PVs (Figure 2.14. A, B). GBP1 is recruited to 65% of the vacuoles, Irga6 to 53%, with the expectation on the basis of independence of 34% double-positive GBP1/Irga6, against 47% observed, a small but possibly meaningful excess (Figure 2.14. C). For Irgb6, the data also show 62% of intracellular PVs loaded with GBP1, 80% loaded with Irgb6 and 54% loaded by both GBP1/Irgb6 against an expectation of 50% (Figure 2.14. D and G and Supplemental table 2.2).

These data are thus consistent with the loading of GBP1 being largely or fully independent of Irga6 and Irgb6 loading. The intensity of labelling for GBP1 is correlated with the loading of Irgb6 better than Irga6 (Figure 2.14. F and G).

On those vacuoles where both an IRG protein and GBP1 are loaded the colocalization of GBP1 and Irga6 or Irgb6 on the *T. gondii* PVs, the location was analyzed by super-resolution microscopy. Evidently GBP1 and Irga6 are recruited to the same area of PVs and are very close to each other, but the resolution does not allow a convincing determination whether they are on different membranes, one on the PVM, one on the plasma membrane of the *T. gondii* (Figure 2.14. E).

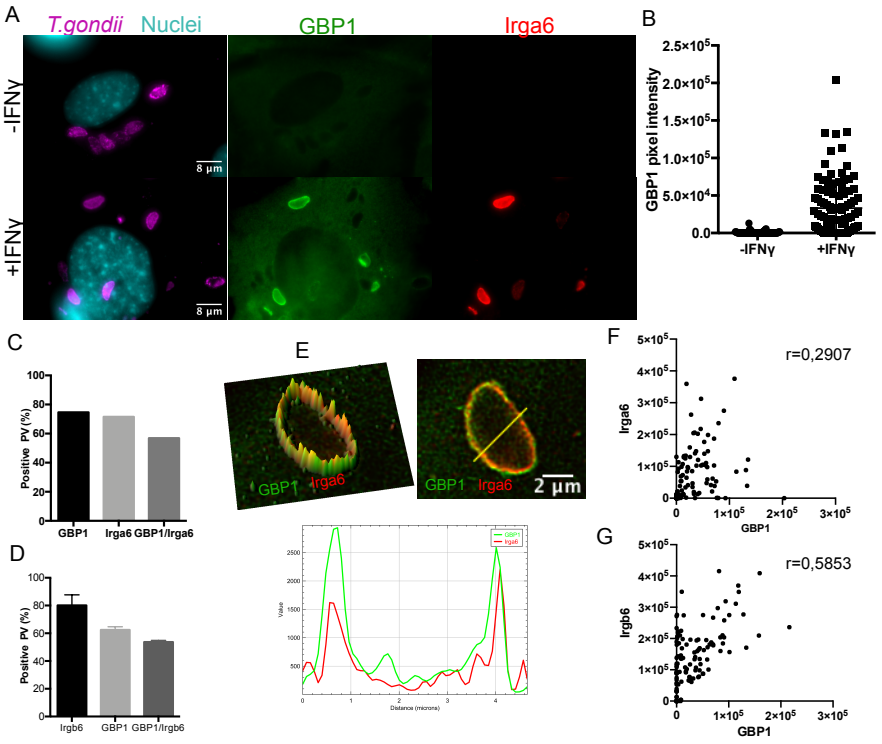

Figure 2.14. GBP1 is recruited to PVs independent of Irga6 and Irgb6.

WT C56BL/6 MEFs were induced with IFNγ (200 U/mL) for 24 hours or left uninduced and infected with *T. gondii* Me49 for 90 minutes. Cells were washed, fixed and stained simultaneously for GRA7 (JH 2.1.2 mAB) using secondary antibodies coupled to AlexaFluorF647 (magenta), GBP1 (pAS) [55] with Alexa Fluor488-conjugated secondary antibody (green) for Irga6 (mAb 10D7) or for Irgb6 (mAb B34) with Alexa Fluor 555-conjugated secondary antibody (red). DAPI was used to label the nuclei (cyan). **A)** Immunofluorescence images are shown merged GRA7 and DAPI, as well as individual GBP1 and Irga6 channels. **B)** GRA7 labelled PVs for IFNγ non-induced and induced conditions were targeted for fluorescent signal intensity of GBP1 measurement, using ImageJ Fiji as described in materials and methods. **C)** and **D)** GRA7 positive PVs were classified as a GBP1, Irga6 or Irgb6 positive PVs, respectively (Supplemental table 2.4). The range between two (C) and 3 (D) independent experiments is shown. **E)** 3D surface plot and plot profile of a transected PV from the representative confocal Image, showing GBP1 and Irga6, was obtained by using ImageJ Fiji. **F)** and **G)** The intensities of each vacuole labelled with GBP1 and Irga6, and GBP1 and Irgb6, were submitted to Pearson correlation analysis. F) P value > 0,002, G) P value < 0,0001.

2.5. Discussion

The process of eliminating *T. gondii* in interferon gamma-induced mouse cells begins with the recruitment of GTPases to the parasitophorous vacuole membrane (PVM) surrounding certain parasites. By an unknown mechanism this induces rupture of the PVM and this is followed by the death of the parasite after exposure to the cytoplasm [39]. Not all vacuoles are loaded with IRG proteins [31] and not all vacuoles are disrupted. These survivor tachyzoites to the IRG attack are probably those that ultimately convert to bradyzoites, form cysts in brain and muscle and establish chronic disease in vivo.
Unravelling and understanding the factors determining IRG recruitment can clarify this whole process. What determines the choice of whether PVs are covered by IRGs or not. Are factors intrinsic to parasites or cells making this determination?

Some previously published data [31] that PV loading is quantitatively and qualitatively heterogeneous has been confirmed. The recruitment of IRGs to the PVs may start immediately after the entry of a parasite into a cell, or with a variable delay. Once started, loading increases for about an hour. The intensity of IRG loading onto PVMs is very variable, from the complete absence of IRG with intensity 0 or close to zero (completely unloaded) until reaching values close to 400000 arbitrary units in MEFs (Figure 2.2. C and E). Despite the phosphorylation and inactivation of the IRGs by virulent RH, a few PVs are covered by a significant intensity of IRGs (Figure 2.2. E), as was noted earlier [31].

Hierarchical loading of Irgs into PVs[31] results in different subsets of PVs. Some PVs are loaded with Irgb6 alone, others with Irgb6 and Irga6, others with Irgb6, Irga6 and Irgd. A similar diversity accompanies loading with Irgb10.

The heterogeneity of the intensity of IRGs in PVs is not explained by the existence of different groups of PVs according to IRG loading, as it is also observed in cells containing single IRGs (Figure 2.5. and 2.6).

It has been supposed that Irgab6 acts as a “pioneer” with a role in anchoring other IRGs to the PVM. However, the recruitment of Irga6 to the PVM is quantitatively independent of the recruitment of Irgb6 (Figure 2.5.) and the removal of Irgb6 affects (but does not eliminate) the recruitment of Irgb10, but not Irga6 (Figure 2.6.). This last result is in complete disagreement with the recently published data using an independently generated Irgb6 knock out [32]. A resolution of these discrepant data is important.

Although Khaminets [31] has shown that the concentration of IRG proteins increases with the concentration of IFNγ and enhanced vacuolar association at the population level, at individual level, it was observed that when a cell with high concentrations of IRG in its cytoplasm is infected by a single vacuole, it can either be loaded by IRG or not (about 22%) (Figure 2.8). We also found that when a cell is infected with 2 parasites, there is no correlation between their IRG intensity on the PVM (Figure 2.8.). Although the intensity of IRG around the PV increases over time [31], the first formed PV does not necessarily have more IRG, a newly formed PV may have more IRG than the earlier entrant [31].

Since neither the variability in time of entry into the cell [31] nor the availability of IRG in the cytoplasm determines whether or not PVMs are loaded, or loaded to what extent, it seems clear that each vacuole independently determines the level of IRG protein loading, both of Irga6 and of Irgb6. Since loading of IRG proteins can begin immediately after entry, this property of “loadability” is already allocated to each PVM at the point of entry, and the heterogeneity is therefore probably a

property of the unit of plasma membrane that forms the PVM rather than a property of the parasite itself. Studies have associated the correct recruitment of IRGs in PVs associated with the presence of ATG proteins. Recruitment of effector IRGs and GBPs for T. gondii PVs is defective in Knockouts Atg3, Atg7 and Atg5 [31,33,64]. Transfer of IRG from the cytoplasm to the PVM occurs by diffusion [31]. The absence of the LC3 conjugation system promotes IRG aggregates, as characterized in Irga6 by recognition by the monoclonal antibody 10D7 [23,31], whether denoting GTP binding or denaturation, somewhat similar to the ones formed in IRGM deficient cells. IRG effector protein concentration were substantially reduced in IFNγ-induced cells, suggesting rapid turnover of the aggregates [31]. This abnormal distribution of effectors, which has not been adequately explained, evidently affects their recruitment to PVs.

It was previously shown that, when *T. gondii* invades cells that are not previously primed with IFNγ, STAT1 transcription signalling downstream is blocked via TgIST [46,61] and ultimately inhibits expression of IRG protein [46], (Figure 2.10., Figure 2.11.) With the prevention of early IRG-mediated elimination, the parasites establish their niche and freely divide in the parasitophorous vacuole (Figure 2.11.). The presence of up to 20% of vacuoles with no loaded IRG proteins stimulated the speculation that, given the heterogeneous delay in the initiation of loading onto vacuoles might for vacuoles with a prolonged delay, allow the development of some unspecified form of “maturation” induced by the resident parasite, whereby if initiation of loading is too long delayed such vacuoles could lose the ability to load IRG proteins. Since there was no reason to suspect that TgIST would be involved in such a process, we used TgIST-deficient *T. gondii* to be able to vary the timing of infection and induction of IRG proteins with IFNγ. Assuming TgIST is the blocker of IRG expression, it was expected to find normal expression and recruitment of IRG in cells infected with

Toxo TgIST KO after 6 and 12 hours of incubation with IFNγ.
However the experimental results showed that the residence of intravacuolar T. gondii parasites in the cell causes a significant reduction in the level of induction of IRG proteins by IFNγ even in the absence of TgIST (Figure 2.12.).

This reduction was also reflected in reduced % of IRG positive PVMs and some reduction in the levels of IRG loading (Figure 2.13.). Neither the concentration of IRG protein in the cytoplasm nor the recruitment of IRG on PVs reached the level expected in cell preincubated with IFNγ that are around 80%. At 12 hours of IFNγ and TgIST parasite coincubation about 60% of PVM are not loaded with IRG proteins (Figure 2.13.)

These preliminary results need to be reconciled with the previous speculation that the concentration of IRG proteins in the cytoplasm is not a limiting factor in recruitment to PVs (Figure 2.12 and 2.13.). The fact is that it appears that T. gondii has another factor that controls the expression of IRG in the absence of TgIST (Figure 2.12. A-D). Even when IRG is already expressed in cells by pre-incubation with IFNγ, the concentration of IRG is affected by the infection, independently of TgIST (Supplemental Figure 2.2.), and the infection impacts both the proportion of vacuoles loaded with IRG proteins and the intensity of loading (Figure 2.12 and 2.13). One possibly additional candidate in the modulation of IFNγ response can be *T. gondii* NCoR/SMRT modulator (TgNSM), described to act together with TgIST in the inhibition of necroptosis [65]. There may also be other modulators, since TgNSM is reported to be secreted only after 8 hours of infection [65] and our data suggested the effect of another factor active even at 6 hours post infection.

Another possibility to account for this anomalous situation is that the

parasite may release agents that reduce the half-life of IRG proteins by increasing their degradation rate.

How *T. gondii* PVs are chosen to be destroyed, whether the heterogeneity of IRG loading has any impact on the outcome of the response and how a small portion of vacuoles survives the immune response remains to be clarified.

2.6. Acknowledgments

I would like to acknowledge: the members of the Howard labs in Lisbon and Cologne for all the inputs in my project; Dr. Colin Adrain as my second adviser for support and encouragement at the early stages of this work. Dr Hakimi for kindly providing the *T. gondii* strains Pru ku80 (WT), Pruku80ΔIST, Pru ku80ΔIST + HA-IST and Pru ku80Δmyr1, Dr Eva Frickel for kindly providing anti-GBP1 antiserum and the services of the facilities of the Advanced Imaging Unit of the IGC, supported by the project PPBI-POCI-01-0145-FEDER-022122, which was fundamental for the development of this study.
This work was supported by funding from FCT (Bolsa FCT: SFRH/BD/114402/2016) and the Gulbenkian Institute of Science, by Sonderforschungsbereiche 670 and 680 and Schwerpunkt 1399 by Deutsche Forschungsgemeinschaft.

2.7. Supplementary material

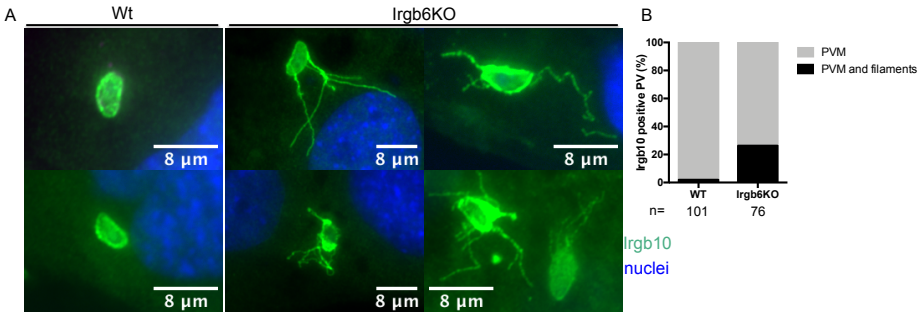

Supplemental Figure 2. 1. Irgb10 location is affected in Irgb6KO cells

IFNγ-stimulated mouse DDCs Wt and Irgb6KO were infected with Me49 tachyzoites (MOI of 5) for 90 min and stained for GRA7 with JH 2.1.2 and for Irgb10 (940/6) with Alexa Fluor 488. **A)** Representative images are shown the nuclei (blue) and Irgb10 (green). **B)** The Irgb10 positive PVs were classified according the location: only on PVM or on PVM associated with filaments and presented in a bar plot.

Supplemental table 2. 1. Duration of IFNγ induction before infection of MEFs with T. gondii.

Treatment	I	II	III	IV	v	VI	VII	VIII	IX	X	XI	XII	XIII
Pre-ind. IFN (h)	24	12	6	0	3	2	1	0	-1	10.5	4.5	0	0
IFNγ & Toxo (h)	1	1	7	13	9	9	9	9	9	1.5	1.5	6	12

Supplemental table 2. 2. Absolute numbers and percentage of colocalization of Irga6 or Irgb6 with GBP1.

PVs	GBP1+	GBP1-	Irga6+	Irga6-	Both	Un/labelled once
Exp1	168	57	133	45	94	84
Exp2	107	65	161	64	128	97
Exp3	122	91	100	113	100	113
Total	397	213	394	222	322	294

PVs	GBP1+	GBP1-	Irgb6+	Irgb6-	Both	Un/labelled once
Exp1	114	64	133	45	94	84
Exp2	67	43	94	16	60	50
Total	181	107	227	61	154	134

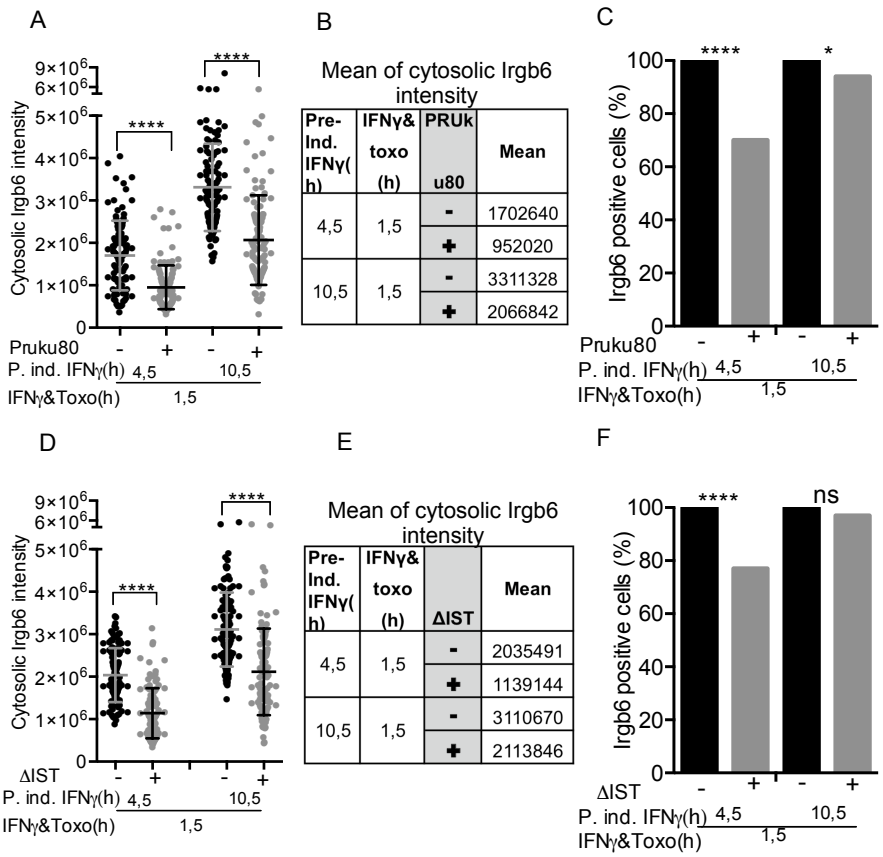

Supplemental Figure 2. 2. Toxoplasma gondii infection impact the IFNγ–induced Irgb6 expression.

DDCs were seeded and pre induced with IFNγ (200 U/ml) for 4,5 and 10,5 (control) hours. The cells were then infected with Pru ku80 (WT) and Pruku80ΔIST at a MOI=10 for 1,5 hours. The samples were processed for Immunofluorescence for GRA7 (**JH 2.1.2 mAB**) and for Irgb6 (serum 141). **A** and **C)** Quantification of cytosolic Irgb6 intensity in infected and non-infected cells were measured and plotted in the graphic and the mean presented in the table. **B** and **D)** The populations of infected and of non-infected cells were classified, according to the intensity, as Irgb6 positive (more than 650000) or Irgb6 negative (less than 650000 au). *, P < 0.05; ****, P<0,0001; n.s., nonsignificant.

Bibliography

1. Rusinova, I. et al. INTERFEROME v2.0: An updated database of annotated interferon-regulated genes. Nucleic Acids Res. 41, (2013).
2. Kim, B. H., Shenoy, A. R., Kumar, P., Bradfield, C. J. & MacMicking, J. D. IFN-inducible GTPases in host cell defense. Cell Host Microbe 12, 432–444 (2012).
3. Schoggins, J. W. Interferon-Stimulated Genes: What Do They All Do? Annu. Rev. Virol. 6, 567–584 (2019).
4. Taylor, G. A., Feng, C. G. & Sher, A. p47 GTPases: regulators of immunity to intracellular pathogens. Nat. Rev. Immunol. 4, 100–109 (2004).
5. Cooper, A. F. & Thakur, R. The group of twenty (G20). The Group of Twenty (G20) 1–194 (2013). doi:10.4324/9780203071236
6. Darnell, J. E., Kerr, I. M. & Stark, G. R. Jak-STAT Pathways and Transcriptional Activation in Response to IFNs and Other Extracellular Signaling Proteins. Adv. Sci. 264, 1415–1421 (1994).
7. Boehm, U. et al. Two families of GTPases dominate the complex cellular response to IFN-gamma. J. Immunol. 161, 6715–6723 (1998).
8. Taylor, G. a., Feng, C. G. & Sher, A. Control of IFN-γ-mediated host resistance to intracellular pathogens by immunity-related GTPases (p47 GTPases). Microbes Infect. 9, 1644–1651 (2007).
9. Tretina, K., Park, E. S., Maminska, A. & MacMicking, J. D. Interferon-induced guanylate-binding proteins: Guardians of host defense in health and disease. J. Exp. Med. 216, 482–500

(2019).

10. Taylor, G. a. IRG proteins: Key mediators of interferon-regulated host resistance to intracellular pathogens. Cell. Microbiol. 9, 1099–1107 (2007).

11. Saeij, J. P. & Frickel, E. M. Exposing Toxoplasma gondii hiding inside the vacuole: a role for GBPs, autophagy and host cell death. Curr. Opin. Microbiol. 40, 72–80 (2017).

12. Kim, B. H. et al. Interferon-induced guanylate-binding proteins in inflammasome activation and host defense. Nat. Immunol. 17, 481–489 (2016).

13. Lindenberg, V. et al. Broad recruitment of mGBP family members to Chlamydia trachomatis inclusions. PLoS One 12, 1–14 (2017).

14. Bernstein-Hanley, I. et al. The p47 GTPases Igtp and Irgb10 map to the Chlamydia trachomatis susceptibility locus Ctrq-3 and mediate cellular resistance in mice. Proc. Natl. Acad. Sci. U. S. A. 103, 14092–14097 (2006).

15. da Fonseca Ferreira-da-Silva, M., Springer-Frauenhoff, H. M., Bohne, W. & Howard, J. C. Identification of the Microsporidian Encephalitozoon cuniculi as a New Target of the IFNγ-Inducible IRG Resistance System. PLoS Pathog. 10, (2014).

16. Biering, S. B. et al. Viral Replication Complexes Are Targeted by LC3-Guided Interferon-Inducible GTPases. Cell Host Microbe 22, 74-85.e7 (2017).

17. Bekpen, C. et al. The interferon-inducible p47 (IRG) GTPases in vertebrates: loss of the cell autonomous resistance mechanism in the human lineage. Genome Biol. 6, 1–18 (2005).

18. Hunn, J. P. et al. Regulatory interactions between IRG resistance GTPases in the cellular response to Toxoplasma

gondii. EMBO J. 27, 2495–2509 (2008).

19. Bougnères, L. et al. A Role for Lipid Bodies in the Cross-presentation of Phagocytosed Antigens by MHC Class I in Dendritic Cells. Immunity 31, 232–244 (2009).

20. Tiwari, S., Choi, H. P., Matsuzawa, T., Pypaert, M. & MacMicking, J. D. Targeting of the GTPase Irgm1 to the phagosomal membrane via PtdIns(3,4)P2 and PtdIns(3,4,5)P3 promotes immunity to mycobacteria. Nat. Immunol. 10, 907–917 (2009).

21. Martens, S. et al. Mechanisms regulating the positioning of mouse p47 resistance GTPases LRG-47 and IIGP1 on cellular membranes: retargeting to plasma membrane induced by phagocytosis. J. Immunol. 173, 2594–2606 (2004).

22. Martens, S. & Howard, J. The interferon-inducible GTPases. Annu. Rev. Cell Dev. Biol. 22, 559–589 (2006).

23. Papic, N., Hunn, J. P., Pawlowski, N., Zerrahn, J. & Howard, J. C. Inactive and active states of the interferon-inducible resistance GTPase, Irga6, in vivo. J. Biol. Chem. 283, 32143–51 (2008).

24. Haldar, A. K. et al. IRG and GBP Host Resistance Factors Target Aberrant, 'Non-self' Vacuoles Characterized by the Missing of 'Self' IRGM Proteins. PLoS Pathog. 9, (2013).

25. Kravets, E. et al. The GTPase activity of murine guanylate-binding protein 2 (mGBP2) controls the intracellular localization and recruitment to the parasitophorous vacuole of Toxoplasma gondii. J. Biol. Chem. 287, 27452–27466 (2012).

26. Degrandi, D. et al. Extensive Characterization of IFN-Induced GTPases mGBP1 to mGBP10 Involved in Host Defense. J. Immunol. 179, 7729–7740 (2007).

27. Vestal, D. J., Gorbacheva, V. Y. & Sen, G. C. Different subcellular localizations for the related interferon-induced GTPases, MuGBP-1 and MuGBP-2: Implications for different functions? J. Interf. Cytokine Res. 20, 991–1000 (2000).

28. Kravets, E. et al. Guanylate binding proteins directly attack Toxoplasma gondii via supramolecular complexes. Elife 5, (2016).

29. Fisch, D. et al. Human GBP1 Differentially Targets Salmonella and Toxoplasma to License Recognition of Microbial Ligands and Caspase-Mediated Death. SSRN Electron. J. 1–28 (2020). doi:10.2139/ssrn.3593524

30. Bassa, A. R. & Shin, S. Human GBP1 promotes pathogen vacuole rupture and inflammasome activation during. (2020).

31. Khaminets, A. et al. Coordinated loading of IRG resistance GTPases on to the Toxoplasma gondii parasitophorous vacuole. Cell. Microbiol. 12, 939–961 (2010).

32. Lee, Y. et al. Initial phospholipid-dependent Irgb6 targeting to Toxoplasma gondii vacuoles mediates host defense. Life Sci. alliance 3, 1–16 (2020).

33. Choi, J. et al. The parasitophorous vacuole membrane of toxoplasma gondii is targeted for disruption by ubiquitin-like conjugation systems of autophagy. Immunity 40, 924–935 (2014).

34. Haldar, A. K. et al. Ubiquitin systems mark pathogen-containing vacuoles as targets for host defense by guanylate binding proteins. Proc. Natl. Acad. Sci. U. S. A. 112, E5628–E5637 (2015).

35. Lee, Y. et al. P62 Plays a Specific Role in Interferon-γ-Induced Presentation of a Toxoplasma Vacuolar Antigen. Cell Rep. 13,

223–233 (2015).

36. Steffens, N. et al. Essential Role of mGBP7 for Survival of Toxoplasma gondii Infection. Biol. Host-microbe 11, 1–14 (2020).

37. Martens, S. et al. Disruption of Toxoplasma gondii parasitophorous vacuoles by the mouse p47-resistance GTPases. PLoS Pathog. 1, 0187–0201 (2005).

38. Selleck, E. M. et al. A Noncanonical Autophagy Pathway Restricts. MBio 6, 1–14 (2015).

39. Zhao, Y. O., Khaminets, A., Hunn, J. P. & Howard, J. C. Disruption of the Toxoplasma gondii parasitophorous vacuole by IFNg-inducible immunity-related GTPases (IRG proteins) triggers necrotic cell death. PLoS Pathog. 5, (2009).

40. Fleckenstein, M. C. et al. A toxoplasma gondii pseudokinase inhibits host irg resistance proteins. PLoS Biol. 10, 14 (2012).

41. Behnke, M. S. et al. Rhoptry Proteins ROP5 and ROP18 Are Major Murine Virulence Factors in Genetically Divergent South American Strains of Toxoplasma gondii. PLoS Genet. 11, (2015).

42. Kim, S.-K., Fouts, A. E. & Boothroyd, J. C. Toxoplasma gondii Dysregulates IFNy Inducible Gene Expression in Human Fibroblasts. J. Immunol. (2007).

43. Zhu, W., Li, J., Pappoe, F., Shen, J. & Yu, L. Strategies developed by toxoplasma gondii to survive in the host. Front. Microbiol. 10, (2019).

44. Liesenfeld, O. et al. The IFN-γ-inducible GTPase, irga6, protects mice against toxoplasma gondii but not against plasmodium berghei and some other intracellular pathogens. PLoS One 6, (2011).

45. Lunde, Milford N. and Jacobs, L. Antigenic Differences between

Endozoites and Cystozoites of Toxoplasma gondii. J. Parasitol. 69, 806–808 (1983).

46. Gay, G. et al. Toxoplasma gondii TgIST co-opts host chromatin repressors dampening STAT1-dependent gene regulation and IFN-γ-mediated host defenses. J. Exp. Med. 213, 1779–1798 (2016).

47. Sabin, A. B. TOXOPLASMIC ENCEPHALITIS IN CHILDREN. J. Amirican Med. Assoc. (1941).

48. Taylor, G. A. et al. Pathogen-specific loss of host resistance in mice lacking the IFN-gamma-inducible gene IGTP. Proc. Natl. Acad. Sci. U. S. A. 97, 751–755 (2000).

49. Johnston, A. C. et al. Human GBP1 does not localize to pathogen vacuoles but restricts Toxoplasma gondii. Cell. Microbiol. 18, 1056–1064 (2016).

50. Alvarez, C. et al. Methods for the Measurement of Early Events in Toxoplasma gondii Immunity in Mouse Cells. 5537, 127–133 (2020).

51. Schindelin, J. et al. Fiji: An open-source platform for biological-image analysis. Nat. Methods 9, 676–682 (2012).

52. Halonen, S. K. et al. Gamma Interferon-Induced Inhibition of. Society 69, 5573–5576 (2001).

53. Ling, Y. M. et al. Vacuolar and plasma membrane stripping and autophagic elimination of Toxoplasma gondii in primed effector macrophages. J. Exp. Med. 203, 2063–2071 (2006).

54. Melzer, T., Duffy, A., Weiss, L. M. & Halonen, S. K. The gamma interferon (IFN-γ)-inducible GTP-binding protein IGTP is necessary for Toxoplasma vacuolar disruption and induces parasite egression in IFN-γ-stimulated astrocytes. Infect. Immun. 76, 4883–4894 (2008).

55. Johnston, A. C. et al. Human GBP1 does not localize to pathogen vacuoles but restricts Toxoplasma gondii. Cellular Microbiology (2016). doi:10.1111/cmi.12579

56. Uthaiah, R. C., Praefcke, G. J. K., Howard, J. C. & Herrmann, C. IIGP1, an interferon-γ-inducible 47-kDa GTPase of the mouse, showing cooperative enzymatic activity and GTP-dependent multimerization. J. Biol. Chem. 278, 29336–29343 (2003).

57. Pawlowski, N. et al. The activation mechanism of Irga6, an interferon-inducible GTPase contributing to mouse resistance against Toxoplasma gondii. BMC Biol. 9, (2011).

58. Lang, C. et al. Impaired chromatin remodelling at STAT1-regulated promoters leads to global unresponsiveness of Toxoplasma gondii-infected macrophages to IFN-γ. PLoS Pathog. 8, (2012).

59. Lüder, C. G. K. et al. Toxoplasma gondii inhibits MHC class II expression in neural antigen-presenting cells by down-regulating the class II transactivator CIITA. J. Neuroimmunol. 134, 12–24 (2003).

60. Rosowski, E. E., Nguyen, Q. P., Camejo, A., Spooner, E. & Saeija, J. P. J. Toxoplasma gondii inhibits gamma interferon (IFN-γ)-and IFN-β-induced host cell STAT1 transcriptional activity by increasing the association of STAT1 with DNA. Infect. Immun. 82, 706–719 (2014).

61. Olias, P., Etheridge, R. D., Zhang, Y., Holtzman, M. J. & Sibley, L. D. Toxoplasma Effector Recruits the Mi-2/NuRD Complex to Repress STAT1 Transcription and Block IFN-γ-Dependent Gene Expression. Cell Host Microbe 20, 72–82 (2016).

62. Franco, M. et al. A novel secreted protein, MYR1, is central to Toxoplasma's manipulation of host cells. MBio 7, 1–17 (2016).

63. Virreira Winter, S. et al. Determinants of GBP recruitment to Toxoplasma gondii vacuoles and the parasitic factors that control it. PLoS One 6, (2011).

64. Haldar, A. K., Piro, A. S., Pilla, D. M., Yamamoto, M. & Coers, J. The E2-like conjugation enzyme Atg3 promotes binding of IRG and Gbp proteins to Chlamydia- and Toxoplasma- containing vacuoles and host resistance. PLoS One 9, (2014).

65. Rosenberg, A. & Sibley, L. D. Toxoplasma gondii secreted effectors co-opt host repressor complexes to inhibit necroptosis. Cell Host Microbe 1–13 (2021). doi:10.1016/j.chom.2021.04.016

Chapter 3

3. Ubiquitination as a mechanism of control of *Toxoplasma gondii* infection.

Ana Rodrigues[1] Claudia Campos[1] and Jonathan C. Howard [1,2]

[1]Fundação Calouste Gulbenkian, Instituto Gulbenkian de Ciência, 2780- 156 Oeiras, Portugal,

[2]Institute for Genetics, University of Cologne, 50674 Cologne, Germany

Author contributions

AR - Study concept and design; Cell culture; Infection experiments; Microscopy and image analyses; Protein quantification; Statistical analysis; Drafting and editing the manuscript.
AC - Parasite propagation; Irgb6 deletion, Cell genotyping
JCH - Study concept and design; Supervision of execution and editing the manuscript.

3.1. Abstract

Ubiquitination is now recognized to be a mechanism involved in cell-autonomous immunity against pathogens. In the mouse it is clearly established that IFNγ priming induces the host cell to respond against *T.gondii*, namely through binding of IRG proteins to the PVM, leading to PVM disruption, death of the parasite and eventually death of the host cell. Ubiquitin also assembles on PVs and some studies have proposed GTPases as possible ubiquitination substrates. Additionally, ubiquitination has been proposed to play a role in the acquired immune response.

We show that about 30 min after the coating of effector IRG proteins onto the PVs of avirulent parasites in IFNγ-induced cells, ubiquitin is recruited to about 70% of parasites coated by IRGs. The ubiquitination on the parasite or PV is typically very weak or absent when the PVM is undisrupted, and strong (intense) on the parasite itself once PVM disruption has occurred. Our results suggest that IRG proteins are not themselves ubiquitinated, but that they are crucial to enable ubiquitination of the parasite through disruption of the PVM. Ubiquitin loading appears to be somewhat dependent on the presence of the pioneer Irgb6 together with concomitant PVM loading by other members of the IRG family (Irga6 and or Irgd), which lead to PVM disruption and allow access of ubiquitin to the parasite itself.

We have been able to demonstrate the presence of K48- and K63-ubiquitin linkages (also known as Lys48- and Lys63) as well as other types of not yet identified ubiquitin linkages on avirulent parasites. We surmise that K48- and K63-ubiquitin coat deposition occurs through machinery that must include not only TRAF6 and TRIM21 but also other E3 ligases. Ubiquitination seems to be independent of parasite strains, but dependent on the efficiency of IRGs to permeabilize and disrupt the PVM and is probably necessary for activation of the host cell

regulated necrosis pathway, but its specific role remains unclear. In-depth research on the precise role of specific ubiquitin linkages and others E3 ligases is needed.

Keywords: ubiquitination; IRGs; *T.gondii***.**

3.2. Introduction

Ubiquitination has recently emerged as a contributor to cell autonomous defense against *Toxoplasma gondii (T. gondii)*, along with the IRG and GBP GTPases [1].

Ubiquitination is a three-step enzymatic process that culminates in the covalent attachment of the 76-aminoacid ubiquitin protein to target proteins, involving the activation of E1, conjugation E2 and ligation E3 enzymes, and is known to regulate many cellular processes. Ubiquitin is either attached to the protein as a single molecule or as polymeric chains of ubiquitin connected by one or more of seven internal lysine residues (Lys6, Lys11, Lys27, Lys29, Lys33, Lys48 and Lys63) and Met1[2]; Ubiquitin attachment can affect every cellular process, through protein turnover by the proteasome or through autophagy (Lys11, Lys27, Lys29, Lys48, Lys63), as well as via non proteolytical signalling regulation (Lys63 and Met1) [2–4].

Ubiquitination plays a role in clearance of microorganisms by autophagy. Several bacteria, including M. tuberculosis and Salmonella, are labeled with Ub chains and are recognized by autophagy receptors on the autophagosomal membrane that contain Ub-binding motifs [5]. Immediately after damage of the Salmonella vacuole (SCV) the bacterium is targeted by ubiquitin and shipped to the microtubule-associated protein 1 light chain 3 (LC3, Atg8) autophagy system via the autophagy markers p62, NDP52 and OPTN, after which the biogenesis of the autophagosome and bacterium degradation are stimulated [6,7].

Immunity-related p47 GTPases (IRG proteins) and 65 kDa guanylate-binding proteins (GBPs) are the front line of cell-autonomous early response against *T. gondii* [8]. In mice, the IRG protein family consists of a) **effector** 47 kDa IRG proteins, all of which possess the conserved GX4GKS sequence in the P-loop, the first nucleotide-binding motif (G1), and are sometimes referred to as the GKS proteins, b) **regulator**

IRGM proteins, Irgm1, Irgm2 and Irgm3, which possess a non-canonical P-loop sequence GX4GMS, originally called the GMS proteins[9] that prevent premature activation of effectors on cytoplasmic membrane systems, and c) highly polymorphic **decoys, 94 kDa** IRG proteins built of two tandem GKS subunits that inhibit a parasite virulence mechanism known from resistance against *Toxoplasma gondii*[10,11]. The accumulation of effector IRG proteins on PV, regulated by regulator proteins (Irgm1, Irgm2 and Irgm3) GBPs, and autophagy components (Atg3, Atg5, Atg7 and Atg16L1)[12–14] is required for the full scale of PVM disruption and subsequent death of the parasite, followed by necrotic death of the host cell[15–17].

T. gondii parasites possessing virulent alleles of the pseudokinase ROP5, ROP17 and ROP18 can block the ability of the IRG system to attack the PVM [18–22] by phosphorylating essential threonines in the nucleotide-binding domain of effector IRG proteins[23,24]. The role of the tandem IRG protein is to deflect the virulence kinase to itself and thereby competitively inhibit the phosphorylation of the effectors. Active tandem decoy proteins have been found in several wild-derived strains of mouse, but are expressed at very low levels in laboratory strains, which are consequently highly vulnerable to *T. gondii* strains carrying active virulence kinases, such as type I strains.

In interferon-induced cells infected with a type 2 or type 3 (avirulent) strain of *T. gondii*, the subset of ubiquitinated PVs has been reported to be correlated with the subset of PVs that is loaded with IRG proteins. In addition, the PVM of type I virulent *T. gondii* is under-loaded with IRG proteins, as well as with ubiquitin [24], It has therefore been proposed that IRG proteins concentrated at the PVM are the main substrate of ubiquitination [1,25,26]. Nevertheless, there has been no formal evidence for this claim and it is still unclear whether ubiquitin recruitment to PV is associated with ubiquitination of IRG or indeed any other membrane proteins.

IFNγ-primed murine cells ubiquitinate vacuoles loaded by several members of the effector IRG proteins that are responsible for PVM disruption. K48- and K63-linkage ubiquitin coat deposition onto the vacuole involves a machinery that must include not only TRAF6 and TRIM21 but also other E3 ligases. In this chapter we will confirm earlier published results, as well as show that ubiquitin concentration at the PV is dependent on the ability of IRGs to permeabilize and disrupt the PVM, and that most of the ubiquitin, if not all, is associated with the parasite membrane and not with the PVM, to which the IRG (and GBP) proteins are bound. The situation thus resembles that in bacterial immunity, where ubiquitination of the organism depends on breakdown of the vacuolar membrane [27]. We therefore surmise that both IRG proteins and at least one of the PVM-associated GBP proteins are probably NOT significant targets of ubiquitination in cell-autonomous immunity against *T.gondii*.

3.3. Material and Methods

3.3.1. Material

3.3.1.1. Mammalian cells and media

Mouse fibroblasts: mouse embryonic fibroblasts (MEFs) and diaphragm-derived cells (DDCs) from C57/BL6 and a wild-derived Indian strain (CIM) were cultured in Dulbecco's modified Eagle's medium (DMEM), high glucose w/o L-glutamine w/o sodium pyruvate (DMEM) supplemented with 10% heat-inactivated fetal bovine serum or HI-FBS, 2mM L-glutamine, 1mM sodium pyruvate, 1x non-essential amino acids, and 1x penicillin/streptomycin. Human Foreskin fibroblast (Hs27) (CVCL_0335) were maintained in Iscove's Modified Dulbecco's medium, high glucose (IMDM) supplemented with 5% heat-inactivated

fetal bovine serum, 2mM L-glutamine, 1mM sodium pyruvate and 1x non-essential amino acids without antibiotic addition.

Table 3.1. Cell types used to perform experiments

Cell type	Ref.	Note
From C57/BL6		
Immortalized WT MEF	[28]	Prepared from mice at day 14 post coitum and immortalized with pSV3-neo plasmid transfected with FuGENE 6 or XtremeGene 9
Immortalized WT DDC	[29]	Cells were prepared from diaphragm tissue of adult mouse
Immortalized *Irga6KO* MEF	[28]	Cells were generated from *Irga6-/- mice* and Immortalized as above
Immortalized *IrgdKO* MEFs	[30]	Kindly provided by Dr. Greg Taylor, cells were immortalized with pSV3-neo plasmid using FuGENE 6 or XtremeGene 9
Immortalized Wt ctrl and *Irgb10KO* ear Fibroblasts	[31]	Kindly provided by Dr. Thirumala-Devi Kanneganti, cells were immortalized with pSV3-neo plasmid using ScreenFect®A Transfection Reagent kit (InCella)
Immortalized *Irgm1/m3KO* MEFs	[32]	Kindly provided by Dr Gregory Taylor, cells were immortalized with pSV3-neo plasmid using FuGENE 6 or XtremeGene 9
Immortalized Wt ctrl and *TRAF6KO* MEF	[33]	Kindly provided by Dr. Jörn Coers, genotype confirmed by PCR
Immortalized Wt ctrl and *TRIM21KO* MEF	[34]	Kindly provided by Dr Eva Frickel, genotype confirmed by PCR
Immortalized *Irgb6 KO* DDCs		Cells were prepared from diaphragm tissue of adult mouse Howard Lab

Cell type	Reference	Note
From CIM		
Immortalized WT DDCs	[35]	Kindly provided by Dr. Tobias Steinfeldt
Immortalized *Irgb2-b1CIM KO* (T17), T17+ Irgb2-b1CIM, T17+ Irgb2-b1P20, T17+ Irgb2-b1BL6	[36]	Kindly provided by Dr Tobias Steinfeldt
Immortalized WT DDC	[36]	Cells were immortalized with pSV3-neo plasmid using ScreenFect®A Transfection Reagent kit (InCella)
From Human		
Hs27	[35]	ATCC (CRL-1634)

The following conditions were used:

- 20.000 cells/well plated on 13mm coverglass into 24 well plates
- 20.000 cells/well plated on Lab-TekII chamber slides (4 well)
- 10.000 cells/well on Lab-TekII chamber slides (8 well)
- 18.0000 cells/well on 12 well plates
- 25.000 cells/well plated on multichannel microscope slides (MMS) (6-channel µ-Slide VI0.4 slides from IBIDI).

3.3.1.2. Toxoplasma gondii (T.gondii) strains

Table 3.2.*T . gondii* used to perform experiments

Strain Name	Origin	Reference	Note
Type II			
Me49	Sheep	[36]	
PRU YFP	Human	[37]	Transgenic RH strain expressing td Tomato

Strain Name	Origin	Reference	Note
Type I			
RH	Human	[38]	
RH-YFP	Human	[37]	
RHΔROP5	Human	[39]	Transgenic RH strain, the *ROP5* locus has been deleted
RHΔGRA7	Human	[40]	
BK	Human	[40]	

Adapted from [41]

3.3.1.3. Plasmids

Irga6-ctag1-GFP (Howard Lab) and RFP-Ubiquitin [42] (kindly provided by Dr Jacques Neefjes) were used.

3.3.1.4. Antibodies:

For all the experiments, the following antibodies were used:

Rat monoclonal anti-GRA7 (2.1.2) at 1/500, rabbit serum anti-Irga6 (165/4) at 1/4000, rabbit serum anti-Irgb6 (141/3) at 1/2000, rabbit serum anti-Irgb10 (940/6) at 1/2000, rabbit serum anti-Irgd (081/3) at 1/3000, rabbit serum anti-Irgb1 (954/1) at 1/4000, mouse monoclonal anti-Irga6 (10D7) at 1/1000, (from the Howard laboratory) mouse monoclonal anti-Irgb6 (B34) at 1/2000 [43], rabbit serum anti-GBP1 (Kindly provided by Dr. Eva Frickel) at 1/500, mouse monoclonal anti-ubiquitin (FK2) (BML-PW8810) from Enzo at 1/300, rabbit monoclonal anti-ubiquitin linkage –specific K48 (ab140601) from Millipore at 1/500, rabbit monoclonal anti-ubiquitin linkage –specific K63 (ab179434) from Millipore at 1/100 and mouse monoclonal anti-SAG1 TP3 at 1/250. Antibodies references followed by slash-number indicate the number of the rabbit bleed.

For primary antibody detection by immunofluorescence we used Goat anti-rabbit Alexa 488, donkey anti-rabbit Alexa 488, goat anti-rat Alexa 647, donkey anti-mouse Alexa 555, donkey anti-mouse Alexa 488, (Molecular Probes) all at 1:1000.

3.3.2. Cell-biological methods

3.3.2.1. Cell culture maintenance

Cells were kept in culture through continuous passage. To passage cells, the stock flask was washed with sterile PBS 1X at RT and then detached with a solution of 1X trypsin-EDTA for 3-5 min at 37ºC, 10%CO2. Cells were harvested and centrifuged at 20-25ºC at 400g for 5 min, and the pellet was resuspended in DMEM and split to a new flask to keep in culture. For freezing, the pellet was resuspended in cold solution of 90%FBS-10%DMSO, which was then aliquoted into cryotubes and placed into a Nalgene Mr. Frosty freezing container to transfer for a slowly cooled down to -80ºC, before storing in liquid nitrogen. When necessary, cells were thawed by rapid resuspension in 15ml of complete DMEM at 37ºC water bath and placed in a 75 cm2 (T75) flask. After attachment, the medium was replaced.

3.3.2.2. Propagation of T. gondii

Tachyzoites from the strains of *T. gondii* enumerated in Table 2 were maintained by serial passaging in T25 confluent monolayers of Hs27 strain human foreskin fibroblasts (HFFs) cultivated in Iscove's modified Dulbecco's medium, high glucose (IMDM) supplemented with 5% FCS, 2 mM L-glutamine, 1mM sodium pyruvate, and 1x non-essential amino acids without antibiotic added at 37ºC in an atmosphere saturated with 10% CO2.

Every 48 hours, a time period more or less coincident with lysis of Hs27 cells, the tachyzoites in suspension were collected. The remaining Hs27 cells were scraped from the flask, and then the suspension was harvested and passed through a 25G syringe needle several times. The parasite suspension was subjected to two differential centrifugations: the first (100 g for 5 min RT) to get rid of cell debris and a second one (700g for 15 min RT) to obtain a small pellet enriched in tachyzoites. Tachyzoites were resuspended in 2ml of medium, a sample counted in a Neubauer chamber, and immediately used for infection of target cells.

3.3.2.3. Transfection of mammalian cells

Transient DNA transfection of cells was conducted using ScreenFect®A Transfection Reagent according to the manufacturer's instructions. Appropriate numbers of target cells were seeded on a 12 well plate 24 hours before transfection in order to obtain 50-70% confluent wells on the day of transfection. A complementary DNA (cDNA) solution (containing cDNAs encoding the fusion proteins Irga6-ctag1-GFP and RFP-Ubiquitin) and a ScreenfectA solution were prepared, mixed and incubated for 20min, after which the mix was added in a dropwise fashion to the target cells. After 24 hours the medium was changed and expression of the protein observed in a fluorescence microscope. Cells were trypsinized, counted and transferred to 6-channel µ-Slide VI0.4 slides for experiments.

3.3.2.4. Cell induction with IFNγ and Infection with T.gondii

Murine fibroblasts were seeded onto UV-sterilized 13mm diameter cover glasses, 12 well plates, Lab-Tek chambers or multichannel microscope slides (MMS), then induced with mouse IFNγ (Cat. 315-05

Peprotech) at 40 ng/ml (200 U/ml) for 18 to 24 hours or were left untreated. The cells were then inoculated with a small volume of the fresh suspension of *T. gondii* ME49, RH and BK tachyzoites at a multiplicity of infection (MOI) of 1,5 to 10 and for the required time of the essay, at 37°C, 10% of CO2. For experiments that require live-cell imaging acquisition, the tachyzoite suspension was filtered through a 3µm pore size filter (Nucleopore Cat No. WHA110612) to get "clean" parasites, i.e., devoid of Hs27 cell debris.

3.3.3. Immunofluorescence

For visualization of IRG proteins and ubiquitin coating on the PVM by fluorescence, cells were allowed to adhere onto a coverslip or onto multichannel microscope slides (MMS) for 24 hours. For more sensitive cells, MMS were pre-treated with 250µg/ml of Poly-D-Lysine for 1hour, following the manufacturer's instructions. The 24 hrs IFNγ- stimulated as well as the unstimulated cells were infected with the indicated strain of *T.gondii* for the indicated amount of time, after which they were extensively washed (2x) with PBS and fixed in 4% paraformaldehyde (PFA) for 30 min at room temperature (RT). Before immunostaining, the cells were washed twice with PBS, permeabilized in 0.1% saponin for 10min and then blocked in blocking buffer (3% bovine serum albumin (BSA) and 0,1% saponin) for 1h at room temperature (RT). These cells were then stained with the indicated antibody reagents specific for *T. gondii* GRA7, for one or more IRG proteins (165/4 , 141/3 , 940/6 , 081/3), for GBP1 and for Ubiquitin (FK2) diluted in blocking buffer, for at least 1 hour at RT.

Subsequently, after three washes with blocking buffer, the antibodies were detected with Alexa Fluor-conjugated secondary antibodies [647 goat anti-rat, 488 donkey anti-rabbit, 488 goat anti-rabbit, 555 donkey anti-mouse, all from Molecular Probes/Invitrogen] diluted in blocking

buffer, for at least 45 min at RT. Cell nuclei/DNA were labelled by 4',6-diamidino-2-phenylindole (DAPI D3571— 889 Life Technologies). The stained cells were washed and mounted into a microscope glass slide with Prolong Gold antifade reagent. Experiments made on other supports follow the same procedures. Lab-Tek chambers were disassembled and covered with cover glass with Prolong gold antifade reagent.

3.3.4. Necrosis assay using PI

3.3.4.1. Preparation of cells

IFNγ-stimulated and non-stimulated cells seeded in an MMS were infected with pore-filtered type I and/or type II (Me49, PRU-YFP, RH) at the indicated desired MOI (from 2 to 10). The filtered tachyzoites were added in a suspension containing complete DMEM supplemented with 0.1 mg/ml of Propidium iodide (PI) (P4170—sigma), 1 µg/ml of Hoechst 33342 trihydrochloride (sc-200,908—Santa Cruz Biotechnology) and 25 mM HEPES [29].

3.3.5. Necrosis and *T. gondii* assays by Flow Cytometry

1,8 x10^5 cells were plated on day -2, stimulated or unstimulated with 200 U/ml IFNγ for 24 hours and infected with Me49 at MOI from 15 to 20 for 7 hours. After that time, the cells and supernatant were harvested with Accutase (BioLegend), pelleted for 5 min at 500g, washed twice with PBS1X and stained with live dead LIVE/DEAD® dye (1:500) in PBS1X. Resuspended cells in 150µl of LIVE/DEAD® dye were incubated for 30 min at RT in the dark. After rinsing the dye off with three washes with PBS, cells were fixed in 4% PFA for 20 min. The PFA was removed by 3 washes in PBS1X and the cells resuspended in

FACS buffer (PBS + 1% BSA) before flow cytometry analysis.

In cases when the aim was also to determine the levels of parasite infection, the pelleted cells free of PFA were equilibrated in ice-cold permeabilization/wash (P/W) buffer—BD Biosciences for 20 min and incubated with an anti-SAG1 TP3 mouse monoclonal antibody (1:250) dissolved in P/W buffer for 30min at 4º C with constant rocking. After two washes with P/W buffer cells were incubated with AF488 goat anti-mouse secondary antibody for 30 min at 4ºC with constant rocking. The secondary antibody was washed off with P/W buffer and cells were resuspended in 250µl FACS buffer (PBS + 1% BSA) for flow cytometry analysis.

$1x10^4$ cells were acquired in two different excitation channels, 405nm giving the live/dead status and 488nm giving the infected status, using LSR Fortessa X20 and recorded using BD FACsDiva software. Data were plotted and quantified using FlowJO software version 10.5.3.

Based on proper control populations (non-infected cells are SAG1 negative and unstained cells are Live/dead negative) four gates were established to which further analysis was restricted: Q1 including alive infected cells, Q2 necrotic infected cells, Q3 necrotic non-infected cells, and Q4 necrotic non-infected cells. The proportion of necrotic cells was obtained considering only infected cell populations[29].

3.3.6. Microscopy and image analyses

3.3.6.1. Fluorescence microscopy

Widefield images were acquired on a Zeiss Axio Observer Z1 fluorescence microscope, using either a 40x 0.94NA or 63x 1.3NA objective, equipped with a Hamamatsu FlashLT camera, a Zeiss Colibri

fluorescence illuminator, and appropriate fluorescence filters all controlled by the Zen 2011 software.
For each condition slides were blinded and a minimum of 100 vacuoles were scored for quantification of GRA7, IRG, Ubiquitin, IRG/Ubiquitin, and GBP1/Ubiquitin positive vacuoles.

Z-series stack images were acquired on a Leica SP5 confocal, equipped with 488, 568 and 633nm laser lines, using a 63x 1.3NA Oil immersion objective, and spectral detection adjusted for the emission of the Alexa488, 568 and 633 fluorochromes. Images were deconvolved with the Huygens software (v17) to enhance contrast and improve resolution.

3.3.6.2. Structured Illumination Microscopy

Images were acquired on a GE HealthCare Deltavision OMX Structured Illumination system, equipped with 2 PCO Edge 5.5 sCMOS cameras, using a 60x 1.42NA Oil immersion objective, GFP + CY5 fluorescence filter sets. Images were deconvoluted/reconstructed with Applied Precision's softWorx software. Images were reconstructed in 3D using Imaris software.

3.3.6.3. Image acquisition of necrosis assay

Images were acquired on an epifluorescence microscope equipped with a digital camera, imaging software, and a heat source to maintain cells at 37ºC. Pictures with 20x magnification of at least 10 random positions per sample were taken each ~4–5.5 min for no longer than up to ~8–10 h post-infection started after 20min post-infection. When the

experiment did not require all the time series, the cells were returned to the incubator until the last required timepoint imaging.

3.3.7. Blinding and unbiased analysis

For all experiments, the acquisition of images was based on the phase contrast channel. To ensure reliable analysis of images microscopic slides prepared and labeled were blinded with adhesive tape before imaging. When this was not possible the files with acquired images were encoded by another person before quantification. To minimize bias in the semiautomatic quantification by applying the macro (described in detail below), the IRG, GBP1 and Ubiquitin proteins were scored in vacuoles selected based on GRA7 expression. This selection ensured that the observed *T. gondii* parasites were intracellular, and that selection was not based on expression of markers of interest.

3.3.8. Quantification of IRG, GBP1 and Ubiquitin on the PVM

3.3.8.1. Proportion of coated vacuoles

The frequency of PVMs carrying IRG proteins, GBP1 or ubiquitin in IFNγ-stimulated and unstimulated cells was determined by blind scoring of a minimum of 100 intracellular parasites, based on the expression of the *T. gondii* GRA7 protein, for each condition [18].

3.3.8.2. Macro design

An ImageJ macro was created to automate the quantification of protein intensity at PVM, by measurement of fluorescence in a defined area.

The macro assumes an original czi format image loaded into ImageJ in

composite mode and based in the scripts creates 3 regions: PV, PVM, and cytosol in the immediate vicinity of the PVM.

Parasite image is identified in a reference channel and then segmented by a mouse click. The macro enlarges the area of the PV by 0,1 µm into the cytosol to generate a Region of Interest (ROI) designated "PV" Then the macro enlarges the frame by 1µm to create an ROI designated "Cytosol". Lastly, the ROI "PVM" is defined by creating a band of 0,8µm of PV inside the ROI "PV".

The table with results contains different measurements, such as fluorescence intensities, shape descriptors and circularity for the 3 areas (PV, PVM, and cytosol) and for each channel [29] (See Chapter 2. 2.3.4.3.).

3.3.8.3. Quantification of protein intensity.

The amounts of IRG, Ubiquitin and GBP1 immunostaining proteins present on the PVM in IFNγ-stimulated and non-stimulated mouse cells were determined by measuring the fluorescence intensity of the fluorochrome correspondent to each protein by using a semi-automated system on the Fiji 2.0.0- rc69/1,52i software [44]. Pixel intensities of the fluorochrome labelling simultaneously or singularly 165, 141, 940, and 81 rabbit antibodies against Irga6, Irgb6, Irgb10, and Irgd, labelling FK2 against ubiquitin and labelling anti-GBP1 were measured in intracellular (GRA7-positive) vacuoles by using the purpose created macro on ImageJ.

The czi composite fluorescent images were loaded in the Fiji software then the macro was run, and the instructions followed. The GRA7 channel was used to detect PVs and the tolerance adjusted for each case when necessary. The pixel intensity was defined as the total pixel

intensity on the PVM after background subtraction. The value is used as a readout for the amount of protein recruited to each PVM.

Corrected brightness of PVM = x-Ay/B

where x = total light from PVM ROI, y = total light from cytosol ROI, A = area of PVM ROI and B = area of cytosol ROI.

3.3.9. Quantification of necrotic and live cells by Image J, Fiji

The total cell number (Hoechst-labeled nuclei) and necrotic cells (PI-positive nuclei) for each position at first and last time point were transformed in particles by using Threshold then analyzed. The Image J-based quantification of the blue and red nuclei was performed separately.
The image was opened and transformed in 8-bit image. The blue and red nuclei were separated from the background using the command Image - Adjust – Threshold, and the ideal threshold was applied to get the binary image. Some nuclei were separated from the adjacent ones by using the command Process – Binary- watershed.
The nuclei were counted by using the command to Analyze Particles.
The total of necrotic cells was given as the total of necrotic cells observed in the images taken at the last time-point minus the total seen at time 0. At least 1000 cells were counted, and the percentage of necrotic cells was given as the Total of Necrotic cells multiplied by 100 divided by the total of Hoechst positive cells in the time 0.

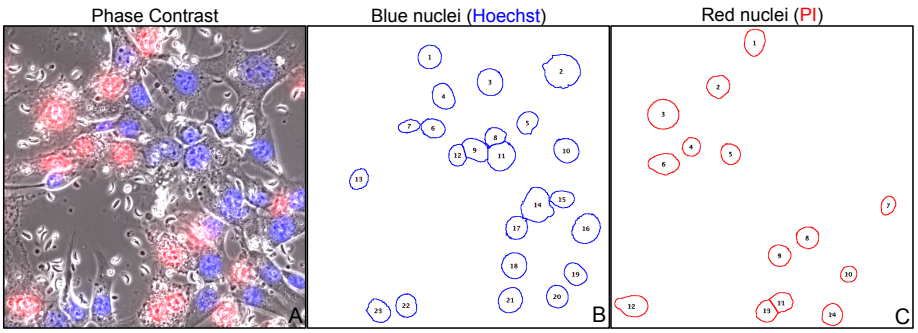

Figure 3.1. Live-cell microscopy-based dual parameter tracking of IFNγ-dependent fibroblast necrosis in response to *T. gondii* infection.

Mouse diaphragm-derived cell cultures (DDCs) were stimulated with 200U/ml of IFNγ and infected with ME49 tachyzoites (MOI of 10). 100 µg/ml PI and 1 µg/ml Hoechst were added to identify necrotic and intact nuclei, respectively. The panel shows merged images obtained from the combination of the Hoechst channel (blue), the PI channel (red), and the phase contrast channel of DDCs at 2,75 hours after infection. Particles in the blue and red channels were defined by color threshold using Fiji 2.0.0-rc69/1,52i software and absolute numbers of blue nuclei in panel (b) or red nuclei in panel (c) were counted to obtain a necrosis proportion within the cell population (see text).

3.3.10. Statistical analysis

Statistical analyses were performed using GraphPad Prism 6.0 and 7.0. Differences of proportion, protein intensities and protein intensities correlation were determined using the Q-square (Fisher exact) t test, Mann-Whitney-test and Pearson correlation coefficient respectively.

3.4. Results

3.4.1. Ubiquitin is recruited to Type II *Toxoplasma gondii* PVs in an Interferon-γ dependent manner.

In previous studies, it was reported that ubiquitin is recruited to avirulent *T. gondii* PVs in IFNγ stimulated MEFs [1] [26]. This recruitment was associated with the presence of IRG proteins on the PVM,

presumably acting as a substrate[25]. To answer the question of whether ubiquitin and IRGs assemble on the same PVs, some previous data were first reproduced. Immortalized wild-type (WT) MEFs and DDCs obtained from C57BL6 mice were stimulated with IFNγ or kept unstimulated (control) for 24 hours. The cells were infected with type II avirulent Me49 or Type I virulent RH Toxoplasma strains for 90 minutes, then fixed and immunostained using a rat anti-GRA7 monoclonal antibody (JH 2.1.2 mAB) detected with a secondary antibody carrying one fluorochrome, to detect intracellular parasites, shown in magenta, as well as immunostained for the set of effector IRGs with rabbit antisera for Irga6 (165/4 pAS), Irgb6 (141/1 pAS), Irgb10 (940/6 pAS) and Irgd (81/3 pAS), with a secondary antibody carrying another fluorochrome shown simultaneously in green, and stained with anti-ubiquitin monoclonal antibody (FK2 mab) detected with a secondary antibody carrying a different fluorochrome in red. The nuclei were stained with DAPI in cyan (Figure 3.2. A). The loading of ubiquitin onto *T. gondii* ME49 and RH PVs was analyzed as a proportion of the total intracellular parasites (detected by staining for GRA7 protein) and plotted as a percentage of maximum (GRA7 positive PVs=100%) (Figure 3.2. C and E) and the pixel intensity determined for each PV as described in Material and Methods (Figure 3.2. B and D).

The immunofluorescence image analyses show a frequency between 50-60% of intracellular Me49 parasites labeled with ubiquitin. The ubiquitin recruitment was much lower on PVs of the type I RH *T. gondii* strain (Figure 3.2. D and E). Ubiquitin accumulation on the PV was entirely dependent on host cell stimulation by IFNγ (Figure 3.2. B and C). The data show a high heterogeneity of the ubiquitin signal on the avirulent ME49 PVM with many vacuoles heavily ubiquitinated, while the RH PVs on IFNγ stimulated cells showed almost no ubiquitin signal (Figure 3.2. D and E). These results confirm previous data[1,26] showing

that ubiquitin recruitment is dependent on IFNγ and is much reduced on PVs of type I strains of Toxoplasma.

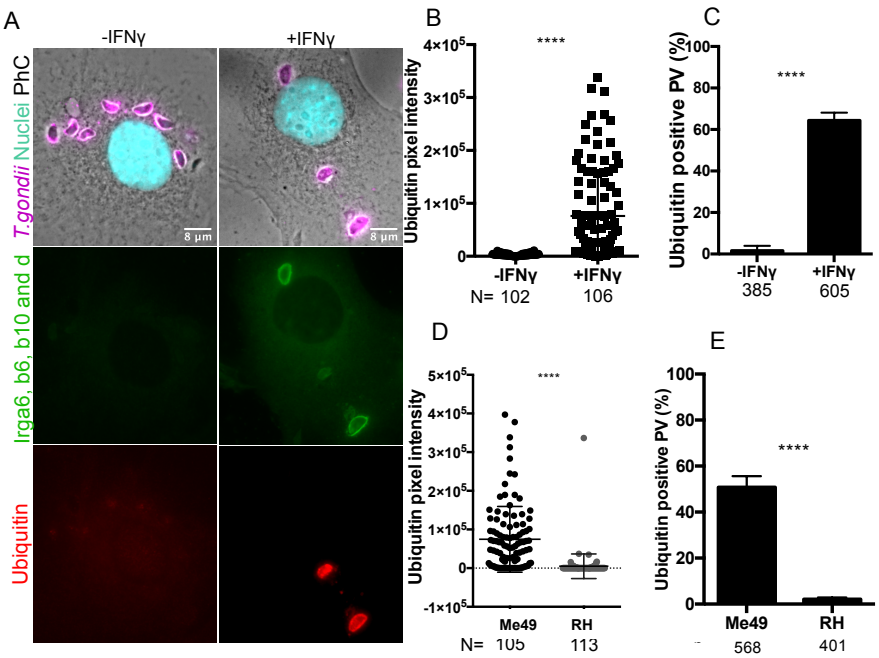

Figure 3.2. Ubiquitin is recruited to Type II Toxoplasma PVs in an interferon-γ dependent manner.

C56BL/6 MEFs (**A, B, C**) and diaphragm-derived cells (DDCs) (**D, E**) stimulated with 200U/ml of IFNγ for 24 hours before infection with **A, B, C**) Me49 and with (**D, E**) either Me49 or RH *T. gondii* strains for 90min. Cells were washed, fixed and stained for Irga6 (serum 165/4), Irgb6 (serum 141/1), Irgb10 (serum 940/6) and Irgd (serum 81/3) with Alexa Fluor 488-conjugated secondary antibody (green), ubiquitin (FK2 mAb) with Alexa Fluor 555-conjugated secondary antibody (red) and GRA7 (JH 2.1.2 mAb) with Alexa Fluor 647-conjugated secondary antibody (magenta). The nuclei were labelled with DAPI (cyan). **A)** Images taken in a fluorescence microscope are shown merged GRA7, DAPI and phase contrast channels, IRGs and ubiquitin individual channels for control and IFNγ treated conditions. **B** and **D)** The fluorescent signal intensities of each PVM in the red channel were measured using the Image J software as described in Material and Methods and analyzed by the Mann-Whitney U test. **C** and **E)** The presence of the ubiquitin was evaluated in every GRA7 labelled PV. Any vacuole in the IFNγ stimulated sample whose intensity was more than 4,5 times the mean intensity in IFNγ unstimulated population was visually distinguished from the cytosol, and was

classified as positive. The graph represents the percentage of ubiquitin-positive with a standard deviation of two independent experiments. ****, P<0,0001

3.4.2. Ubiquitin is recruited to PVs decorated by IRG proteins.

It is now a well established fact that the presence and activation of GTPases on the PV membrane is the key to the immune response of mouse cells against *T. gondii*, and that mouse GTPases act by destroying the PV and killing the parasite [45]. IRG proteins accumulate coordinately and collaboratively at the PVs, but there are always some IRG-negative vacuoles as described in the previous chapter [46]. From previous studies reproduced in this chapter, it appears that more than half of the intracellular PVs are covered by IRG proteins and ubiquitin in an IFNγ-dependent manner. Ubiquitin accumulation is not seen on virulent type I PVs, where accumulation of IRGs is also inefficient. On the basis of this evidence, Coers and Haldar [1,25] reasonably proposed that IRG proteins could be the substrates for ubiquitination in vacuoles.

To clarify whether ubiquitin and IRG proteins accumulate on the same PVs, immortalized MEFs were stimulated with IFNγ for 24 hours to express IRGs and infected with avirulent type II *T. gondii* for 90min. The cells were processed for immunofluorescence using a rat anti-GRA7 monoclonal antibody to detect intracellular parasite, anti-ubiquitin monoclonal antibody, and rabbit antisera against Irga6, Irgb6, Irgb10, and Irgd simultaneously to detect vacuoles carrying any of the set of effector IRGs or for the combination of rabbit antisera against Irgb6 and Irgb10.

The co-staining for effector IRG proteins and ubiquitin shows that approximately 80% of intracellular parasites are covered by one or more of the 4 IRG effectors, as described in detail in the previous chapter. About 60% are ubiquitinated, of which approximately 94% are

vacuoles that are also labelled for the set of effector IRG proteins, representing 55% of the total intracellular parasites (Figure 3.3. A).

Co-staining of Irgb6 and Irgb10 together with ubiquitin shows a similar pattern to the previous one, with almost 74% of PVs covered by IRG, 66% by ubiquitin and 59% by both proteins. However, a small proportion of ubiquitinated PVs are recorded not covered by any of these two Irgs (Figure 3.3. B).

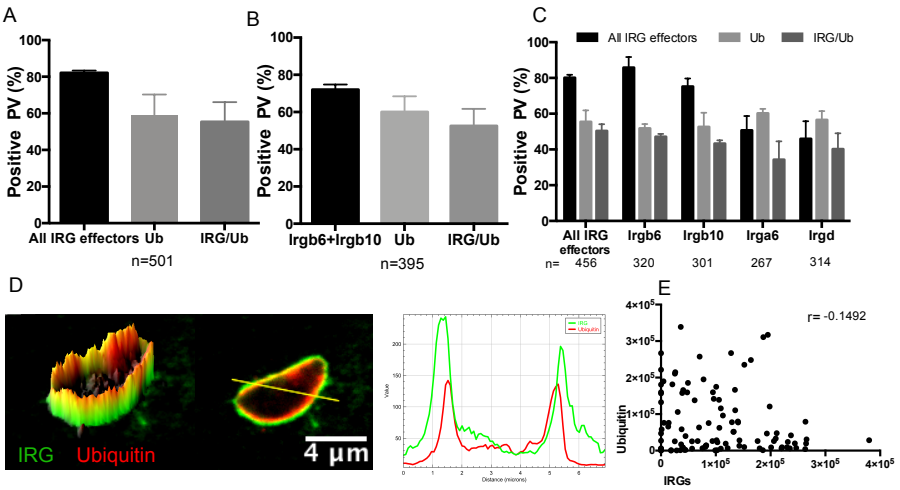

Figure 3.3. Ubiquitin is recruited to PVs decorated by IRG proteins.

C57BL/6 MEFs were induced with IFNγ for 24 hours or kept uninduced. The cells were infected with *T. gondii* ME49 strain for 90 min. The cells were washed, fixed and co-stained with immunoreagents against GRA7 (JH 2.1.2 mAb) with Alexa Fluor 647-conjugated secondary antibody, ubiquitin (FK2 mAb) with Alexa Fluor 555-conjugated secondary antibody and **(A)** Irga6 (serum 165/4), Irgb6 (serum 141/1), Irgb10 (serum 940/6) and Irgd (serum 81/3) simultaneously; **(B)** Irgb6 (serum 141/1) and Irgb10 (serum 940/6) simultaneously or **(C)** IRGs individually with Alexa Fluor 488-conjugated secondary antibody as shown in Figure 1. **A-C)** From fluorescent images, all GRA7-labelled PVs were visually classified as IRG, ubiquitin and double-positives and the proportion represented in the bar graph. Mean +/- SD of two independent experiments is shown, a total of GRA7–labeled PVs (n shown in the graphics) was counted. **D)** 3D surface plot and plot profile of a transected PV from the representative confocal image was obtained by using ImageJ Fiji. **E)** IRG (Irga6, Irgb6, Irgb10 and Irgd) and Ubiquitin

signal intensities on the PVM were measured, using ImageJ software as described in Material and Methods and analyzed by Pearson correlations analysis. P value >0,1

Different IRGs are recruited to the same PVs, resulting in 4 different kinds of PV, no IRG protein, b6 only, b6+a6 only, b6+b10+a6 only and b6+a6+d. To determine whether the PVs that have more IRG proteins on them are more likely to have ubiquitin, single IRGs were colocalized with ubiquitin by processing IFNγ stimulated and infected MEFs for immunostaining with GRA7 antibody, anti-ubiquitin monoclonal antibody, and rabbit antisera against either Irga6, Irgb6, Irgb10, and Irgd (Figure 3.3. C).

The data for colocalization of Ubiquitin with single IRGs show that the frequency of PVs covered by Irgb6 and Irgb10 is substantially higher than the frequency of PVs covered by ubiquitin, while the reverse is the case for IRG proteins Irga6 and Irgd, both lower in the loading hierarchy defined by Khaminets [46]. These data suggest that the proportion of ubiquitinated PVs roughly matches the proportion of PVs covered by Irgb6, Irga6 and Irgd (Figure 3.3 C), suggesting that vacuoles covered only by Irgb6 (and also Irgb10) represent the majority of PVs that are not ubiquitinated. Expressed in another way, this would suggest that the loading of Irgb6 alone is not sufficient to initiate whatever is required for ubiquitination of the vacuole, and that the other effector IRG proteins play an essential role in the process.

In those vacuoles in which both the IRG protein and ubiquitin are loaded, the location of ubiquitin in relation to the PVM marker, IRG, was analyzed by confocal microscopy. Evidently, ubiquitin and Irga6 are recruited to the same PV area and are very close to each other, but the resolution does not allow to determine if they are in the same membrane or in different membranes, one in the PVM, one in the *Toxoplasma* plasma membrane (Figure 3.3. D). In the image shown

(Figure 3.3. D) the scanned profile suggests that the ubiquitin signal is internal to the IRG signal, but this is not apparent in all ubiquitinated PVs.

The pixel intensity quantification data show that the intensity of labelling for the set of effector IRG proteins is not correlated with the labeling for ubiquitin, suggesting that the amount of ubiquitin accumulating on the PV does not depend on the amount of IRG protein present there, even if they tend to be found on the same vacuoles (Figure 3.3. E). The data suggest that the presence of ubiquitin on the PVM is related to the presence of the set of IRG proteins, but not to any single IRG protein, while the lack of quantitative correlation across the large range of IRG loading intensity argues against IRG proteins themselves being the true molecular targets for ubiquitination.

3.4.3. The presence of the family of effector IRGs, not single IRGs on the PVM, is crucial to its ubiquitination.

In IFNγ-induced MEFs effector IRG proteins and ubiquitin (Ub) are recruited largely to the same PVs. About 60% of avirulent type II Me49 PVs are doubly loaded with IRGs and Ub, and IRG proteins have been proposed as a substrate for this ubiquitination [47].

We set out to reinvestigate whether the absence of individual effector IRGs affects PV ubiquitination using cells derived from Irga6, Irgb6, Irgb10 and Irgd knockout (KO) mice. We also looked at cells with global IRG effector dysregulation due to the absence of both IRG protein regulators, Irgm1 and Irgm3. When these cells are induced with IFNγ, effector IRG proteins are constitutively activated, form cytoplasmic aggregates, and do not accumulate on the PVM [48,49].

We used Irga6 KO and Irgd KO MEFs, Irgb6KO DDCs as well as Irgb10 KO ear fibroblasts [31]. Cells were pre-induced with IFNγ for 24 hours and infected with Me49 for 90 minutes. The cells were prepared for immunofluorescence and stained with anti-ubiquitin mAb FK2, and with mAb anti-GRA7 as a marker of intracellular parasites. Fluorescence microscopy images were used to determine the proportion of intracellular parasites labelled for ubiquitin and to measure the intensity of ubiquitin loading at the PVM.

The frequency of ubiquitin-loaded PVs was not significantly reduced in Irga6 KO, Irgb10 KO and Irgd KO cells compared to WT cells (Figure 3.4. A, C and E), but was significantly reduced in the absence of the pioneer Irgb6 protein (Figure 3.3. G). On the other hand, the intensity of ubiquitin at the PVM was reduced in Irga6 KO MEFs, Irgd KO MEFs and Irgb6 KO DDCs compared with WT MEFs and WT DDCs (Figure 3.4. B, F and H), but not in Irgb10KO (Figure 3.4. D).

These results reinforce the notion that a single IRG protein, be it Irga6, Irgb10 or Irgd, or even Irgb6, does not constitute a (unique) target of ubiquitin at the PV nor is it uniquely crucial to the ubiquitination process. The data strongly support the idea that ubiquitination of the PV follows from a synergistic interaction between effector IRG proteins.

As expected and in complete agreement with previous results [1], we found that in the absence of the regulators Irgm1 and Irgm3, not only are the effector IRGs absent from the PVM [49] but also the accumulation of ubiquitin is completely lost (Figure 3.4. I and J). Taken together, these results suggest that the presence of Irgb6 accompanied by other effector proteins, probably Irga6 and Irgd at the PVs, enhanced the ubiquitin accumulation there, which in turn is not strongly affected by the absence of a single IRG protein. Again, the status of Irgb10 as an effector against *T. gondii* is unclear.

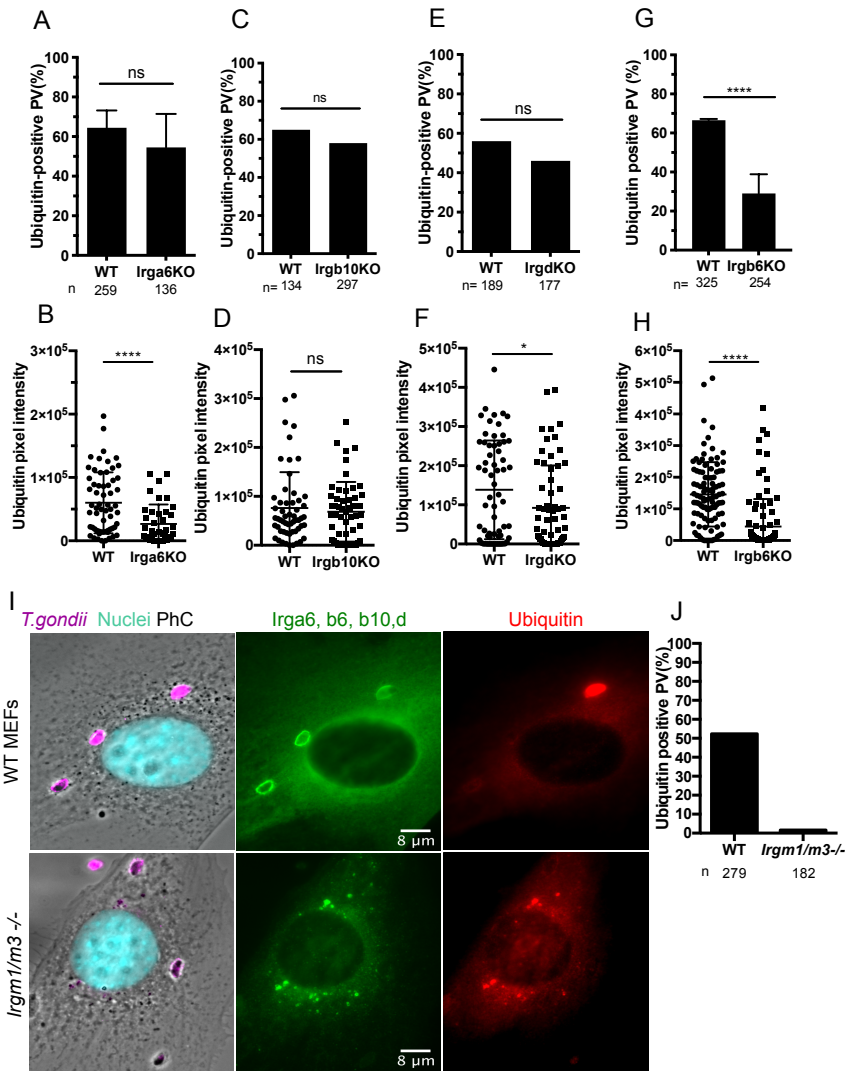

Figure 3.4. Ubiquitination may be slightly reduced in the absence of single Irg proteins (A-F), strongly reduced in absence of the pioneer Irgb6 (G, H), but is eliminated in Irgm1/Irgm3-deficient cells in the absence of the family of effectors IRGs on the PV.

WT, Irga6, Irgd, Irgm1/Irgm3 knock-outs (KO) MEFs, WT, and Irgb10KO ear fibroblasts, WT, and Irgb6KO DDCs were induced with 200 U/ml IFNγ for 24 hours and then infected with Me49 for 90 min. Cells were stained for: ubiquitin (FK2 mAb) with Alexa Fluor 555-conjugated secondary antibody, GRA7 (JH 2.1.2 mAb) with Alexa Fluor 647-conjugated secondary antibody. **A, C, E** and **G)** From the images taken, the proportions of ubiquitin-positive vacuoles in WT and IRGs KO cells were obtained and the contingency data were compared by Fisher's exact test. **A)** and **E)** Mean +/- SD of two

independent experiments is shown. **B, D, F** and **H)** The fluorescent signal intensity from the ubiquitin channel was measured by using ImageJ Fiji as described in Material and Methods. The Mann-Whitney U test was applied. I and **J)** WT and Irgm1/Irgm3 KO infected MEFs were stained for Irga6 (serum 165/4), Irgb6 (serum 141/1), Irgb10 (serum 940/6) and Irgd (serum 81/3) with Alexa Fluor 488-conjugated secondary antibody (green); ubiquitin (FK2 mAb) with Alexa Fluor 555-conjugated secondary antibody (red) and GRA7 (JH 2.1.2 mAb) with Alexa Fluor 647-conjugated secondary antibody (magenta). The nuclei were labeled with DAPI (cyan). Representative images of GRA7, IRG and Ubiquitin staining and Phase contrast (PhC) are shown. **G)** The total of GRA7 positive PVs was classified as a ubiquitin-positive or not and the proportion is shown. Fisher's exact test was applied. * P < 0.05; **** P<0,0001; n.s. nonsignificant.

3.4.4. Ubiquitin colocalizes with mislocalized IRG effector proteins in Irgm1 + Irgm3 deficient cells.

The results so far give no support to the idea that IRG proteins loaded onto the vacuoles of avirulent Toxoplasmas are directly ubiquitinated. Since it is known, at least for Irga6, that the protein bound to the PVM is in the GTP-bound, activated state, unlike the free cytosolic Irga6[50], it is unlikely that the conformational change associated with GTP-binding at the vacuole is a trigger for ubiquitination. It has been shown, however, that in IFNγ-induced cells lacking at least one of the GMS proteins, such as IFNγ-induced Irgm1 KO, Irgm3 KO or Irgm1/Irgm3 KO mouse embryonic fibroblasts (MEFs), GKS proteins form aggregate-like structures in the cytoplasm and are unable to accumulate at the *T. gondii* PVM[49] consistent with unregulated activation by cytoplasmic GTP[50]. Unexpectedly in view of the lack of evidence that activated IRG proteins are ubiquitinated at the PV, these cytosolic aggregates are heavily ubiquitinated. Irgm1/m3 double knockout MEFs were induced with IFNγ for 24 hours then infected with Me49 for 90 minutes. Cells were fixed and stained for ubiquitin with mAb FK2, for GRA7 with mAb anti-GRA7 and for either Irga6 or Irgb6 or Irgb10. Immunofluorescence images revealed within a weak cytosolic background a distribution of

intensely stained Irga6, Irgb6 and Irgb10 aggregates. These aggregate structures were not clearly resolved for Irgd. Ubiquitin also appeared in small aggregate-like structures some of which colocalized with mislocalized IRGs, pointed by white arrows **(**Figure 3.5. A). The quantification of IRG loading onto structures labeled with Ubiquitin, analyzed as a proportion of the total individualized aggregates IRG positive and plotted as a percentage of maximum (ubiquitin positive aggregates =100%) showed significant overlaps of ubiquitin with Irgb6 and with Irga6, to a considerably lesser extent with Irgb10 (Figure 3.5. B). Previous studies have shown that IRG effector proteins in these cells (Irgm1/Irgm3KO) are largely located on lipid droplets[48,51]. To discriminate the different effector IRG locations, IFNγ stimulated and infected cells were co-stained with Irga6 and either Irgb6 or Irgb10 and for GRA7. In accordance with previous results, none of the effector IRGs was found on the PVs. Representative fluorescence Images showed a substantial overlap of activated Irga6, stained with the monoclonal antibody 10D7, with Irgb6 positive structures but not with Irgb10 (Figure 3.5. C). Thus Irga6 and Irgb6 associate with same heavily ubiquitinated structures, probably the lipid droplets[48,51], while Irgb10 associates with other structures. The co-localization of IRG effector aggregates with ubiquitin in the Irgm1/Irgm3 double-deficient cells is consistent with ubiquitination of the IRG proteins themselves. Up to now, we have assumed that the activation of IRG proteins on *T. gondii* vacuoles in genetically intact cells is functionally equivalent to their ectopic activation on organellar membranes in the absence of the regulator IRG proteins [51]. This conclusion is based on the expression by Irga6 in the aggregates of the epitope recognized by the monoclonal antibody, 10D7, which identifies the GTP-bound state of the protein[46]. However, 10D7 also recognizes denatured Irga6, for example on Western blots, where the epitope is also exposed. Thus the binding of ubiquitin to Irga6 and other aggregated IRG proteins in the regulator

deficient cells may reflect denaturation rather than ectotopic activation by GTP. However, the precise colocalization with ubiquitin in aggregates in the Irgm1/m3 double-deficient cells seems to be distinct from the close but incomplete colocalisation on the PVM in Irgm1 and Irgm3 wt cells.

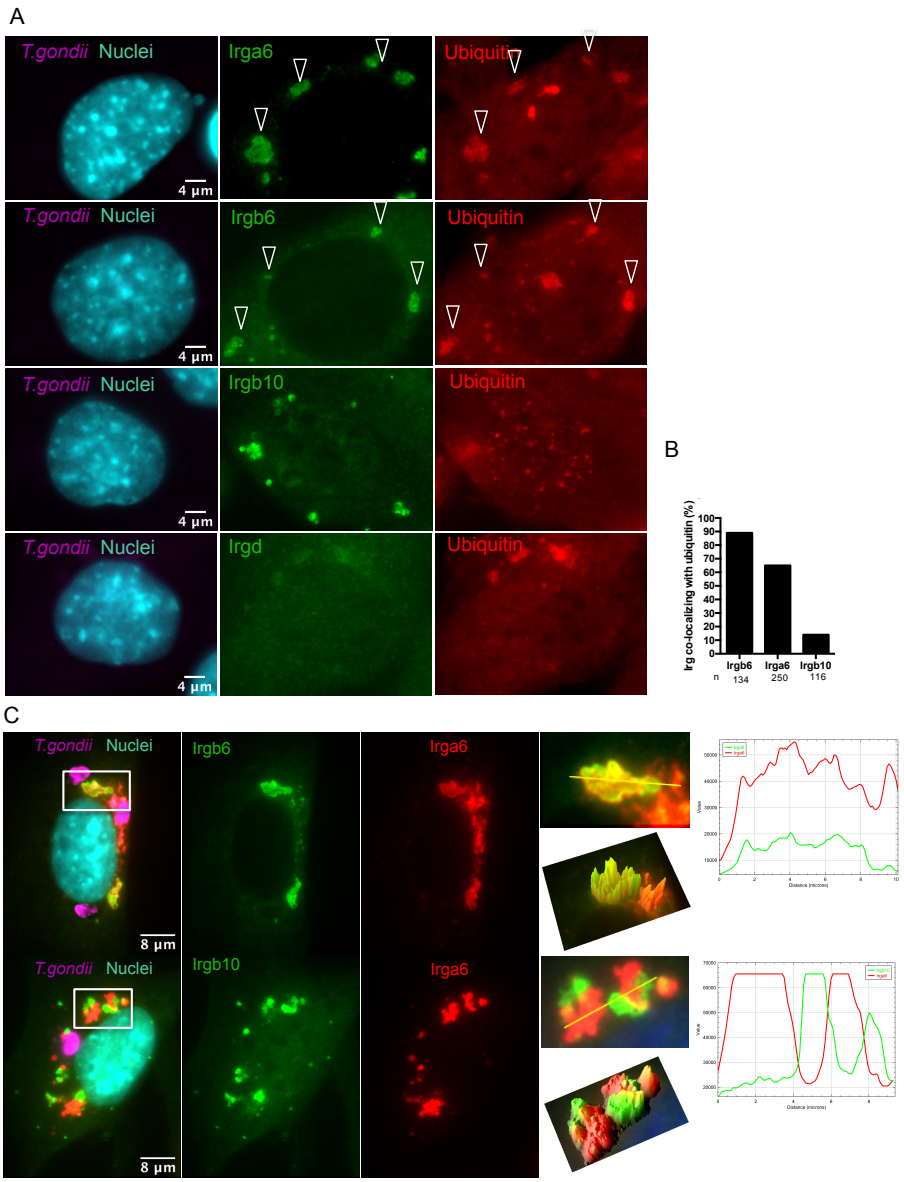

Figure 3.5. Ubiquitin colocalizes with mislocated IRG effectors in Irgm1 and Irgm3 deficient cells.

Irgm1-/Irgm3- MEFs were induced with 200 U/ml IFNγ for 24 hours and then infected with Me49 for 90 min. Cells were stained for: **A)** ubiquitin (FK2 mAb) with Alexa Fluor 555-conjugated secondary antibody; Irga6 (serum 165/4) or Irgb6 (serum 141/1) or Irgb10 (serum 940/6) or Irg

(serum 81/3) with Alexa Fluor 488-conjugated secondary antibody (green); GRA7 (JH 2.1.2 mAb) with Alexa Fluor 647-conjugated secondary antibody. **C)** for Irga6 (10D7 mAb) and Irgb6 (serum 141/1) with Alexa Fluor 555-conjugated secondary antibody and Alexa Fluor 488-conjugated secondary antibody (green) respectively or Irgb10 (serum 940/6) and Irga6 (10D7 mAb) with Alexa Fluor 488-conjugated secondary antibody (green) respectively and GRA7 (JH 2.1.2 mAb) with Alexa Fluor 647-conjugated secondary antibody. **A)** Representative microscopic images of each IRG and ubiquitin are shown. Arrowhead indicates IRG and ubiquitin colocalization on the aggregates. **B)** More than 100 aggregates of Irga6, Irgb6, and Irgb10 were evaluated by eye, and the percentage of these aggregates that co-localize with ubiquitin was presented. **C)** Representative microscopic images of individual channels of Irgb6 and Irga6 (top) and Irgb10 and Irga6 (bottom) and their overlay are shown. The magnified rectangular areas are represented in 3D surface plot (bottom) and profile of the transect, by using ImageJ Fiji.

3.4.5. Ubiquitin accumulates on PVs decorated with GBP1.

It was shown in chapter 2 that GBP1 and Irga6 cover 56,8 % of the PVs, it was also demonstrated in this chapter that almost all vacuoles covered by IRGs are covered by ubiquitin. To verify whether the ubiquitin correlated with the presence of GBP1 at PVs, C56BL/6 MEFs and DDCs were stimulated with IFNγ or kept unstimulated for 24 hours, and then infected with type II *T. gondii* strain for 90 min. Intracellular Immunostaining was processed with anti-GRA7 mAb, FK2 anti-ubiquitin mAb and with serum anti-GBP1.

Immunofluorescence images revealed subcellular and PV distributions of GBP1. Analyses of intensity at PVM show a high accumulation of the protein at PV in cells treated with IFNγ**,** whereas hardly any accumulation of GBP1 in non induced cells in concordance with previous reports [52] (Figure 3.6. A-B). Around 65% of the intracellular parasite PVs were associated with GBP1 and close to 60% of all PVs are also GBP1 and ubiquitin double positives. Only a few GBP1-loaded PV (5%) showed no colocalization with ubiquitin (Figure 3.6. D). Although representative double-positive PVs show both protein in the

same area Figure 3.6. C, the intensity of the GBP1 and ubiquitin was not convincingly correlated (Figure 3.6. E). Indeed the weak correlation is itself elevated by the small subset of very weakly stained or negative PV. These data show that ubiquitin and GBP label the same subset of PVs, but do not show that GBP1 is itself ubiquitinated, as also concluded for IRG proteins. Following the argument expressed above, the data suggest that loading of GBP1 is also dependent on loading of Irgb6 and either or both of Irga6 and Irgd.

Previous studies demonstrated that an extended deletion in chromosome 3, lacking the GBPs 1, 2, 3, 5 and 7 genes, does not affect the accumulation of ubiquitin on PVs [26], suggesting that IRG proteins are sufficient to drive ubiquitination and the GBPs to PVs. This idea is consistent with the fact that GBP1 and ubiquitin label the same PV.

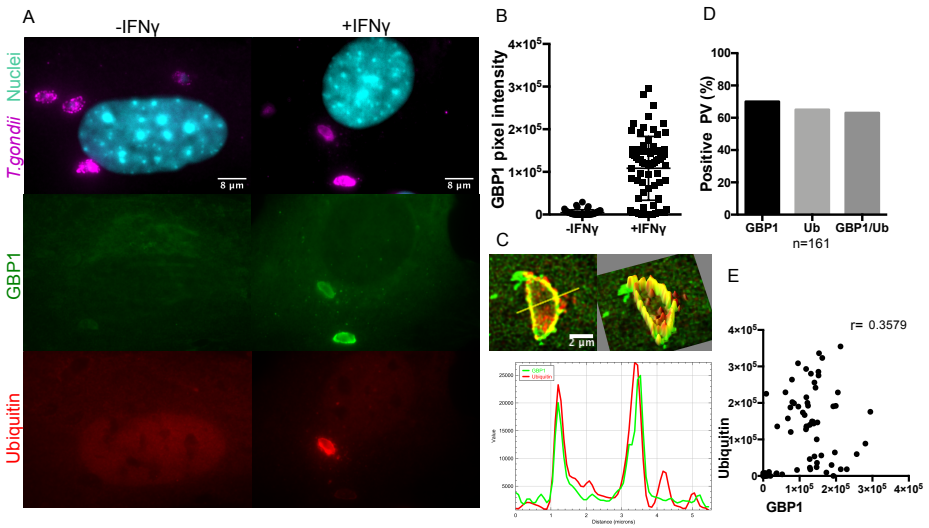

Figure 3.6. Ubiquitin accumulated on PVs decorated by GBP1.

C56BL/6 MEFs were stimulated with 200 U/ml of IFNγ for 24 hours and then infected with *Toxoplasma gondii* Me49 for 90 minutes. Cells were washed, fixed and stained simultaneously for GBP1[53] with Alexa Fluor 488-conjugated secondary antibody (green); ubiquitin (Fk2) with Alexa Fluor 555- conjugated secondary antibody (red) and GRA7 (JH 2.1.2 mAb) with Alexa Fluor 647-conjugated secondary antibody (magenta). The nuclei were labelled with DAPI (cyan). **A)** Representative images of GBP1 and ubiquitin are shown. **B)** GBP1 pixel intensity on PVM was measured and the

significance of difference tested by the Mann-Whitney test. **C)** 3D surface plot and plot profile of overlapping GBP1 and Ubiquitin channels are shown. **D)** The proportion of GBP1, ubiquitin and double positives PVs are shown**. E)** The signal intensity of GBP1 and ubiquitin on the PVM were measured by using Image J Fiji and analyzed by Pearson correlation. P value <0,002.

3.4.6. Ubiquitin recruitment to the PV is dependent on IRG loading

As described by Khaminets [46], and confirmed in Chapter 2, the recruitment of effector IRG proteins to the PV starts immediately after infection. To assess the kinetics of ubiquitin recruitment in relation to the effector IRG from 15 up to 120 minutes after infection, IFNγ induced MEFs were infected for 15, 30, 60 and 120 minutes and processed for intracellular immunostaining for GRA7, ubiquitin, and the set of effector IRG proteins (Irga6, Irgb6, Irgb10 and Irgd) detected together (See 3.1) (Figure 3.7. A). Subsequently, IRG and ubiquitin loading intensities were measured from over 100 GRA7 labeled PVs (Materials and Methods, chapter 2.3.4.3).

A time-course analysis of this experiment revealed a delay of ubiquitin recruitment in relation to IRG proteins (Figure 3.7.). At 15 minutes after infection, a significant proportion of PVs were already covered by IRGs, and that proportion increased with longer durations of the infection. The recruitment of ubiquitin to the PVs followed the loading of the IRGs, appearing visible only after 30 minutes of infection with a small proportion of Ub-positive PVs. The latter increased significantly to a plateau of about 66% of all PVs at 120 minutes, at a time when the proportion of IRG-positive PVs seemed to decrease. At 120 min a small proportion of PVs was loaded only with ubiquitin and devoid of IRG proteins, suggesting that such PVs might have lost the IRG-loaded PVM. This possibility was supported by decrease in the proportion of

PVs loaded with IRGs and the presence of IRG-positive aggregates typical of material from damaged PVs (Figure 3.7. B).

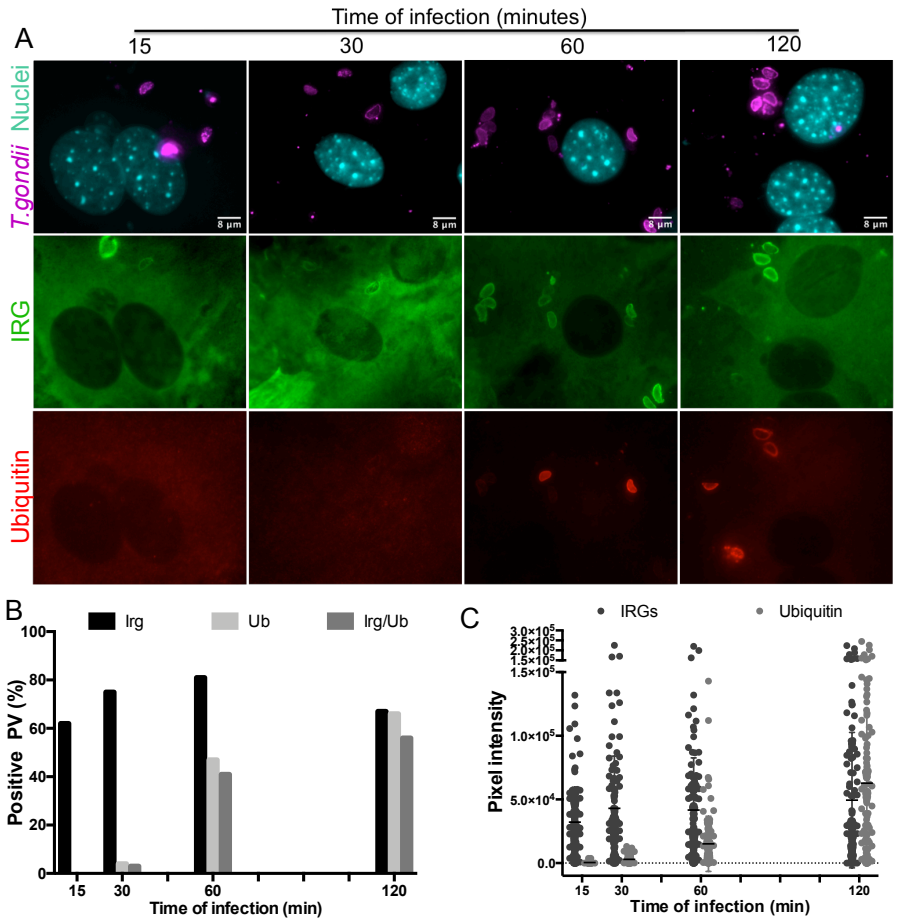

Figure 3.7. Ubiquitin recruitment to the PV is dependent on IRG loading.

C56BL/6 MEFs were stimulated with IFNγ (200 U/mL) for 24 hours and then infected with *Toxoplasma gondii* Me49 for 15, 30, 60 and 120 minutes. Cells were fixed and stained simultaneously for Irga6 (165/4 pAS), Irgb6 (141/1 pAS), b10 (940/6 pAS) and d (81/3 pAS) with each secondary antibody coupled with Alexa Fluor488 (green), ubiquitin (Fk2 mAb) with Alexa Fluor 555- conjugated secondary antibody (red) and GRA7 (JH 2.1.2 mAb) with Alexa Fluor 647-conjugated secondary antibody (magenta). The nuclei were labelled with DAPI (cyan). A) Merged GRA7 and DAPI, IRG and ubiquitin individual channels are shown. B) 117, 131, 188 and 222 PVs visibly labelled with GRA7 antibody were classified as IRG, ubiquitin, and double-positives and presented as a percentage of GRA7 positive vacuoles. C) The pixel intensity of IRG

and ubiquitin proteins on 105 individual GRA7 labelled PVs at each time point were measured using the Image J Fiji software as described in Materials and Methods. Horizontal bars represent the arithmetic mean values.

Accordingly, the pixel intensity of the measurable ubiquitin on PVs suggests a starting point for Ub accumulation on PVs at 30 minutes post infection and an increase in frequency up to 120 minutes. The ubiquitin intensity of individual vacuoles also increased, suggesting that in addition to the increase in the number of Ub-positive vacuoles, there was also an increase in Ub protein accumulation on individual vacuoles (Figure 3.7. C). Taken together, the data suggest that ubiquitination follows IRG protein recruitment to the vacuole and persists well after membrane damage caused by IRG loading has occurred.

3.4.7. Ubiquitination of PVs is associated with the efficiency with which IRGs destroy the PVM.

3.4.7.1. There is more ubiquitin on disrupted PVs.

The previous data showed that at 120 minutes after infection a proportion of PVs (10%), appeared to be loaded only by ubiquitin and not by IRG proteins. Because the data suggested that ubiquitination follows IRG recruitment, we proposed that ubiquitin remained associated with the parasite itself, rather than the PVM, after the disappearance of the IRGs upon PVM disruption. To test this hypothesis, IRG protein labelling was used to classify vacuoles in a preliminary manner as apparently intact or apparently disrupted. “Intact“ was defined as when the IRG labelling on the vacuole appeared to be continuous, including smooth and rough [16], and “disrupted” when it showed interruptions as shown in the overlapped confocal images and the plot profile along the indicated transects (Figure 3.8. A) which

locate the ubiquitin signal as clearly inside the IRG signal. The quantification of intensity shows lower ubiquitin intensities in intact PVs, contrasting with higher ubiquitin intensities on disrupted vacuoles (Figure 3.8. B). Taken together, this and the previous data seem to indicate that ubiquitin starts to be recruited to PVs already covered by IRGs and that Ub recruitment is strongly enhanced probably on the parasite membrane itself after the disruption of the PVM.

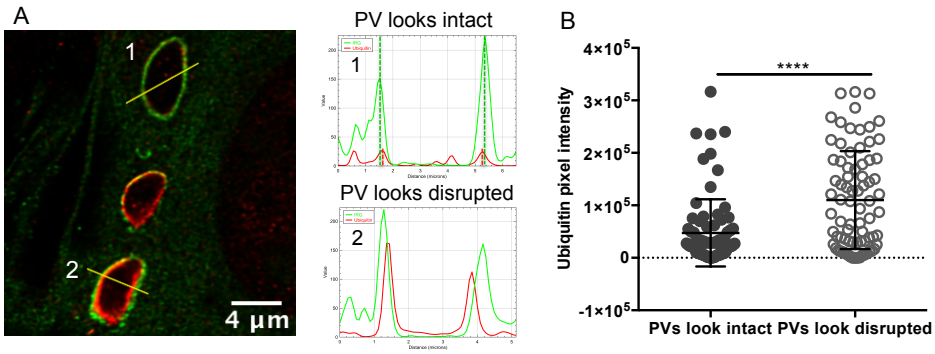

Figure 3.8. There is more accumulation of ubiquitin in disrupted PVs.

IFNγ stimulated C56BL/6 MEFs were infected with *Toxoplasma gondii* Me49 strain for 90 minutes. Cells were fixed and stained simultaneously for Irga6 (165/4 pAS), Irgb6 (141/1 pAS), Irgb10 (940/6 pAS) and Irgd (81/3 pAS) with the same secondary antibody coupled with Alexa Fluor 488 (green), ubiquitin (Fk2 mAb) with Alexa Fluor 555-conjugated secondary antibody (red) and GRA7 (JH 2.1.2 mAb) with Alexa Fluor 647-conjugated secondary antibody (magenta). The nuclei were labelled with DAPI (cyan). **A)** Confocal representative IRG and ubiquitin overlapped images and two transected PVs are shown: 1 (apparently intact) and 2 (apparently disrupted), represented by profiles, showing the pixel intensity of the IRG and ubiquitin channels along these transects. The perpendicular lines in profile 1 shows the location of the peaks on the x axis. **B)** The PVs were evaluated and classified as apparently intact (with IRG signal apparently continuous) and visually destroyed (with the IRG signal apparently discontinuous). The ubiquitin intensity on the PVM was measured by using Image J Fiji and shown as a scatter dot plot: closed circles: PVs look intact; open circles: PVs look disrupted. Horizontal bars represent the arithmetic mean values. ****, P<0,0001

3.4.7.2. Toxoplasma gondii type I PVMs are disrupted by IRG proteins in CIM cells.

As previously shown, the PVMs of virulent parasites are not loaded by IRG effectors due to ROP5/ROP18-mediated phosphorylation [24]. Cells derived from the wild-derived *Mus musculus castaneus* strain CIM are able to interfere with virulent *T. gondii* strains such as RH allowing effector IRGs to load PVs of these strains [41]. To determine whether cells from CIM mice are able to ubiquitinate vacuoles containing virulent RH strain parasites, we first examined whether those PVs are destroyed, just as avirulent PVs are destroyed in C57BL6 DDCs. IFNγ-stimulated CIM DDCs were infected with tachyzoites of the type I virulent RH strain of *T. gondii* for 90min after which immunofluorescence was performed. Cells were stained for a pool of effector IRG proteins, Irga6, Irgb6, Irgb10 and Irgd. The PVs were evaluated and classified (as described in the previous experiment) as apparently "intact" (with IRG continuous line) and "disrupted" (visually destroyed, with IRG discontinuous line), by using fluorescent microscopy images (Figure 3.9. A). We found that IFNγ-stimulated cells from CIM mice were able to disrupt about 80% of the IRG-covered PVs (Figure 3.9. B).

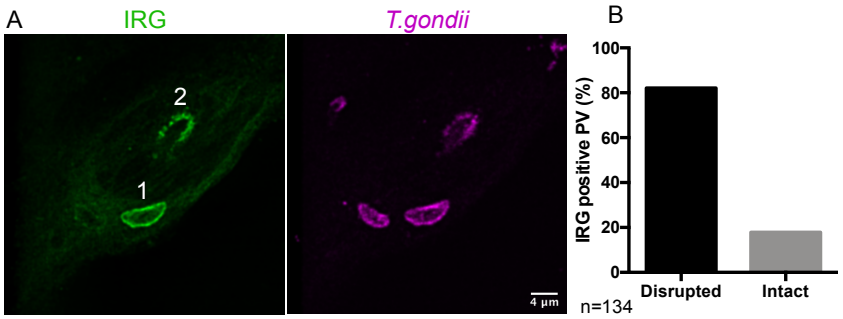

Figure 3.9. IRG proteins in cells from the CIM mouse strain are able to disrupt type I PVM.

IFNγ stimulated CIM diaphragm-derived cells (DDCs) were infected with type I RH *T. gondii* strain for 90min. Cells were washed, fixed and stained for Irga6 (serum 165/4), Irgb6 (serum 141/1), Irgb10 (serum 940/6) and Irgd (serum 81/3) simultaneously with Alexa Fluor 488-conjugated secondary antibody (green); ubiquitin (FK2 mAb) with Alexa Fluor 555-conjugated secondary antibody (red) and GRA7 (JH 2.1.2 mAb) with Alexa Fluor 647-conjugated secondary antibody (magenta). The nuclei were labeled with DAPI (cyan). **A)** Representative confocal Images for IFNγ treated condition are shown IRG and GRA7 channels **B)** GRA7 and IRG labelled PVs were visually classified as intact (1) or disrupted (2) based in the continuity or discontinuity of the IRG signal around the vacuole respectively, and presented in the bar plot.

3.4.7.3. PVs of virulent strains are ubiquitinated by CIM DDCs

Just as effector IRG proteins from C57BL/6 (BL/6) cells are recruited to and disrupt the PVs of avirulent *T. gondii* strains, so effector IRG proteins from CIM cells are recruited to virulent RH strain tachyzoite PVs, disrupt virulent RH strain PVs, and inhibit RH tachyzoite proliferation [41].

To answer whether the disruption of RH PVs is required for ubiquitination, IFNγ-stimulated C57BL/6 and CIM DDCs were infected with tachyzoites of the type I virulent strains RH, BK and tachyzoites of the type II avirulent strain Me49 for 90min. These cells were later fixed and simultaneously stained for ubiquitin, for the set of effector IRGs (Irga6, Irgb6, Irgb10 and Irgd) with the secondary antibodies coupled to the same fluorochrome and for GRA7. Pictures of the samples were taken and GRA7-positive PVs were manually blind-classified as Ub-positive or Ub-negative.

Vacuole counting and quantification of ubiquitin intensity on PVs revealed that IFNγ-induced CIM cells, which allow IRG recruitment to RH PVs and PVM disruption, significantly ubiquitinate these RH PVs,

much more than C57BL6 cells. In fact, in BL/6 cells, in a manner that is consistent with lack of IRG recruitment, ubiquitin does not seem to be recruited to the PVs of type I parasites. The control avirulent strain Me49 PVs are ubiquitinated to a similar extent in both cell lines (Figure 3.10. C and D). The extension of the experiment to tachyzoites of another type I strain, BK, the replication of which is also controlled by IFNγ-induced CIM cells, showed ubiquitination much like that seen for RH strain PVs in CIM cells (Figure 3.10. E). Assuming that these vacuoles are destroyed in CIM cells much like non-virulent PVs are destroyed in BL/6 DDCs, the conclusion would be that disruption of the PVM is a requisite for ubiquitination of parasites, dependent on the mouse strain but independent of *T. gondii* strain.

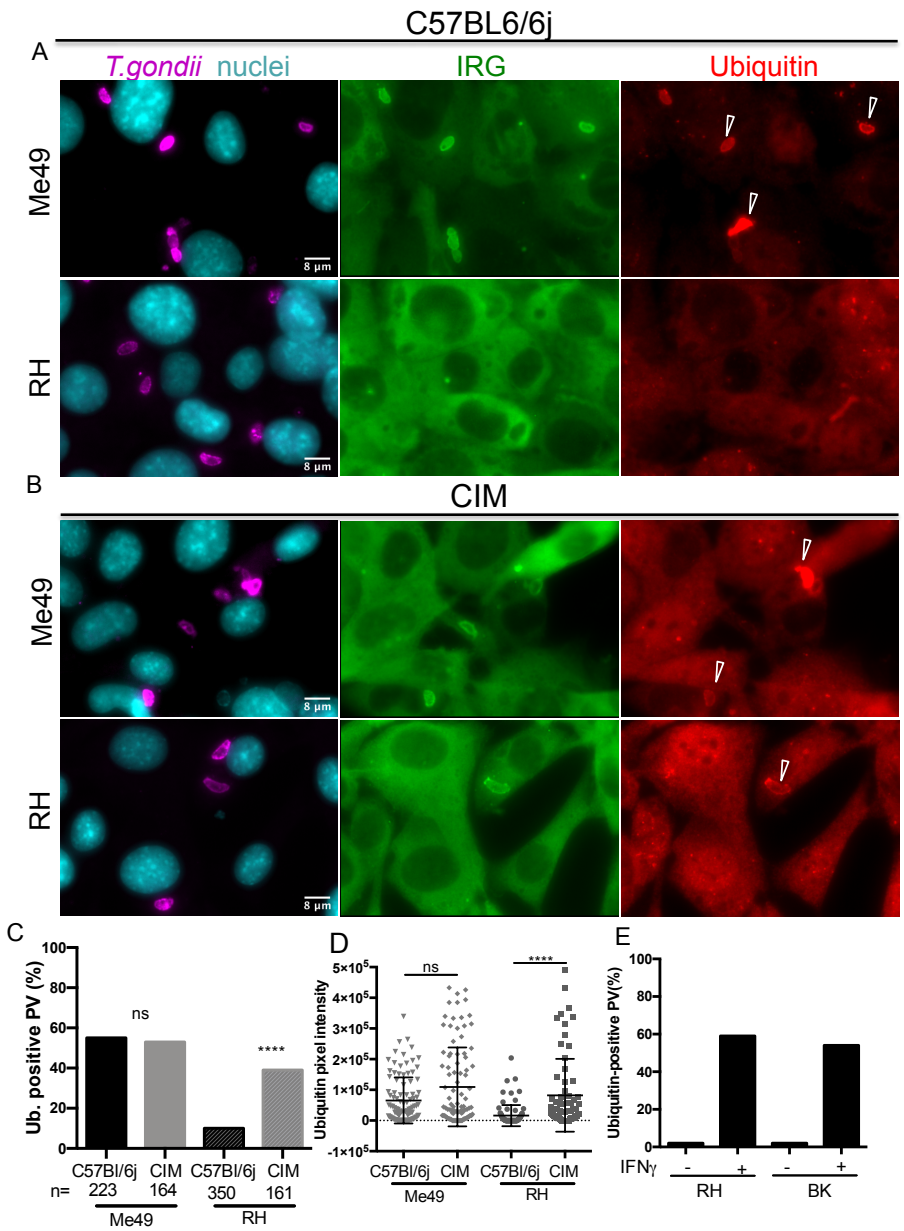

Figure 3.10. Cells from the CIM mouse strain are able to ubiquitinate type I PVM.

C56BL/6 and CIM diaphragm-derived cells (DDCs) were stimulated with 200U of IFNγ for 24 hours prior to infection with type II Me49 and type I RH and BK *T. gondii* strain for 90min. Cells were washed, fixed and stained for: Irga6 (serum 165/4), Irgb6 (serum 141/1), Irgb10 (serum 940/6) and Irgd (serum 81/3) simultaneously with Alexa Fluor 488-conjugated secondary antibody (green); ubiquitin (FK2 mAb) with Alexa Fluor 555-conjugated secondary antibody (red) and GRA7 (JH 2.1.2 mAb) with Alexa Fluor 647-conjugated secondary antibody (magenta). The nuclei were labelled with DAPI (cyan).

A) and **B)** Representative images for the IFNγ-treated condition, taken in a widefield microscope are shown. Arrows point at the PVs positive for ubiquitin. **C)** and **E)** More than 150 PVs GRA7 positive were quantified and the proportion of ubiquitin-positive PVs are shown. **D)** The pixel intensity of ubiquitin in the PV area was measured as described in Material and Methods, plotted and analyzed by Mann- Whitney U test. ****P<0,0001; n.s., nonsignificant

3.4.8. Ubiquitination of PVs in mouse CIM strain cells requires the presence of Irgb2-b1

The presence of Irgb2-b1 (tandem IRG) is required for resistance against *T. gondii* virulent strains due to the ability of this IRG tandem protein to interfere with the phosphorylation of effector IRG proteins. Irgb2-b1$_{CIM}$ (KO) CIM cells display phosphorylation of Irga6 on the PVM but do not have the ability to control replication of a *T. gondii* virulent strain; however, when these KO cells are complemented with the Irgb2-b1$_{CIM}$ gene/protein, the resistance is restored to levels observed for the wild-type CIM cells [36].

Assuming that ubiquitination happens downstream of the disruption of the PVM, which in the case of virulent *T. gondii* strains occurs only in cells such as CIM strain cells that carry the b2-b1 tandem IRG, it was investigated whether this IRG is necessary for the ubiquitination of RH PVs. IFNγ-stimulated CIM DDCs, CIM DDCs KO for *Irgb2-b1$_{CIM}$* (T17) and T17 cells complemented with *Irgb2-b1$_{CIM}$* were infected with type I virulent RH *T. gondii* strains for 90min, fixed and then simultaneously stained with specific antibody for ubiquitin and for GRA7.

Although the levels of effector IRG proteins Irga6, Irgb6, Irgb10 and Irgd are not different between CIM wt cells and T17 cells [36] the frequencies of RH vacuoles carrying ubiquitin was greatly reduced compared with frequencies in wild type cells (Figure 3.11. A and B).

Complementation of KO cells with Irgb2-b1$_{CIM}$ partially restored the frequencies of ubiquitinated PVs to frequencies seen for wild type cells, suggesting that Irgb2-b1 is necessary and sufficient to interfere with virulence factors and allow the effector IRGs to disrupt PVs.

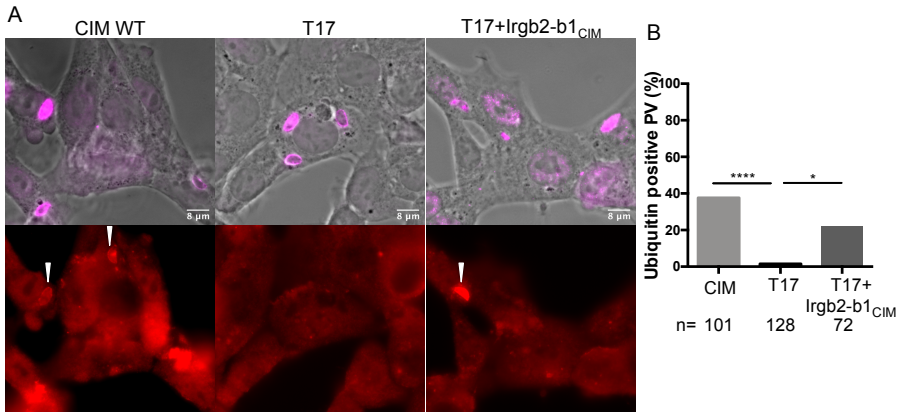

Figure 3.11. The presence of the Irgb2-b1 allele is required for ubiquitination of type I *T. gondii* PV.

WT CIM DDCs, Irgb2-b1 KO CIM DDCs (T17) and T17 DDCs complemented with Irgb2-b1 from CIM, were stimulated with 200U of IFNγ for 24 hours before infection with type I RH *T. gondii*. Cells were fixed and ubiquitin (Ub) and GRA7 were detected by using the FK2 mAb with Alexa Fluor 555-conjugated secondary antibody (red) and JH 2.1.2 mAb with Alexa Fluor 647-conjugated secondary antibody (magenta) respectively. The nuclei were labelled with DAPI (cyan). **A)** Representative images for IFNγ-treated conditions taken in a widefield fluorescent microscope are shown. Arrows point at the PV loaded by Ub. **B)** PVs labelled with anti-GRA7 were evaluated and the proportion of Ub-positive ones is shown. Fisher's exact test was applied to test the difference between the cells. *, P < 0.05; **** P<0,0001; n.s., nonsignificant.

3.4.9. Parasite membranes are the target of ubiquitination.

To clarify the ambiguity of ubiquitin location, samples from IFNγ-induced MEFs infected with Me49 strain tachyzoites were co-stained for a combination of antigens/proteins consisting of ubiquitin and effector IRGs (Figure 3.12. A and C) or ubiquitin and GBP1 (Figure 3.12. B and D). Images were taken with high resolution using confocal

microscopy (Figure 3.12. A and B) and super resolution microscopy (Figure 3.12. C and D).

Vacuoles where both ubiquitin and IRG protein are loaded, or ubiquitin and GBP1 are loaded, were analyzed. Two distinct situations were identified: in vacuoles where the PV is disrupted, and the PVM has partially separated from the parasite, the IRG and GBP proteins are on the PVM, while the ubiquitin is on the parasite; conversely, in ubiquitinated vacuoles where IRG and GBP1 labelling suggest the PVM is still intact, evidently ubiquitin and IRG or GBP1 are very close to each other, but the resolution does not allow a clear determination of whether they are on the same membrane or on different membranes (in the latter proposition, one protein may be on the PVM while the other may be on the parasite's membrane, as in the image shown in Figure 3.8. A, profile 2). The first situation is consistent with previous indications that ubiquitin is recruited to the parasite's membrane. The accumulation of ubiquitin that begins with the permeabilization of the PVM is seen in low intensity while the PVM looks intact and intensifies with its disruption, hence explaining the strong intensity observed in the vacuoles where the PVM is clearly disrupted, some with small residual portions of PVM loaded with IRGs.

Additionally the transect Figure 3.12. E) of disrupted PVs in which the PVMs is already isolated from parasites revealed no presence of ubiquitin coincident with IRG or GBP, suggesting that the small peak of ubiquitin coincident with continuous IRG on PVM (Figure 3.8. A, profile 1) was perhaps "leakage" of a damaged but still mostly impermeable PVM, called rough PV[16], onto the parasite underneath.

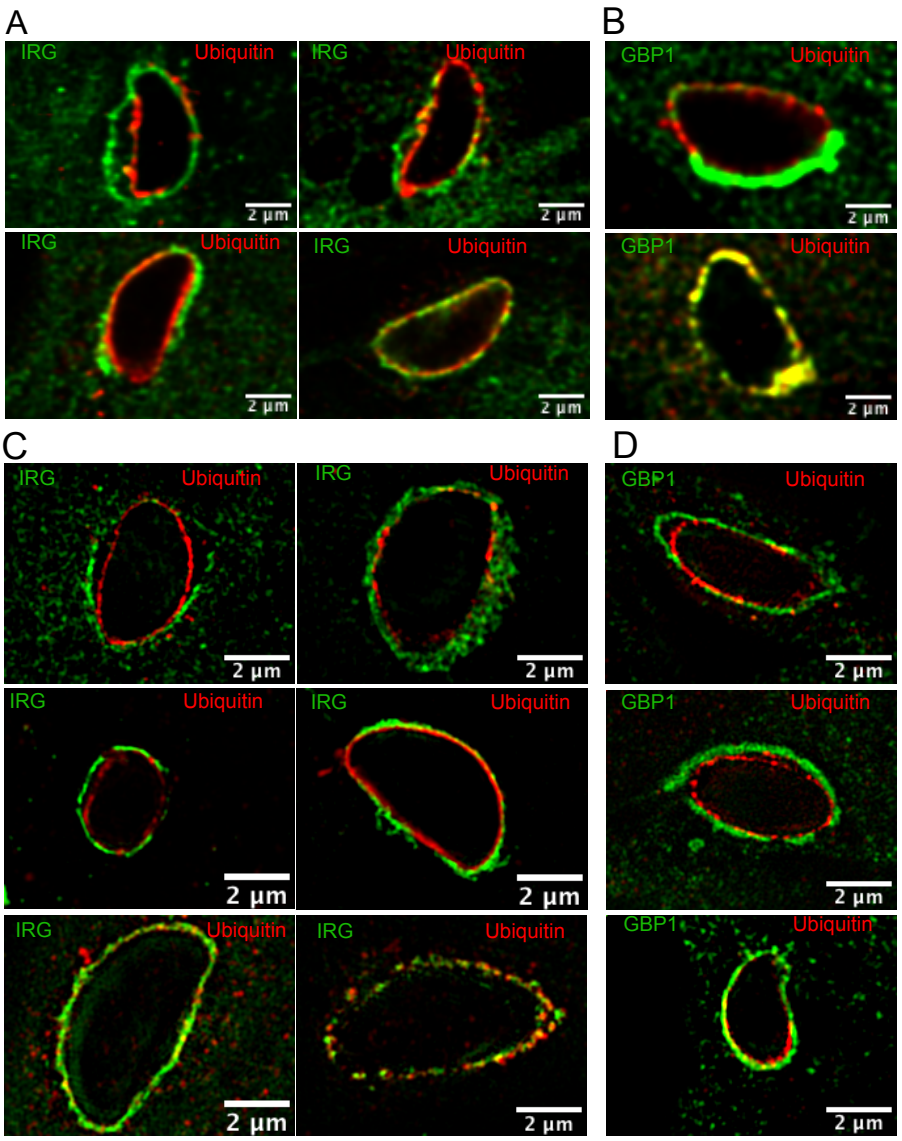
A
IRG
Ubiquitin
2 µm
B
GBP1
Ubiquitin
C
D

E

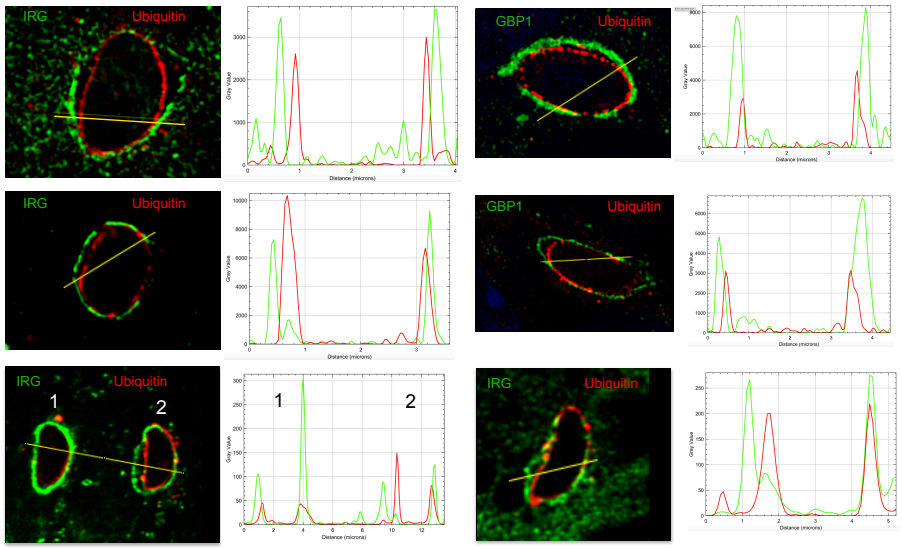

Figure 3.12. Ubiquitin is recruited to the parasite membrane dependent on IRG loading and PVM disruption.

IFNγ-stimulated C56BL/6 MEFs were infected with *Toxoplasma gondii* Me49 for 90 minutes. Cells were fixed and stained simultaneously for GRA7 (JH 2.1.2 mAB) with Alexa Fluor 647-conjugated secondary antibody (magenta); ubiquitin (Fk2 mAb) with Alexa Fluor 555- conjugated secondary antibody (red) and for **A, C)** Irga6 (serum 165/4), Irgb6 (serum 141/1), Irgb10 (serum 940/6) and Irgd (serum 81/3); **C)** Irga6 (serum165/4); **B, D)** GBP1 serum[53] with secondary antibody coupled with Alexa Fluor 488 (green). Representative images of IRG or GBP1 and ubiquitin overlapped channels from the confocal microscope **(A and B)** and structured illumination microscope **(C. and D)** are shown. **E)** The plot profile of each transected PV was obtained by using ImageJ Fiji**.**

3.4.10. Neither TRAF6 nor TRIM21 E3 ligases are individually required for ubiquitination of PVs

The E3 ligases TRAF6 and TRIM21 are partially associated with PVs[1,54]. To examine the requirement of these E3 ligases for ubiquitin association with PVs, BL/6 MEFs in which the TRAF6 or TRIM21 gene(s) had been deleted[33,34] ((FK2 mab) ary figure 3.7) were induced with IFNγ for 24 hours and infected with Me49 strain tachyzoites for 90

minutes. The samples were stained for GRA7, IRGs and ubiquitin, as shown in the representative images (Figure 3.13. A and D). The results of this experiment show no significant reduction in the frequency of PVs covered by ubiquitin in both cases (Figure 3.13. B and E). The intensity of ubiquitin also shows no significant variation in TRIM21 KO cells compared to wild type cells, but a possibly non-significant increase in ubiquitin intensity was observed in TRAF6 KO cells (Figure 3.13. C). Evidently neither TRIM21 nor TRAF6 is uniquely associated with parasite ubiquitination, though these results would be consistent with both E3 ligases redundantly active on the parasite membrane.

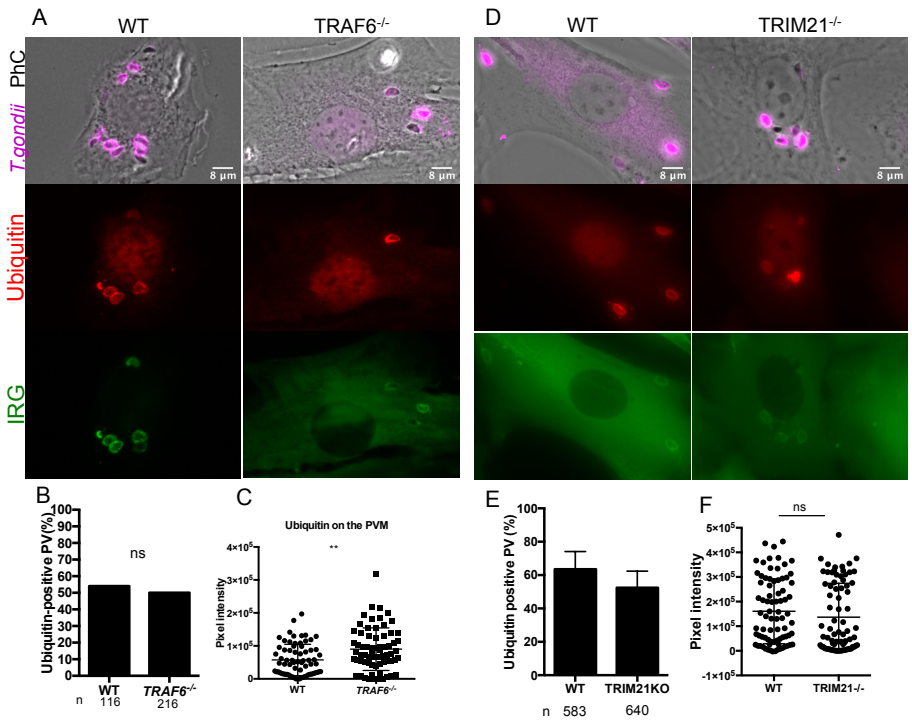

Figure 3.13. The ubiquitination of PVs is not affected in TRAF6 and TRIM21 knockouts cells.

Wildtype, TRAF6, and TRIM21 knockout (KO) MEFs (all genotypes confirmed by PCR) were induced with 200U of IFNγ for 24 hours or kept uninduced. The cells were infected with *T. gondii* ME49 strain for 90 min. The cells were washed, fixed and co-stained with immunoreagents against GRA7 (JH 2.1.2 mAB) with Alexa Fluor 647-conjugated secondary antibody; ubiquitin (Ub) (FK2 mab) with Alexa Fluor 555-

conjugated secondary antibody; **(A, B** and **C)** Irgb6 (serum 141/1), Irgb10 (serum 940/6) **(D, E,** and **F)** Irga6 (serum 165/4), Irgb6 (serum 141/1), Irgb10 (serum 940/6) and Irgd (serum 81/3) simultaneously with Alexa Fluor 488-conjugated secondary antibody. **A, D**) Images taken in a wide field microscope are shown. **B, E)** GRA7-labelled PVs were visually classified as Ub-positive and the proportions are represented in the bar graph. Mean +/- SD of four independent experiments is shown. **C, F)** By using ImageJ Fiji software the Ub signal intensity on the PVM was measured, as described in Material and Methods and analyzed by the Mann-Whitney test. **, P<0,01; n.s., nonsignificant.

3.4.11. K48- and K63-type ubiquitin linkages are both involved in parasite ubiquitination.

Because the type of ubiquitin linkage determines the different fate of the ubiquitinated substrates 55,56, we set out to investigate the type of ubiquitination involved in IFNγ-mediated T. gondii control. IFNγ-induced MEFs were infected with Me49 strain tachyzoites for 90 minutes and the cells were prepared for indirect immunofluorescence. Intracellular parasites were identified with anti-GRA7, and ubiquitination was assessed with FK2 and anti-K48- or anti-K63-linked ubiquitin- specific antibodies. Representative images and merged channels are shown (Figure 3.14. A).

The results of the quantification on PVs of mono- and poly-ubiquitinylated proteins with the FK2 antibody, and quantification of specific poly-ubiquitinylated proteins with the K48- and K63-specific antibodies, showed that both K48- and K63-linkage poly-ubiquitin conjugates are associated with ubiquitinated PVs. The form of K48-linked poly-ubiquitination localized with 62% of ubiquitinated PVs detected by FK2 and the K63-linked poly-ubiquitination with 71% of FK2-positive vacuoles. The ubiquitinated vacuoles are mainly covered by K48-linked and K63-linked, together representing 84% of FK2-positive vacuoles. About 15% of vacuoles are presumably ubiquitinated by other type(s) of lysine-linkage(s) (Figure 3.14. B). The extension of

the experiment to TRIM KO cells showed a slight defect in ubiquitination by lysine K63 (Supplemental Figure 3.9)

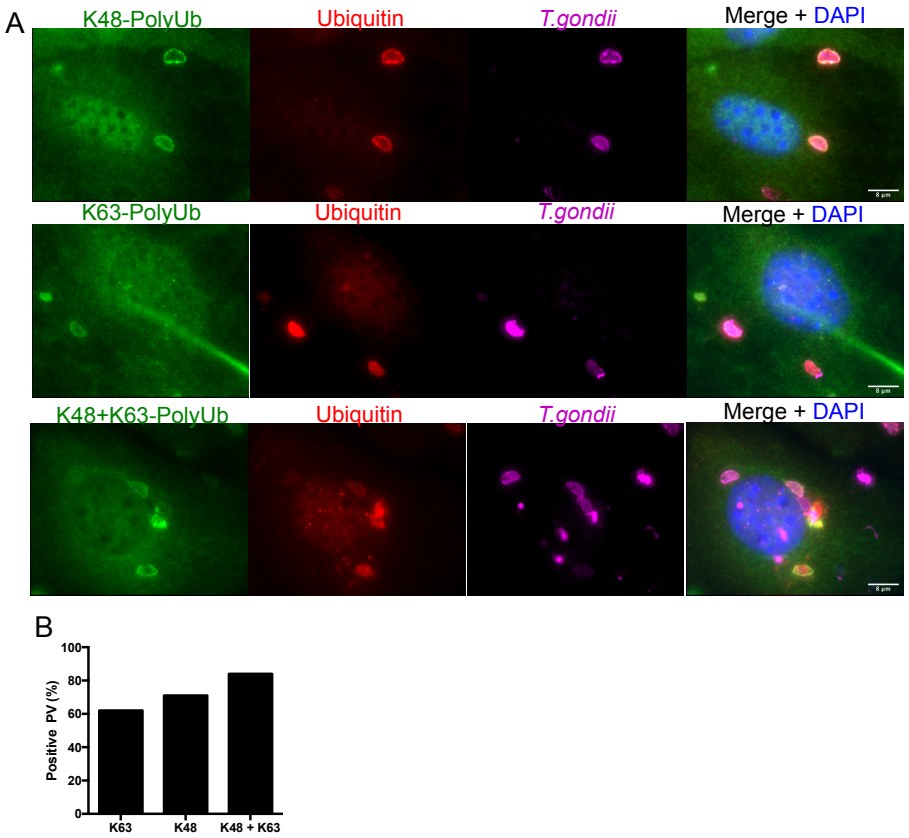

Figure 3.14. Lysine K48 and K63-type linkages both contribute to the polyubiquitination of PVs.

IFNγ-stimulated and unstimulated C56BL/6 MEFs were infected with *T. gondii* ME49 strain tachyzoites for 90 min. The cells were prepared and co-stained for GRA7 with JH 2.1.2 mAb and Alexa Fluor 647-conjugated secondary antibody (magenta); ubiquitin with FK2 mAb and Alexa Fluor 555-conjugated secondary antibody (red) and for Lysine 48 and Lysine 63 with simultaneously K48- or K63-polyUb-specific Ab or both with Alexa Fluor 488-conjugated secondary antibody (green). **A)** Individual channels and overlay images are shown. **B)** More than a hundred of GRA7- and ubiquitin- double labelled PVs were visually classified as K48- or K63- polyubiquitinated PVs or both, and the proportions are presented in the bar graph.

3.4.12. IRG and ubiquitin recruitment to PVs is followed by host cell programmed necrosis.

IFNγ-treated cells infected with avirulent *T. gondii* have been observed to undergo a form of necrotic death after the death of the parasite [57] (Figure 3.15). Shortly after cell invasion and establishment of the PV, GTPases coat the *T. gondii* PVM, a step that is generally followed by PV permeabilization and later death of the parasite, after which the cells undergo a death that displays morphological characteristics of "programmed necrosis" or "regulated necrosis", in which the nuclear membrane condenses, the plasma membrane breaks down and there is release of cellular contents (Figure 3.15). The mechanisms by which parasite and host cell death occur are not well understood. First, to decide whether cell death is exclusively dependent on infection, necrotic host cell death was assessed as described in Material and Methods (see section 333.4 and 3.3.6.3) in IFNγ-treated DDCs infected with the PRU-YFP fluorescent reporter strain of *T. gondii*. The quantification results demonstrated that only infected cells underwent necrosis (Figure 3.15). To understand whether there is a correlation between the presence of ubiquitin and programmed cell death, IFNγ-treated cells infected with avirulent *T. gondii* were immunostained, following the standard protocol (see 3.1.), for the set of effector IRGs (Irga6, Irgb6, Irgb10 and Irgd), ubiquitin and GRA7. Fluorescent images were used to visually select necrotic cells, according to the description above, and to examine the presence of IRG protein and ubiquitin on the PV within these cells. Live cell image analysis shows that some parasites egress early and others remain in the necrotic cell. We don't yet know whether these egressed parasites are able to reinvade neighbouring cells or not (Supplemental Figure 3.2.). IRG and ubiquitin recruitment to the remaining PVs was followed by necrotic cell death: consistently, close to 95% of necrotic cells contained IRG and ubiquitin-

positive PVs (Figure 3.15. A). These data suggest that only host cells carrying IRG and ubiquitin-coated *T. gondii* PV go on to commit a type of necrotic death.

Cells carrying PVs covered by IRG and ubiquitin appear to be differentiated from the others, the contracted nucleus losing incorporated ubiquitin (Figure 3.15. A.).

Our observations suggest that either the presence of IRG and ubiquitin together on the PV trigger a signal that initiates the host cell necrosis pathway, or that the signaling is activated by the permeabilization of the PV by IRGs, as previously described[57] and that all PVs that are covered by IRGs end up being covered by ubiquitin as a consequence of permeabilization.

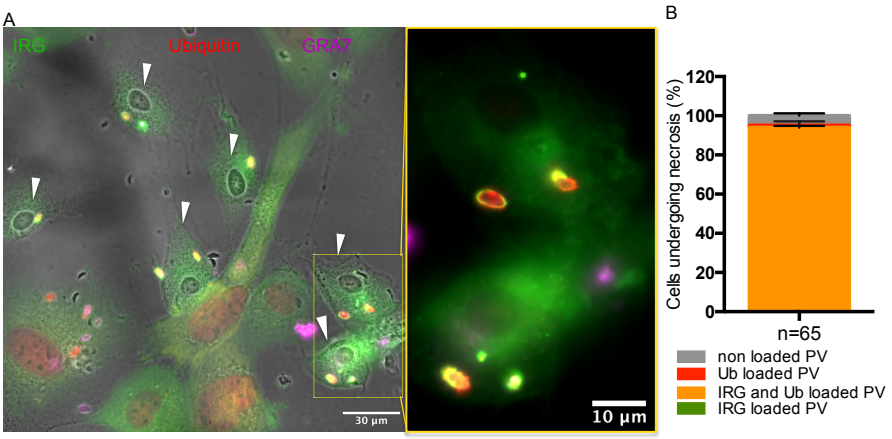

Figure 3.15. IRG and ubiquitin recruitment to PVs is followed by necrotic death of the host cell.

IFNγ-stimulated C56BL/6 MEFs were infected with *Toxoplasma gondii* Me49 strain for 90 minutes. Cells were fixed and stained simultaneously for Irga6 (165/4 pAS), Irgb6 (141/1 pAS), Irgb10 (940/6 pAS) and Irgd (81/3 pAS) with the same secondary antibody coupled with Alexa Fluor 488 (green), ubiquitin (Ub) (Fk2 mAb) with Alexa Fluor 555-conjugated secondary antibody (red) and GRA7 (JH 2.1.2 mAb) with Alexa Fluor 647-conjugated secondary antibody (magenta). **A)** Representative image show Infected necrotic cells. Cells were examined for the presence in the PV of IRG and Ub, demonstrated by the Zoom in of the insert. **B)** The percentage of cells undergoing

necrosis in which there was IRG and Ub recruitment to the same PV (orange), only Ub recruitment (red) and unloaded PVs, as determined by fluorescence microscopy, are displayed in the graphic bar. The range between three independent experiments was shown.

3.5. Discussion

The cell-autonomous response of mouse cells to *T. gondii* invasion relies on interferon-dependent mechanisms, more precisely the action of the IRG proteins in the disruption of the PV. Studies on ubiquitination have pointed to GTPases as possible substrates for ubiquitination in the PVM [1,26,58] but it has remained uncertain whether the IRGs assembled on PVs are themselves ubiquitinated.

We show that ubiquitin enrichment on PVs is totally dependent on IFNγ confirming previous studies [1,26,58]. Although 95% of ubiquitinated PVs are also coated with IRG proteins, demonstrating an association between the presence of ubiquitin and the presence of IRGs, most individual IRG proteins such as Irga6, Irgb10 and Irgd are not essential for IFNγ-mediated ubiquitination. However the absence of the pioneer effector protein, Irgb6, significantly affects ubiquitination levels, but does not eliminate it. It is important to recall that some vacuoles are loaded with Irgb6 alone, others with Irgb6 and Irga6, and yet others with Irgb6, Irga6 and Irgd. The data shown in Figure 3.3. are fully consistent with the idea that efficient ubiquitination requires the presence of Irgb6 plus at least one of Irga6 and Irgd, and that vacuoles loaded with Irgb6 alone are not or rarely ubiquitinated. Presently, any significance of Irgb10 in this context is unclear, since despite its high representation on vacuoles, equal to that of Irgb6, its absence has no effect on the level of ubiquitination.

We confirmed earlier data [49] that absence of the regulatory IRG proteins, Irgm1 and Irgm3 results in a complete loss of effector IRG

binding to the PV and consequent absence of ubiquitination (Figure 3.4.) [1,26]. In this situation the effector IRG proteins are mislocalised to other organelles, especially lipid droplets [48,51] and are intensely ubiquitinated (Figure 3.5. A). It is not clear whether these mislocalised IRG aggregates are activated by GTP or denatured. This uncertainty arises from the fact that the monoclonal antibody 10D7 recognises both GTP-activated Irga6 and denatured Irga6 [50]. Since Irga6 at the PVM is activated but almost certainly not ubiquitinated it becomes probable that the aggregated IRG proteins present in Irgm1/Irgm3-deficient cells are denatured, possibly after unregulated activation by GTP.

Ubiquitin deposition occurs after IRG loading on the PVM. We show that in IFNγ-primed C57BL/6 (BL/6) cells infected with avirulent tachyzoites, the ubiquitin coat on the PV starts to appear about 30min after the initiation of IRG coating of the PVM and increases over time until it reaches a maximum of 65% of all PVs at 2 hours post-infection. The intensity of ubiquitin on PVs also increases over time. The delay in the accumulation of ubiquitin relative to the accumulation of IRGs suggests the existence of a time window in which the vacuoles are damaged by the action of the IRG proteins to allow the infiltration of ubiquitin (Figure 3.7.). This assumption is supported by our findings of stronger ubiquitin accumulation on fully disrupted PVs, perhaps because access to the parasite membrane is no longer impeded by the PVM (Figure 3.8.).

In C57BL/6 (BL/6) cells IRG proteins can disrupt PVs containing avirulent Me49 strain tachyzoites, but not RH strain PVs [46]. Virulent strains carry the virulence factors ROP5 and ROP18 that phosphorylate and thereby inactivate effector IRG proteins, preventing their activation and stable binding to the PVM and preventing PVM disruption. We show, in agreement with others [1,26] that ubiquitin recruitment does not occur on virulent *T.gondii* strain PVMs. The wild-derived *Mus musculus*

castaneus strain CIM cells express the Irgb2-b1 tandem protein at high level, which acts as a decoy, diverting the active ROP5/ROP18 kinase complex of virulent strains from effector IRG proteins (e.g. Irga6 and Irgb6) and allowing the effector IRG proteins to bind and disrupt PVs of these strains[35]. We found that diaphragm-derived cells (DDCs) obtained from CIM mice, which inhibit proliferation of RH strain tachyzoites when IFNγ-induced, also significantly ubiquitinate these RH PVs (Figure 3.10) after disruption by IRGs (Figure 3.9.) In addition, [48,51] in cells lacking regulatory IRGMs the effector IRGs do not reach the PVs and there is no PVM disruption and no Ub deposition. The conclusion that disruption of the PVM is a requisite for ubiquitination of the parasite is supported by these data.

Shortly after cell membrane invasion and formation of the PV, IRG proteins start to assemble on the PVM of avirulent tachyzoites, ultimately leading to the disruption of PVM followed by the death of the host cell [57]. We demonstrate that sometime between these two events, probably coinciding with the rupture of the PVM, the parasite starts to become ubiquitinated. Although its specific role is not yet clear, ubiquitin accumulation may be required to trigger the necrosis pathway since we can detect at least one ubiquitinated parasite inside virtually every necrotic cell (Figure 3.15). We show that some *T. gondii* PVs are covered only by K48-linkage polyubiquitin conjugates, others by only K63-linked polyUb, and others still by both, suggesting the possibility of different fates for the ubiquitinated parasites. What seems evident is that K48- and K63-linkage polyubiquitin conjugates are equally associated with *T. gondii* PVs, contrasting with previous data [26,59] which indicate that the majority of PVs are coated by K48-linked polyubiquitinylated conjugates. Another type (or types) of polyUb linkage, perhaps linear M1-linkage [1,26,60], cooperate with K48- and K63-linked polyUb to make up the parasite's full ubiquitin coat. This

unknown linkage may be partially overlapping or not with the K48- and K63-linked poly-Ubiquitinated PVs. The involvement of K63-linked ubiquitination has been shown in autophagic events during the elimination of another vacuolar pathogen, the bacterium Salmonella enterica serovar Typhimurium [61] in a process involving the autophagy adaptors P62 and NDP53. Salmonella is also coated by M1-linked Ub chains to promote NF-κB activation [62].

However, in the case of *T. gondii* control this K63 polyubiquitination seems to be unrelated to autophagy. ATG proteins are the core of canonical autophagy machinery[63]. There is evidence suggesting that Atg3, Atg5, Atg7, and Atg16L1 mediate the recruitment of ubiquitin and p62 to PVs [26] and that Atg3, Atg5, Atg7 and Atg8 are crucial for IRG and GBP recruitment [12,64,65]. The interpretation of these data has, however, consistently ignored the phenotype of IRG proteins in IFNγ-induced cells lacking one or more of these Atg proteins. IRG effector proteins in such cells spontaneously form 10D7+ aggregates apparently similar to those formed following loss of IRGM proteins, and are no longer able to associate with the PVM [46,66]. No explanation for this anomalous behaviour has been proposed. On the evidence, it is reasonable to assert that the core autophagy proteins are required for normal behaviour of the IRG effectors even in uninfected cells, but it does not follow that these proteins “mediate the recruitment” of IRG effectors to the parasitophorous vacuole.

The autophagy adaptor P62 was described to succeed ubiquitin recruitment to PVM in an IFNγ-dependent manner[26], and K48- and K63-polyUb were shown to interact with P62 [67]. The data were not sufficient to clarify which cellular processes, proteasome-mediated degradation, autophagic degradation or signalling regulation, result from said ubiquitination, but some preliminary data argue against proteasome degradation role (Supplemental Figure 3.6).

We investigated whether either of the PV-localized E3 ligases TRAF6 and TRIM21 are solely responsible for the build up of ubiquitin on the parasite as others have indicated[1,59]. Our results showed no effect of the absence of either of these adaptors. Unless TRAF6 and TRIM21 are both redundantly active on the parasite, we conclude that other E3 ubiquitin ligases must be responsible for the K48- and K63-linked polyubiquitination detected on *T. gondii* PVs. Preliminary data suggested that the E3 ligase TRIM21 is more specialized in the K63 ubiquitination than K48 (Supplemental Figure 3.9). Other E3 ligases commonly implicated in the context of ubiquitination of pathogens, such as Parkin which mediates K63-linked polyubiquitination in the selective autophagy of *Mycobacterium tuberculosis* and *Listeria monocytogenes* [5], Smurf1, which mediates K48-linkage polyubiquitination, LRSAM1, ARIH, HOIPI, mediators of Salmonella clearance [6] should be considered for investigation.

3.6. Acknowledgments

I would like to acknowledge: the members of the Howard labs for all the imputs in my project; Dr. Joana Loureiro who developed the flow cytometry-based method for quantifying host cell necrosis; the services of the facilities of the Advanced Imaging Unit of the IGC, supported by the project PPBI-POCI-01-0145-FEDER-022122, which was fundamental for the development of this study, the Animal Facility, supported by the research infrastructure Congento, project LISBOA-01-0145-FEDER-022170 and the Transgenic Unit for the Crispr of Irgb6.
Dr Eva Frickel for kindly providing TRIM21KO cells and anti GBP1 antiserum, Dr. Jörn Coers for kindly providing the TRAF6KO cells, Dr. Thirumala-Devi Kanneganti for kindly providing the Irgb10KO cells, Dr Tobias Steinfeldt for kindly providing the CIM Irgb2b1 KO cells.

This work was supported by funding from FCT (Bolsa FCT: SFRH/BD/114402/2016) and the Gulbenkian Institute of Science, by Sonderforschungsbereiche 670 and 680 and Schwerpunkt 1399 by Deutsche Forschungsgemeinschaft.

3.7. Supplementary material

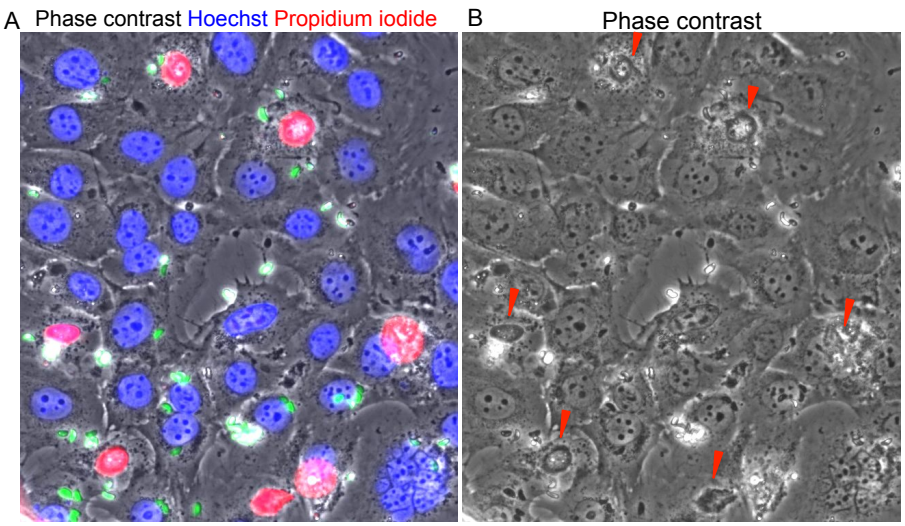

Supplemental Figure 3. 1. Necrotic cells death is featured by condensed nucleus

IFNγ-stimulated mouse DDCs were infected with PRU-YFP tachyzoites (MOI of 10) for 6 hours and observed microscopically by time-lapse photography. Simultaneously with infection 100 µg/ml PI and 1 µg/ml Hoechst were added to identify necrotic and intact nuclei, respectively. The panel A) shows merged images obtained from the combination of the Hoechst channel (blue), the PI channel (red), and the phase contrast channel of DDCs at 2,75 hours after infection and the panel B) shows the phase contrast. Condensed nuclei are visually identified in phase contrast and pointed by red arrows.

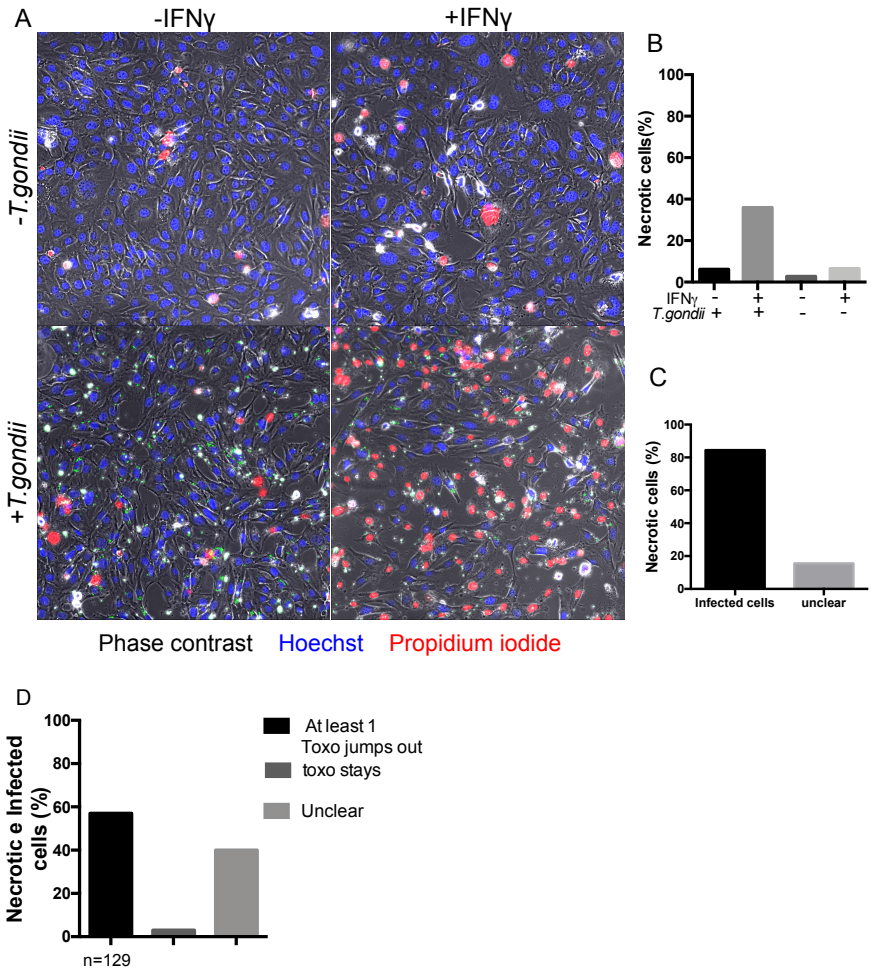

Supplemental Figure 3. 2. Necrosis is IFNγ-induced cells is triggered by avirulent T. gondii infection

IFNγ-stimulated mouse DDCs were infected with PRU-YFP tachyzoites (MOI of 10) for 6 hours observed microscopically by time-lapse photography. Simultaneously with infection 100 µg/ml PI and 1 µg/ml Hoechst were added to identify necrotic and intact nuclei, respectively. The panel A) shows merged images obtained from the combination of the Hoechst channel (blue), the PI channel (red), and the phase contrast channel of DDCs at 6 hours after infection. Particles in the blue and red channels were counted using Fiji 2.0.0-rc69/1,52i software and B) the proportion of necrotic cells within the cell population was obtained (see Material and Methods 333.7). C) Necrotic cells (red nuclei) were followed back in time-lapse and classified as infected or unclear (when it is not possible to determine the infection) and the proportion is depicted in the plot. D) Necrotic and single and multiple infected cells (red nuclei) were followed back in time-lapse and classified into 3 groups: At least 1 tachyzoite (toxo) jumps out (even more

toxos stay), toxos stay and unclear (when is not possible to determine within the time frame, or when is not clear if the toxo jumps out) the proportion is depicted in the plot.

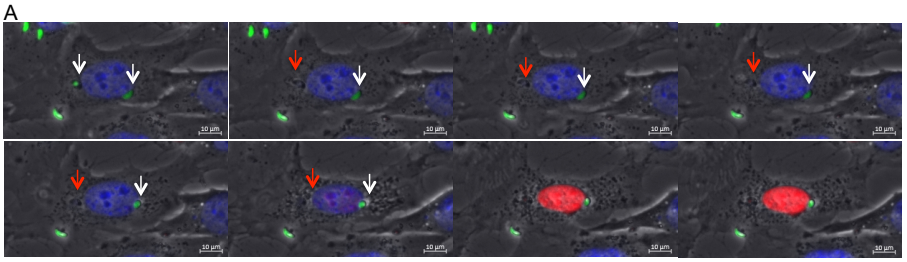

Supplemental Figure 3. 3. The IFNγ Induced cells undergo necrosis after at least one included T. gondii dies.

IFNγ-stimulated mouse DDCs were infected with PRU-YFP tachyzoites (MOI of 10) for 6 hours observed microscopically by time-lapse photography. The imaging started 30 minutes after infection and the scenes Images were taken at 4,4 minutes intervals and selected images are shown. Simultaneously with infection 100 µg/ml PI and 1 µg/ml Hoechst were added to identify necrotic and intact nuclei, respectively. The panel A) shows merged images obtained from the combination of the Hoechst channel (blue), the PI channel (red), and the phase contrast channel of DDCs at 2,5 hours after infection. White and red arrows pointed to green parasite (seems alive) and black parasite (seems dead) respectively.

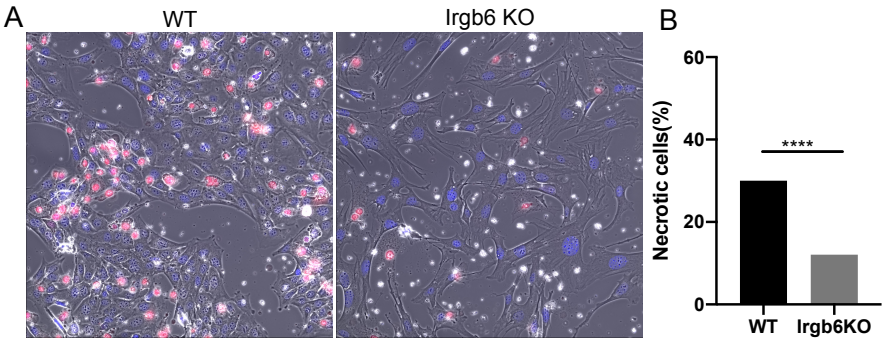

Supplemental Figure 3. 4. Infection dependent necrosis is partially affected in Irgb6 KO cells.

IFNγ-stimulated mouse DDCs Wt and Irgb6KO were infected with Me49 tachyzoites (MOI of 5) for 6 hours observed microscopically by time-lapse photography. Simultaneously with infection 100 µg/ml PI and 1 µg/ml Hoechst were added to identify necrotic and intact nuclei, respectively. The panel A) shows merged images obtained from the combination of the Hoechst channel (blue), the PI channel (red), and the phase contrast channel of DDCs at 6 hours after infection. Particles in the blue and red

channels were counted using Fiji 2.0.0-rc69/1,52i software and B) the proportion of necrotic cells within the cell population was obtained (see Material and Methods 333.7).

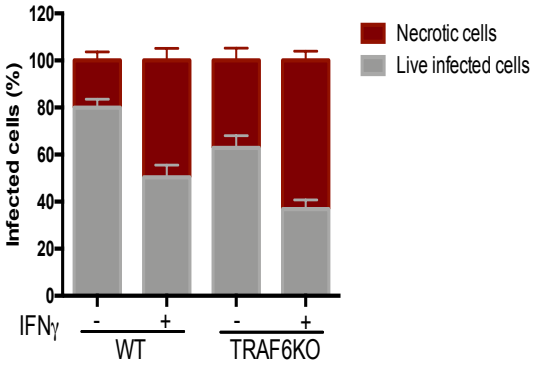

Supplemental Figure 3. 5. The absence of TRAF6 does not affect the infection dependent necrosis.

Wildtype and TRAF6 knockout (KO) MEFs were induced with 200U of IFNγ for 24 hours or kept uninduced. The cells were infected with *T. gondii* ME49 strain at MOI15 for 7 hours. The cells were washed and processed for Live/dead staining. Cells were harvested, washed with PBS, permeabilized prior the incubation with the violet LIVE/DEAD® dye to detect live/dead cells. Cells were fixed and stained with the TP3 antibody against the SAG1 *T.gondii* protein. Necrotic cells and live infected cells were assessed by FACS as detailed in Material and Methods.

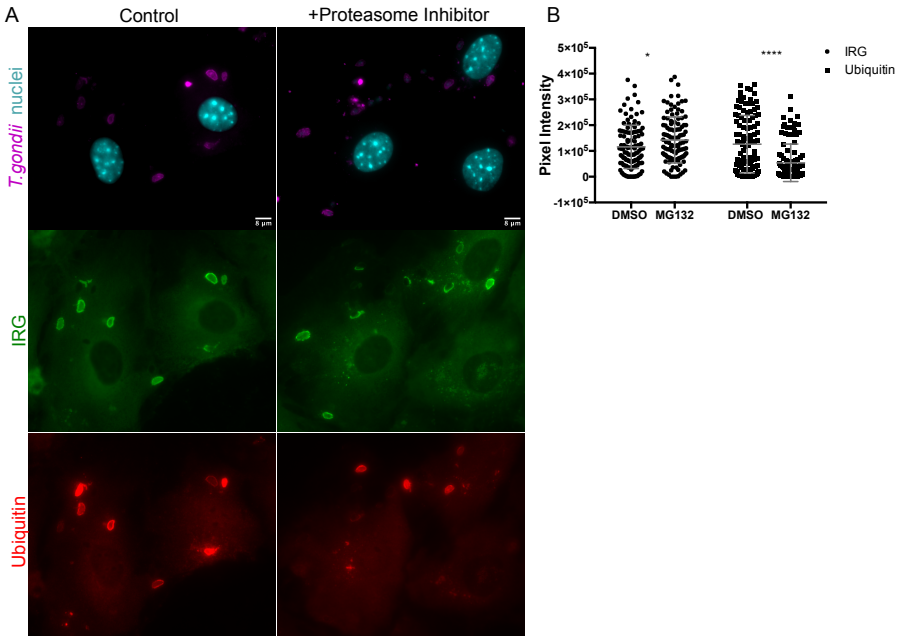

Supplemental Figure 3. 6. roteasome inhibition does not increase T. gondii ubiquitination.

IFNγ-stimulated C56BL/6 MEFs were incubated with DMSO or MG132 (20μM) for 3 hrs and infected with *Toxoplasma gondii* Me49 strain for 90 minutes. Cells were fixed and stained simultaneously for Irga6 (165/4 pAS), Irgb6 (141/1 pAS), Irgb10 (940/6 pAS) and Irgd (81/3 pAS) with the same secondary antibody coupled with Alexa Fluor 488 (green), ubiquitin (Fk2 mAb) with Alexa Fluor 555- conjugated secondary antibody (red) and GRA7 (JH 2.1.2 mAb) with Alexa Fluor 647-conjugated secondary antibody (magenta). The nuclei were labelled with DAPI. The intensity of IRG and ubiquitin were measured as determined by fluorescence microscopy and displayed in the graphic bar.

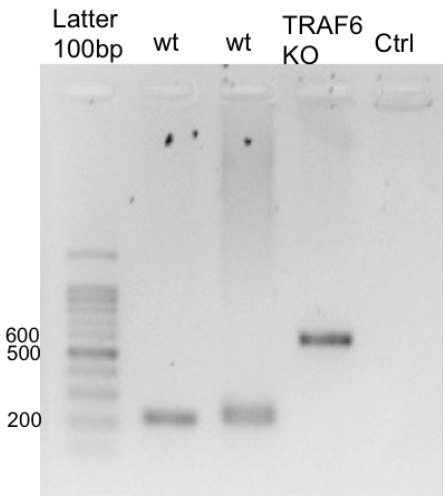

Supplemental Figure 3. 7. Verification of TRAF6KO- cells by PCR

Wt and TRAF6 KO MEFs were genotyped by using the Kapa express extraction kit. Traf6 rev 1 TCTTGCTCTTCAAGAGGATCG and the Traf6 rev 2 TTCATGGCGTGGTGCTATATA. PCR product of 245bp indicates the PCR product of wt cells genomic and 517bp indicate the TRAF6 knockout cells.

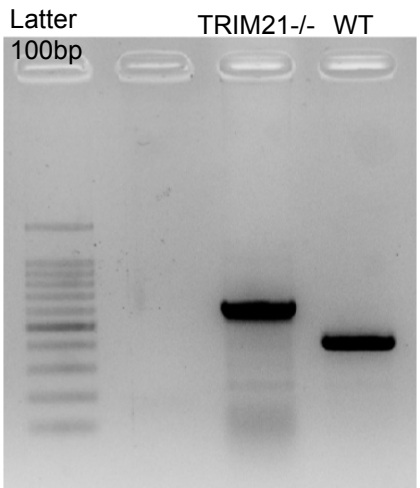

Supplemental Figure 3. 8. Wt and TRIM21KO genotyping PCR

Wt and TRIM21 KO MEFs were genotyped by PCR (the Kapa express extraction kit), using the primers FW (5′-CCTTGGCATTATTTGGGGGA-3′) and RV (5′-CTCCATGCTTCATGCAGTGC-3′) for the wild-type allele and FW (5′-CCTTGGCATTATTTGGGGGA-3′) and RV (5′-GCG GATCTTGAAGTTCACCT-3′) for the mutated allele. The WT amplicon has 400bp, and the KO amplican has 500bp[34].

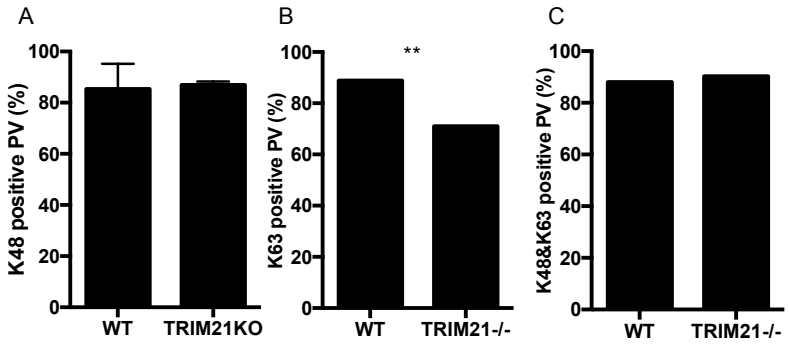

Supplemental Figure 3. 9. K63 Ubiquitination is reduced in TRIM21KO cells.

Wildtype, and TRIM21 knockout (KO) MEFs were induced with 200U of IFNγ for 24 hours or kept uninduced. The cells were washed, fixed and co-stained with immunoreagents against GRA7 (JH 2.1.2 mAB) with Alexa Fluor 647-conjugated secondary antibody; ubiquitin (Ub) (FK2 mab) with Alexa Fluor 555-conjugated secondary antibody and either with K48, K63-polyUb-specific Ab and with K48- and K63-polyUb-specific Ab simultaneously with Alexa Fluor 488-conjugated secondary antibody. **A, B** and **C)** More than a hundred of GRA7- and ubiquitin- double labelled PVs were used to get the proportions of K48, K63 or K48 and K63 positive PVs labeled with GRA7 and Ubiquitin were visually classified as K48, K63 or K48 and K63 positive and the proportions are represented in the bar graph. Mean +/- SD of 2 independent experiments is shown. . **, P<0,01.

Bibliography

1. Haldar, A. K. et al. Ubiquitin systems mark pathogen-containing vacuoles as targets for host defense by guanylate binding proteins. Proc. Natl. Acad. Sci. U. S. A. 112, E5628–E5637 (2015).
2. Husnjak, K. & Dikic, I. Ubiquitin-binding proteins: Decoders of ubiquitin-mediated cellular functions. Annu. Rev. Biochem. 81, 291–322 (2012).
3. Komander, D. & Rape, M. The ubiquitin code. Annu. Rev. Biochem. 81, 203–229 (2012).
4. Swatek, K. N. & Komander, D. Ubiquitin modifications. Cell Res. 26, 399–422 (2016).
5. Franco, L. H. et al. The Ubiquitin Ligase Smurf1 Functions in Selective Autophagy of Mycobacterium tuberculosis and Anti-tuberculous Host Defense. Cell Host Microbe 21, 59–72 (2017).
6. Sharma, V., Verma, S., Seranova, E., Sarkar, S. & Kumar, D. Selective autophagy and xenophagy in infection and disease. Front. Cell Dev. Biol. 6, 1–17 (2018).
7. Wang, L., Yan, J., Niu, H., Huang, R. & Wu, S. Autophagy and ubiquitination in Salmonella infection and the related inflammatory responses. Front. Cell. Infect. Microbiol. 8, 1–14 (2018).
8. Sasai, M., Pradipta, A. & Yamamoto, M. Host immune responses to Toxoplasma gondii. Int. Immunol. 30, 113–119 (2018).
9. Boehm, U. et al. Two families of GTPases dominate the complex cellular response to IFN-gamma. J. Immunol. 161, 6715–23 (1998).
10. Bekpen, C. et al. The interferon-inducible p47 (IRG) GTPases in vertebrates: loss of the cell autonomous resistance mechanism

in the human lineage. Genome Biol. 6, 1–18 (2005).

11. Müller, U. B. & Howard, J. C. The impact of Toxoplasma gondii on the mammalian genome. Curr. Opin. Microbiol. 32, 19–25 (2016).

12. Zhao, Z. et al. Autophagosome-Independent Essential Function for the Autophagy Protein Atg5 in Cellular Immunity to Intracellular Pathogens. Cell Host Microbe 4, 458–469 (2008).

13. Ohshima, J. et al. Role of Mouse and Human Autophagy Proteins in IFN-γ–Induced Cell-Autonomous Responses against Toxoplasma gondii . J. Immunol. 192, 3328–3335 (2014).

14. Haldar, A. K., Piro, A. S., Pilla, D. M., Yamamoto, M. & Coers, J. The E2-like conjugation enzyme Atg3 promotes binding of IRG and Gbp proteins to Chlamydia- and Toxoplasma- containing vacuoles and host resistance. PLoS One 9, (2014).

15. Ling, Y. M. et al. Vacuolar and plasma membrane stripping and autophagic elimination of Toxoplasma gondii in primed effector macrophages. J. Exp. Med. 203, 2063–2071 (2006).

16. Martens, S. et al. Disruption of Toxoplasma gondii parasitophorous vacuoles by the mouse p47-resistance GTPases. PLoS Pathog. 1, 0187–0201 (2005).

17. Zhao, Y. O. et al. Toxoplasma gondii and the immunity-related GTPase (IRG) resistance system in mice - A review. Mem. Inst. Oswaldo Cruz 104, 234–240 (2009).

18. Fleckenstein, M. C. et al. A toxoplasma gondii pseudokinase inhibits host irg resistance proteins. PLoS Biol. 10, 14 (2012).

19. Behnke, M. S. et al. The Polymorphic Pseudokinase ROP5 Controls Virulence in Toxoplasma gondii by Regulating the Active Kinase ROP18. PLoS Pathog. 8, (2012).

20. Niedelman, W. et al. The rhoptry proteins ROP18 and ROP5 mediate Toxoplasma gondii evasion of the murine, but not the human, interferon-gamma response. PLoS Pathog. 8, (2012).

21. Panas, M. W. et al. Translocation of Dense Granule Effectors across the Parasitophorous Vacuole Membrane in Toxoplasma-Infected Cells Requires the Activity of ROP17, a Rhoptry Protein Kinase . mSphere 4, 1–15 (2019).

22. Etheridge, R. D. et al. Virulence in Mice. 15, 537–550 (2015).

23. Fentress, S. J. et al. Phosphorylation of immunity-related GTPases by a toxoplasma gondii-secreted kinase promotes macrophage survival and virulence. Cell Host Microbe 8, 484–495 (2010).

24. Steinfeldt, T. et al. Phosphorylation of mouse immunity-related gtpase (IRG) resistance proteins is an evasion strategy for virulent Toxoplasma gondii. PLoS Biol. 8, (2010).

25. Coers, J. & Haldar, A. K. Ubiquitination of pathogen-containing vacuoles promotes host defense to Chlamydia trachomatis and toxoplasma gondii. Commun. Integr. Biol. 8, 1–3 (2015).

26. Lee, Y. et al. P62 Plays a Specific Role in Interferon-γ-Induced Presentation of a Toxoplasma Vacuolar Antigen. Cell Rep. 13, 223–233 (2015).

27. Wu, S., Shen, Y., Zhang, S., Xiao, Y. & Shi, S. Salmonella Interacts With Autophagy to Offense or Defense. Front. Microbiol. 11, 1–13 (2020).

28. Liesenfeld, O. et al. The IFN-γ-inducible GTPase, irga6, protects mice against toxoplasma gondii but not against plasmodium berghei and some other intracellular pathogens. PLoS One 6, (2011).

29. Alvarez, C. et al. Methods for the Measurement of Early Events

in Toxoplasma gondii Immunity in Mouse Cells. 5537, 127–133 (2020).

30. Collazo, C. M. et al. Inactivation of LRG-47 and IRG-47 reveals a family of interferon gamma-inducible genes with essential, pathogen-specific roles in resistance to infection. J. Exp. Med. 194, 181–188 (2001).

31. Man, S. M. et al. IRGB10 Liberates Bacterial Ligands for Sensing by the AIM2 and Caspase-11-NLRP3 Inflammasomes. Cell 167, 382-396.e17 (2016).

32. Henry, S. C. et al. Balance of Irgm protein activities determines IFN-gamma-induced host defense. J. Leukoc. Biol. 85, (2009).

33. Lamothe, B. et al. The RING domain and first zinc finger of TRAF6 coordinate signaling by interleukin-1, lipopolysaccharide, and RANKL. J. Biol. Chem. 283, 24871–24880 (2008).

34. Yoshimi, R. et al. Gene Disruption Study Reveals a Nonredundant Role for TRIM21/Ro52 in NF-B-Dependent Cytokine Expression in Fibroblasts. J. Immunol. (2009). doi:10.4049/jimmunol.0804121

35. Lilue, J., Müller, U. B., Steinfeldt, T. & Howard, J. C. Reciprocal virulence and resistance polymorphism in the relationship between Toxoplasma gondii and the house mouse. Elife 2013, 1–21 (2013).

36. Murillo-León, M. et al. Author Correction: Molecular mechanism for the control of virulent Toxoplasma gondii infections in wild-derived mice. Nat. Commun. 10, 79104 (2019).

37. Gubbels, M. J., Li, C. & Striepen, B. High-throughput growth assay for Toxoplasma gondii using yellow fluorescent protein. Antimicrob. Agents Chemother. 47, 309–316 (2003).

38. Sabin, A. B. TOXOPLASMIC ENCEPHALITIS IN CHILDREN. J.

Amirican Med. Assoc. (1941).

39. Behnke, M. S. et al. Virulence differences in Toxoplasma mediated by amplification of a family of polymorphic pseudokinases. Proc. Natl. Acad. Sci. U. S. A. 108, 9631–9636 (2011).

40. Caffaro, C. E. & Boothroyd, J. C. Evidence for host cells as the major contributor of lipids in the intravacuolar network of toxoplasma-infected cells. Eukaryot. Cell 10, 1095–1099 (2011).

41. Lilue, J., Müller, U. B., Steinfeldt, T. & Howard, J. C. Reciprocal virulence and resistance polymorphism in the relationship between Toxoplasma gondii and the house mouse. Elife 2013, 1–21 (2013).

42. Salomons, F. A. et al. Selective Accumulation of Aggregation-Prone Proteasome Substrates in Response to Proteotoxic Stress. Mol. Cell. Biol. 29, 1774–1785 (2009).

43. Carlow, D. A., Teh, S. J. & Teh, H. S. Specific antiviral activity demonstrated by TGTP, a member of a new family of interferon-induced GTPases. J. Immunol. 161, 2348–55 (1998).

44. Schindelin, J. et al. Fiji: An open-source platform for biological-image analysis. Nat. Methods 9, 676–682 (2012).

45. Martens, S. et al. Mechanisms regulating the positioning of mouse p47 resistance GTPases LRG-47 and IIGP1 on cellular membranes: retargeting to plasma membrane induced by phagocytosis. J. Immunol. 173, 2594–2606 (2004).

46. Khaminets, A. et al. Coordinated loading of IRG resistance GTPases on to the Toxoplasma gondii parasitophorous vacuole. Cell. Microbiol. 12, 939–961 (2010).

47. Coers, J., Starnbach, M. N. & Howard, J. C. Modeling infectious disease in mice: Co-adaptation and the role of host-specific IFNγ

responses. PLoS Pathog. 5, (2009).

48. Haldar, A. K. et al. IRG and GBP Host Resistance Factors Target Aberrant, 'Non-self' Vacuoles Characterized by the Missing of 'Self' IRGM Proteins. PLoS Pathog. 9, (2013).

49. Hunn, J. P. et al. Regulatory interactions between IRG resistance GTPases in the cellular response to Toxoplasma gondii. EMBO J. 27, 2495–2509 (2008).

50. Papic, N., Hunn, J. P., Pawlowski, N., Zerrahn, J. & Howard, J. C. Inactive and active states of the interferon-inducible resistance GTPase, Irga6, in vivo. J. Biol. Chem. 283, 32143–51 (2008).

51. Maric-Biresev, J. et al. Loss of the interferon-γ-inducible regulatory immunity-related GTPase (IRG), Irgm1, causes activation of effector IRG proteins on lysosomes, damaging lysosomal function and predicting the dramatic susceptibility of Irgm1-deficient mice to infection. BMC Biol. 14, 1–20 (2016).

52. Degrandi, D. et al. Extensive Characterization of IFN-Induced GTPases mGBP1 to mGBP10 Involved in Host Defense. J. Immunol. 179, 7729–7740 (2007).

53. Johnston, A. C. et al. Human GBP1 does not localize to pathogen vacuoles but restricts Toxoplasma gondii. Cell. Microbiol. 18, 1056–1064 (2016).

54. Saeij, J. P. & Frickel, E. M. Exposing Toxoplasma gondii hiding inside the vacuole: a role for GBPs, autophagy and host cell death. Curr. Opin. Microbiol. 40, 72–80 (2017).

55. Chen, Z. J. & Sun, L. J. Nonproteolytic Functions of Ubiquitin in Cell Signaling. Mol. Cell 33, 275–286 (2009).

56. Akutsu, M., Dikic, I. & Bremm, A. Ubiquitin chain diversity at a glance. J. Cell Sci. 129, 875–880 (2016).

57. Zhao, Y. O., Khaminets, A., Hunn, J. P. & Howard, J. C. Disruption of the Toxoplasma gondii parasitophorous vacuole by IFNg-inducible immunity-related GTPases (IRG proteins) triggers necrotic cell death. PLoS Pathog. 5, (2009).

58. Lee, Y. et al. Initial phospholipid-dependent Irgb6 targeting to Toxoplasma gondii vacuoles mediates host defense. Life Sci. alliance 3, 1–16 (2020).

59. Foltz, C. et al. TRIM21 is critical for survival of Toxoplasma gondii infection and localises to GBP-positive parasite vacuoles. Sci. Rep. 7, 1–13 (2017).

60. Clough, B. et al. K63-Linked Ubiquitination Targets Toxoplasma gondii for Endo-lysosomal Destruction in IFNγ-Stimulated Human Cells. PLoS Pathog. 12, (2016).

61. van Wijk, S. J. L. et al. Fluorescence-Based Sensors to Monitor Localization and Functions of Linear and K63-Linked Ubiquitin Chains in Cells. Mol. Cell 47, 797–809 (2012).

62. Wijk, S. J. L. Van et al. Linear ubiquitination of cytosolic Salmonella bacterial proliferation. 17066, (2017).

63. Morishita, H. & Mizushima, N. Diverse cellular roles of autophagy. Annu. Rev. Cell Dev. Biol. 35, 453–475 (2019).

64. Choi, J. et al. The parasitophorous vacuole membrane of toxoplasma gondii is targeted for disruption by ubiquitin-like conjugation systems of autophagy. Immunity 40, 924–935 (2014).

65. Selleck, E. M. et al. Guanylate-binding Protein 1 (Gbp1) Contributes to Cell-autonomous Immunity against Toxoplasma gondii. PLoS Pathog. 9, (2013).

66. Könen-Waisman, S. & Howard, J. C. Cell-autonomous immunity to Toxoplasma gondii in mouse and man. Microbes Infect. 9,

1652–1661 (2007).

67. Waters, S., Marchbank, K., Solomon, E., Whitehouse, C. & Gautel, M. Interactions with LC3 and polyubiquitin chains link nbr1 to autophagic protein turnover. FEBS Lett. 583, 1846–1852 (2009).

Chapter 4

4. General discussion

Cells rely on activating the Jak / STAT signalling pathway and expressing IFN-induced GTPase genes to respond against one of the most successful parasites in the world, *T. gondii*. Mouse cells initiate the anti-Toxoplasma process with the recruitment of GTPases, particularly IRGs and GBPs that accumulate on the PVM immediately after infection, leading to its disruption and consequently death of the parasite and subsequent elimination of the parasite's niche via programmed host cell death.

The parasite's ability to escape this GTPase-dependent immune system response ensures the parasite's progression to differentiation to eventually establish chronic toxoplasmosis, ensuring parasite transmission. However, only a small number of parasites escape the action of GTPases.

What differentiates the elimination-prone and elimination-resistant parasites underlies lifelong parasite persistence in the host, with dangerous scenarios of reactivation in immunocompromised individuals.

One hypothesis is that a differential modification of the PVM during and after *T. gondii* invasion generates PVMs that carry or do not carry one or more tags allowing the binding of IRG proteins. Despite lack of data to assume that all PVMs have the same composition, here we focused on the events taking place within the first hours of infection to understand what determines the selection of PVs such that they are initially covered by IRGs and destined for elimination, or not covered by IRGs, as well as the relationship between the recruitment of ubiquitin and the subsequent processes.

Are factors intrinsic to parasites or cells making this determination? Although it is relatively well described that IRG proteins target the PVM to destroy *T. gondii*, the molecular mechanisms and decision making that direct GTPases to particular PVs and avoid others and how GTPases locate and recognize these PVs remain unclear.

Previous studies have shown that ubiquitin and protein components of the autophagy process are also deposited in PVs. These studies suggest that ubiquitin marks PVs for the deposition of GBPs in an IRG-dependent process, but the role of these proteins in the death of the parasite and downstream pathways is unknown. In this thesis I have attempted to clarify some aspects of the relation between IRG proteins and the destructive events associated with the elimination of the parasite.
This work led to the main conclusions presented and discussed below.

4.1. Summary of the findings.

This work began as described in Chapter 2 with an analysis of factors that determine the qualitative and quantitative heterogeneity of effector IRGs recruited onto the PVM that decide whether the parasite's vacuole is loaded for destruction or not. Firstly, we evaluated whether the cytosolic availability of IRGs explains the frequency of unloaded PVs for disruption. We found that regardless of the amount of IRGs available within the cytoplasm after 24 hours of IFNγ induction, immediately after infection by avirulent *T. gondii*, effector IRGs initiate an individual PVM loading process, with each IRG covering different proportions of PVs, which together complete around 80% of all PVs; about 20% of PVs remain uncovered, even when cytosolic IRG protein concentration is high and cells are infected with a single parasite. Additionally, we analyzed whether the selection of PVs to be destroyed is determined once the pioneer IRG (Irgb6) is recruited to the PVM, and is used as a platform for others IRGs. Our analyses revealed that the recruitment of other IRG proteins are not completely dependent on the pioneer Irgb6 on the PVM, and that the loading of Irgb6 alone is not sufficient to destroy the PVM.

Then we moved on to investigate the intrinsic parasite factor that might explain the existence of unloaded parasite vacuoles, which persist within the cell and allow tachyzoite differentiation to bradyzoites.

Earlier findings (Khaminets) [1] showed that the initiation of IRG protein loading is a stochastic event that may begin immediately after entry of the parasite into the cell, or be delayed for a variable interval. We considered the possibility that if loading is not initiated soon enough, vacuoles might have time to undergo some form of maturation that would permanently inhibit IRG protein access. To approach this question we first confirmed that when *T. gondii* invades cells that are either not primed with IFNγ or induced for less than 3 hours with IFNγ, the parasite interferes with global IRG expression and recruitment to the PVM. TgIST, secreted in the host cell cytosol [2], and possibly other unknown factor(s), block IRG protein expression and accumulation at the PVM. However, in the absence of TgIST we found no evidence that the PVM "matures" and becomes unloadable by IRG proteins with time of residence in the absence of IFNγ, thus the "unloaded" vacuoles in IFNγ-induced cells cannot be explained by vacuolar maturation.

In chapter 3 we focused on the determination of whether ubiquitin recruitment to the PV is due to the ubiquitination of IRG proteins. Firstly, we analyzed the behavior of ubiquitin relative to the recruitment to IRG proteins described in chapter 2. We demonstrated that in mouse cells induced previously with IFNγ, ubiquitin assembles on about 70% of PVs that have already been loaded by IRGs, coincident with PVs loaded with both Irgb6 and Irga6, or Irgb6, Irga6 and Irgd. Vacuoles loaded only with Irgb6 are not ubiquitinated. While IRGs begin to accumulate in PVs 15 min after infection, we can begin to visualize ubiquitin accumulation around 30 min after infection; ubiquitin accumulation increases over time, reaching greater intensities on IRG-labeled vacuoles. We analyzed whether the buildup of ubiquitin may be a consequence of the destruction of the PVM by the IRGs. In later

times of infection we found some strongly ubiquitinated PVs displaying only fragments of IRG-labelled material, indicative of disrupted PVs. Higher intensities of ubiquitin appear associated with the parasite within the disrupted PVM. In contrast, a low or absent ubiquitin is more frequent on PVs that appear to have a layer of intact IRGs.

The resistance of CIM to virulent parasites requires the presence of Irgb2-b1. We found that mouse cells that possess Irgb2-b1 decoys are capable of ubiquitinating virulent *T. gondii* PVs. This ability to ubiquitinate virulent *T. gondii* disappears with the removal of Irgb2-b1 and is partially recovered with the reintroduction of Irgb2-b1. This behaviour is consistent with the known ability of certain allelic forms of Irgb2b1 to inhibit the phosphorylation and inactivation of effector IRG proteins by the active ROP5/ROP18 kinase complex secreted by virulent strains of Toxoplasma.

When the spatial separation between the PVM and the parasite allowed it, we were able to show that ubiquitin is exclusively associated with the membrane of the parasite itself, while both IRG and GBP proteins are exclusively associated with the PVM.

Finally, through the analysis of the structural characteristics of the ubiquitination seen on *T. gondii* PVs, we tried to infer its possible functions and participation in downstream pathways. We found that K63- and K48-linkage ubiquitin chains cooperate with other ubiquitin lysines in the assembly of ubiquitin chains on PVs before the host cells progress to the process of necrosis.

4.2. Cooperative loading of effector IRG proteins on the PVM are the key to the cell's autonomous resistance to *T. gondii*

The ability of mouse cells to destroy *T. gondii* is attributed to IRGs. Multiple effector IRG proteins and GBPs rapidly surround susceptible PVs, leading to the disruption of the PVM. IRG loading is highly ordered: it starts with Irgb6, followed by Irga6 and Irgd [1], leading to the concept of Irgb6 as a “pioneer” in the loading process.

We decided not to include Irgb10 in this analysis, since the data repeatedly demonstrates independence in loading between Irgb10 and Irgb6 (Figure 2.4 and see also Khaminets 2010 Fig. 6). It is not strictly relevant to this thesis, but the accumulating evidence is that Irgb10 plays a role in resistance to certain bacteria and is probably not relevant to immunity against T. gondii. The role of Irgb10 in bacterial resistance [3,4] is unquestionable, but it is not clear in *T. gondii* resistance since it behaves independently of others IRGs. In cells lacking the regulators Irgm1 and Irgm3, Irgb10 was observed to mislocalize to different aggregates than other effector IRGs (Figure 3.5), and Irgb10-deficient fibroblasts show no deficiency in cell-autonomous resistance against T. gondii [5]. Although Irgb10 localizes with the PVM, as do other effector IRGs, it may be behaving like the non-immune IRG homologue, IRGC, expressed exclusively in haploid spermatids [6] (Christoph Rohde, unpublished data), which, when transfected into IFNγ-induced, infected cells, is also recruited with the immune IRG effectors to the PVs (Julia Hunn, unpublished data).

The loading process results in about 80% of PVs covered by Irgb6, about 50% by Irga6, and about 40% by Irgd, generating 4 categories of PVs: a significant proportion covered by Irgb6, a6, d; in small proportions by Irgb6, Irga6; by Irgb alone, and others PVs completely unloaded [1] (Figure 2.4). The impact of IRG loading is the disruption of

the vacuole, followed by death of the parasite and subsequently of the host cell[7]. From our data, it appears likely that loading of Irgb6 alone, as occurs on about 20% of PV, is not sufficient to lead to PV destruction as indicated by ubiquitination of the parasite. Whether there is a further distinction between the fates of the Irgb6+Irga6+ PV and the Irgb6+Irga6+Irgd+ PV is not apparent.

The rupture of the PV was first observed in IFNγ-induced cells transfected with Irga6-ctag1-EGFP[7]. Since essentially 100% of Irga6 positive PVs are also Irgb6 positive we can assume those interrupted PVM were also Irgb6 positive. The same morphology was also observed in the PVs positive for Irgb6, and our evidence suggest that it is probably only the double- or triple-positive PVs that become disrupted.

After pre-stimulation with IFNγ, all IRGs are "equally" available in the cytoplasm. With infection, the IRGs are constitutively activated (GTP), and by diffusion, they accumulate at the PVM, first Irgb6, followed by Irga6 and Irgd [1]. We demonstrate that the concentration of IRGs available in the infected cytosol does not limit the loading of IRG on the PVM (Figure 2.8).

Although the effector IRGs clearly demonstrate the “Russian Doll” inclusion hierarchy [1] they are quantitatively and to some degree also qualitatively independent. The absence of Irga6 somewhat reduces the intensity of Irgb6 recruited to the PVM [1], but the absence of Irgb6 does not significantly reduce Irga6 recruitment (Figure 2.6). We show that IRG loading on the PVM is essentially independent of the concentration of IRG in the cytoplasm of the invaded cell (Figure 2.8), there is no correlation between the loading intensities of two vacuoles in the same cell, and that the loading of Irgb6 and the loading of Irga6 are quantitatively independent (Figure 2.5). Loading of Irga6 occurs in the absence of Irgb6 but is somewhat reduced in intensity, thus it is unlikely that the dominance of Irgb6 loading is due to competition for a specific

target on the PVM with Irgb6 having a higher affinity, since absence of Irgb6 would then predict an increase in Irga6 loading. We conclude that each vacuole is “tagged” at the point of entry by specific ligands for individual IRG proteins.

On this hypothesis, we assume that the cytosolic leaflet of the host plasma membrane carries distinct tags for different IRG proteins, which are captured in the PVM during parasite invasion and retained after the PV is detached. On this hypothesis the existence of heterogeneous local concentrations (clustering) of tags may also explain the heterogeneity of Irg loading observed on individual PVMs, and the clear hierarchy of loading frequency b6>a6>d can be explained by a hierarchy in the membrane concentrations of the different tags for the three IRG effectors. Very recently it was shown that Irgb6 has specificity to bind monophosphorylated phosphoinositide (PI) 5P and phosphatidylserine (PS) on the PVM, but cannot bind PI3P, PI4P, PI(3,5)P2, PI(3,4,5)P3, and PA[5]. Binding of PI5P was shown to be due to specific residues in C-terminal predicted helices of Irgb6. Earlier studies showed a remarkable sequence homology in the alpha-K helical region of the three regulator IRG proteins, Irgm1, Irgm2 and Irgm3 with the phosphoinositide binding pocket of phospholipase [8]. More studies are needed to correlate effector IRG proteins with specific tags on the PVM.

4.3. Partial regulation of IRG expression and recruitment by TgIST is important for parasite.

Cells rely on the IFN-dependent STAT1 transcriptional activity, which regulates the expression of genes induced by IFN, to defend themselves against *T. gondii*. On the other hand, the parasite uses an

arsenal of secreted proteins to maintain itself in the cell in opposition to IFN-inducible proteins.

Previous studies have shown that parasites can suppress the interferon-dependent response by interfering with STAT1 transcriptional activity via the TgIST inhibitor [9]. After host cell invasion, *T. gondii* secretes TgIST, which mediates the interaction of Mi-2 nucleosome and deacetylase (Mi-2 / NuRD) with STAT1 and thereby blocks the transcription of STAT1-dependent genes [9].

By using IRG proteins as probes for STAT1 functionality, we demonstrated that WT parasites can block the expression of Irga6 and Irgb6 to allow parasite replication. This immune response evasion was observed at the cytoplasm level and also at recruitment of IRGs to the PVM (Figure 2.10 and 2.11). The parasite's ability to escape the immune system leads to the tachyzoite-to-bradyzoite transition stage [10].

Using *T. gondii* parasites deficient in TgIST (IST KO parasites) to infect mouse cells, we demonstrated that, despite the absence of the IRG blocker (IST), the TgIST KO parasite can still cause moderate attenuation of Irgb6 expression compared to the wild type (WT) parasite or the IST KO parasite complemented with IST.

We found that in the absence of TgIST, cells cannot allow complete IRG expression at 6h and 12h, as observed at 6 and 12 h with pre-stimulation with IFNγ (Figure 2.13). The recruitment of IRGs to PVs expected at 6 and 12 hours is also incomplete compared with the control situation (Figure 2.14). This leads us to assume that secreted TgIST cooperates with an additional unknown effector to inhibit the transcription of IRGs in the first 12 hours of interferon stimulation.

Previous studies have shown that in more advanced stages of bradyzoite infection, TgIST suppresses the IFN-dependent response partially in both mice and humans [9,11]. This second unknown effector may be as important as TgIST in blocking the expression of IRGs, or maybe one enhances the activity of the other when more than the

effect of TgIST is necessary to get the expected IRG expression at 6 and 12 hours of IFNγ induction.

T. gondii secretes TgIST immediately after host cell invasion, as TgIST protein can be identified in the cytoplasm at 20 minutes of infection [9]; it takes more than 3 hours for TgIST to translocate to the cell nucleus, where it accumulates over time: it has been identified in the nucleus from 9 hours post-infection onwards and persisted for a long time, with reduction after 48 hours until 6 days [9,12].

The arrival of IST in the nucleus, and therefore the initiation of STAT1 inhibition, after 3 hours may explain the moderate effect of the absence of IST in relation to wild type TgIST in the expression of IRGs at 6 hours of infection. Still, it does not explain the incomplete expression of IRGs observed at 12 hours (Figure 2.13).

Our suspicions for the additional unknown effector that inhibits the transcription of IRGs rest with the *Toxoplasma* NCoR / SMRT modulator (TgNSM), that has been shown to down-regulate IFNγ signalling and inhibit necroptosis in human and mouse cells [9]. Unlike TgIST, TgNSM is secreted by the parasite after 8 hours of infection and translocates to the nucleus; although its arrival time is unknown, TgNSM was identified in the nucleus at 20 hours. Although studies describe the role of TgNSM protein in a more advanced stage of infection, it is plausible that, as early as 12 hours after parasite entry, it is possible to observe its effect on the expression of IRGs in such a way that it may explain the difference observed between TgIST KO parasites at 12 hours with and without pre-stimulation with IFNγ. TgIST and TgNSM alone do not have a significant impact on the survival of the cysts and host cell necrotic death, but together they have a significant inhibitory effect on the survival of the cysts and prevention of necroptosis. The two effectors may act in combination and thus have a considerable impact on the suppression of IRG expression. The effect of these effectors is seen in cells infected with IST KO parasite

complemented with IST shows many more parasites sitting in cells, which Irgb6 expression downregulated than in cells Expressing Irgb6 (Suplemental figure 5.1.)

Myc regulation 1 (Myr1) is a complex located on the PVM, responsible for transporting various GRA effectors, from the parasite to host cell nucleus, including TgIST and TgNSM [13]. Since the absence of MYR1 also does not allow full expression of IRGs at 6 and 12 hours of infection (Supplemental Figure 5.2.) we consider other parasite effectors, which translocation to nucleus is in a MyR1-independent way, to complement the effect of TgIST in IRG expression;

These data leave open the possibility of other complementary effectors in suppressing the transcription of IFNγ-dependent genes.

By excluding all the secreted factors of the parasite that interfere with IRG expression we can analyze over time a parasite completely susceptible to IRG and test the hypotheses that the duration of residence of the PV within the cell leads to PV maturation that makes it resistant to elimination by preventing IRG coverage. So far, our results suggest that failure to load IRG proteins on a PV is not due to maturation, and requires another kind of explanation. The “tag” model put forward above would suggest that such vacuoles are surrounded by a patch of membrane that was simply devoid of sufficient tags to load IRG proteins.

4.4. Ubiquitin at the parasite surface marks the disruption of the PVM.

The *T. gondii* tachyzoite establishes the PV shortly after cell invasion to protect itself against the host immune effectors and allow its persistence and progression to the next stage. However, several host cell effector proteins associated with the immune response conspire to bind to PVs, including IRGs, GBPs, autophagy adapters and ubiquitin.

Previous studies have shown that IRGs arrive at the PV very early and that they are responsible for its permeabilization and disruption [1,14]. By analyzing the recruitment of IRGs and ubiquitin in parallel, we demonstrate that the ubiquitination of the PV is a process that starts with the recruitment of IRGs and that it signals PV disruption. The permeabilization of PVs begins 30 minutes after infection[14], and coincides with the starting point for ubiquitin accumulation (Figure 3.7.). After permeabilization of the PV, ubiquitin joins IRGs in the PV area with a rise in frequencies of ubiquitinated PVs and ubiquitin signal intensification at later timepoints of infection. We demonstrate that ubiquitin accumulates more intensely in clearly destroyed PVMs (Figure 3.8. and 3.12.) and that the presence of effector IRGs at the PVM is essential for the buildup of ubiquitin.

Deficiency or disturbance in the disruption of PVs either in Irgb6-deficient cells or in cells altogether deficient in IRG effector functions on PVs due to the absence of the IRG regulator proteins Irgm1 and Irgm3 [15] results in blockage of ubiquitin recruitment on the PVs (Figure 3.4. and 3.5., respectively).

As described above, the recruitment of Irga6 and Irgd onto PVs already covered by Irgb6 enhances PVM disruption and leads to more efficient ubiquitination than that seen on PVs in Irgb6-deficient cells that are positive only for Irga6 and Irgd (Figure 3.3. C).

Infection studies of virulent *T. gondii* parasites and susceptible laboratory mice have shown that ROP kinases prevent the disruption of the PV by inactivation of IRGs [1,16] and consequently the parasites are not ubiquitinated [17] (Figure 3.2). In the case of wild-derived mouse strains whose cells contain the Irgb2-b1 tandem IRG decoy, cells containing Irgb2-b1 avoid the inactivation of effector IRGs, leaving the PVs vulnerable to disruption, presumably resulting in exposure of parasite membrane targets that are the substrate for the observed ubiquitin accumulation (Figure 3.9, 3.10).

Members of the autophagy (ATG) protein family, which include ATG5-12-16L1, ATG3, Atg5, ATG7 and GABARAP, are crucial for ubiquitin recruitment in PVs [17,18] unrelated with xenophagy [19] and P62 for the parasites [17]. Defect in ATG components mislocalise IRG effectors spontaneously in form of aggregates, when cells are treated with IFNγ, in a very similar manner to loss of the IRGM regulator proteins. The disturbance in ubiquitin accumulation in the autophagy KO cells is the result of the inaccurate functioning of GTPases like Irga6 [1,18–20] Irgb6 [1,21], Irgd [1] and GBPs [18,19,21]. Lack of GTPase accumulation on the PV means that there is no PV disruption. Perhaps these ATG effectors act in some way as chaperones for IRG proteins, protecting the activated state against spontaneous denaturation

In human cells, *T. gondii* has been shown to become ubiquitinated and subsequently recruit autophagy adaptors such as NDP52, p62, optineurin as well as LC3B adaptors, which presumably control parasite replication without PV disruption [22–25]. Although the cellular significance of this ubiquitination is not yet clear, our work denotes PVMs decorated by IRGs and parasites decorated by ubiquitin as a marker for the immune targeting of host cell necrosis. The chronology of events is unclear, but all necrotic cells seem to harbour at least one heavily ubiquitin-loaded tachyzoite (Figure 3.15).

After recruitment of the IRGs to the PVM, the *T. gondii* PV is additionally decorated by P62 [15], and ubiquitin is assembled by TRAF6, TRIM21, and probably other E3 ligase(s) onto the parasite (Figure 3.13).
Whether P62 has a role in ubiquitin recruitment to the PV is still inconclusive, since previous data showed opposite tendencies, with P62 seemingly mediating ubiquitin deposition [15] or not [17]. Work by

others in the Howard lab suggests that host cell necrosis is impaired in NDP52 knockdown cells, i.e. MEFs expressing shRNAs against NDP52, and to some extent in MEFs expressing shRNAs against P62, suggesting the existence of a role for autophagy adaptors in the necrotic response of IFNγ-primed cells to avirulent *Toxoplasma* (Joana Loureiro, unpublished data). Although the presence of P62 is certainly dependent on PV disruption [5], we do not yet know whether autophagy acts upstream or downstream of the ubiquitination step.

The closest well studied example that links ubiquitination and programmed cell death is the elimination of Salmonella [26,27]. The cytosolic exposed bacteria are ubiquitinated and directed to autophagy through the adapters [28]. GBPs that colocalize with NDP52 [29] accumulate in the membrane of bacteria, forming a signal activation platform for pyroptosis [29,30].

4.5. Concluding remarks and future perspectives

Many recent studies have integrated ubiquitin into early defence mechanisms against *T. gondii*, a process which is initiated in mice by the essential presence of IRG proteins whose activity at the parasitophorous membrane determines subsequent events.

Our lab has made primary contributions to the primordial role of IRGs in the control of avirulent *Toxoplasma* parasites. Upon inactivation by virulence factors, IRG proteins are not efficient against virulent strains of *T. gondii*. A small portion of avirulent parasites also evades binding by the IRGs and these almost certainly represent the parasites that go on to survive the immune response and achieve chronicity.

The key to parasite elimination in mouse cells lies in the recognition of PVs by the IRGs. The work developed in this thesis explored the first events that determine the elimination of PVs by IRGs. It demonstrated that the cooperation of different IRGs in PVs is crucial for their elimination and probably results from the stochastic distribution of as yet unidentified “tag” molecules in the host cell's plasma membrane. Our work demonstrated that each IRG independently covers a proportion of PVs and that Irgb6 binding is necessary but not sufficient to disrupt the PVM.

Accumulation of Irga6 and Irgd along with Irgb6 stimulate the disruption of the PV and the subsequent accumulation of ubiquitin. Irgb6 is necessary but not sufficient. IRGs are not themselves ubiquitinated but they are necessary for PV permeabilization and access of ubiquitin to the parasite within. Thus the presence of ubiquitin is a strong marker for a disrupted PV.

Further studies are needed to better understand how PV selection works, through the identification of the tag molecules(s) for IRGs on the PVM, such as, for example, a correlation study between Irgb6 and its specific tag on the PVM, as well the colocalization of the specific tag for

Irgb6 with all effectors, which would allow us to know about the non IRG-covered PVs. Additionally, colocalization studies of each IRG Irgb6 tag will allow us to know about common or independent tags for other IRGs.

With more in-depth studies, it may be possible to identify whether the parasites develop additional strategies such as a change, or "maturation" process over time once inside the cell that would render PVs progressively les susceptible to IRG proteins. Our experiments using TgIST - deficient cells so far showed no such process, although they indicated the existence of an additional parasite function capable of reducing IRG protein binding. This function probably coincides with the recently identified TgNSM [9].

These statements provide useful contributions for studies on these or other molecular defence mechanisms against this or other pathogens that use similar strategies.

4.6. Supplementary material

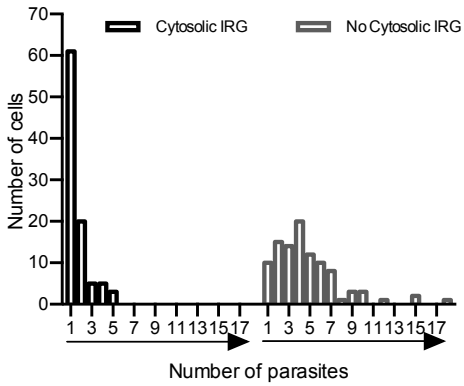

Supplemental Figure 4. 1. Cells that do not express IRG harbour more PVs, than cells that express IRG

MEFs were simultaneously induced with IFNγ and infected with Pru ku80 delta IST + HA-IST. After 12 hours the samples were processed for Immunofluorescence for GRA7 (**JH 2.1.2 mAB**) and for Irgb6 (serum 141). The number of PV within positive cytosolic IRG and negative cytosolic IRG populations were counted and the number was plotted as a frequency distribution.

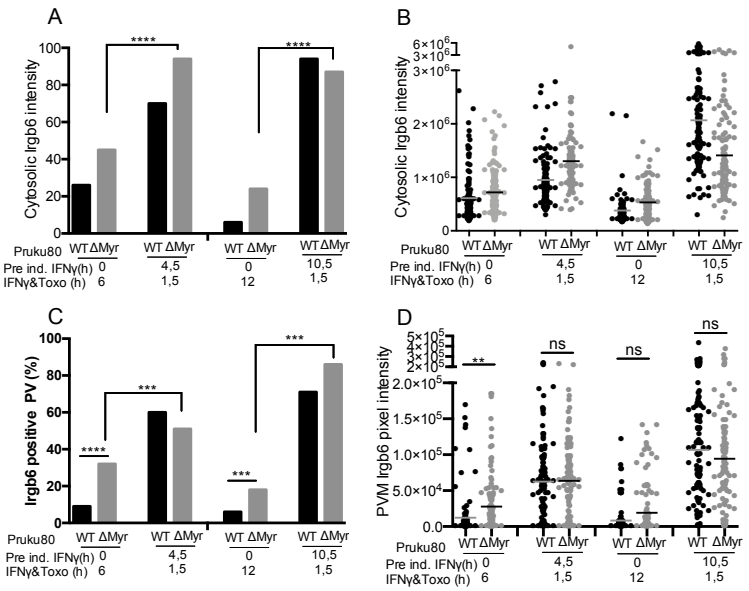

Supplemental Figure 4. 2 MYR-independent factor impact Irgb6 expression. T. gondii

Mouse DDCs were split in 3 populations, and two populations was pre-induced with IFNγ (200 U/ml), either for 4,5 hours or for 10,5 hours and another was not induced. The cells were then incubated with T.gondii (either Pru ku80 (WT) or Pru ku80Δmyr1) suspension in medium with IFNγ (200 U/ml), at a MOI=10 for 1,5 hours for 6 and 12 hours. The samples were processed for Immunofluorescence for GRA7 (**JH 2.1.2 mAB**) and for Irgb6 (serum 141). **A** and **B)** The intensity of Irgb6 on infected cytosol was accessed as described in Material and Methods and the proportion of infected Irgb6 positive cells was displayed. **C)** The percentage of PVs carrying Irgb6 and **D)** the intensity were displayed.

Bibliography

1. Khaminets, A. et al. Coordinated loading of IRG resistance GTPases on to the Toxoplasma gondii parasitophorous vacuole. Cell. Microbiol. 12, 939–961 (2010).
2. Olias, P., Etheridge, R. D., Zhang, Y., Holtzman, M. J. & Sibley, L. D. Toxoplasma Effector Recruits the Mi-2/NuRD Complex to Repress STAT1 Transcription and Block IFN-γ-Dependent Gene Expression. Cell Host Microbe 20, 72–82 (2016).
3. Bernstein-Hanley, I. et al. The p47 GTPases Igtp and Irgb10 map to the Chlamydia trachomatis susceptibility locus Ctrq-3 and mediate cellular resistance in mice. Proc. Natl. Acad. Sci. U. S. A. 103, 14092–14097 (2006).
4. Man, S. M. et al. IRGB10 Liberates Bacterial Ligands for Sensing by the AIM2 and Caspase-11-NLRP3 Inflammasomes. Cell 167, 382-396.e17 (2016).
5. Lee, Y. et al. Initial phospholipid-dependent Irgb6 targeting to Toxoplasma gondii vacuoles mediates host defense. Life Sci. alliance 3, 1–16 (2020).
6. Howard, J. C., Hunn, J. P. & Steinfeldt, T. The IRG protein-based resistance mechanism in mice and its relation to virulence in Toxoplasma gondii. Curr. Opin. Microbiol. 14, 414–421 (2011).
7. Martens, S. et al. Disruption of Toxoplasma gondii parasitophorous vacuoles by the mouse p47-resistance GTPases. PLoS Pathog. 1, 0187–0201 (2005).
8. Martens, S. et al. Mechanisms regulating the positioning of mouse p47 resistance GTPases LRG-47 and IIGP1 on cellular membranes: retargeting to plasma membrane induced by phagocytosis. J. Immunol. 173, 2594–2606 (2004).

9. Rosenberg, A. & Sibley, L. D. Toxoplasma gondii secreted effectors co-opt host repressor complexes to inhibit necroptosis. Cell Host Microbe 1–13 (2021). doi:10.1016/j.chom.2021.04.016

10. Di Cristina, M. et al. Temporal and spatial distribution of Toxoplasma gondii differentiation into bradyzoites and tissue cyst formation in vivo. Infect. Immun. 76, 3491–3501 (2008).

11. Mayoral, J., Shamamian, P. & Weiss, L. M. crossm In Vitro Characterization of Protein Effector Export in the. 11, 1–17 (2020).

12. Gay, G. et al. Toxoplasma gondii TgIST co-opts host chromatin repressors dampening STAT1-dependent gene regulation and IFN-γ-mediated host defenses. J. Exp. Med. 213, 1779–1798 (2016).

13. Wang, Y., Sangaré, L. O., Paredes-Santos, T. C. & Saeij, J. P. J. Toxoplasma Mechanisms for Delivery of Proteins and Uptake of Nutrients across the Host-Pathogen Interface. Annu. Rev. Microbiol. 74, 567–586 (2020).

14. Zhao, Y. O., Khaminets, A., Hunn, J. P. & Howard, J. C. Disruption of the Toxoplasma gondii parasitophorous vacuole by IFNg-inducible immunity-related GTPases (IRG proteins) triggers necrotic cell death. PLoS Pathog. 5, (2009).

15. Haldar, A. K. et al. Ubiquitin systems mark pathogen-containing vacuoles as targets for host defense by guanylate binding proteins. Proc. Natl. Acad. Sci. U. S. A. 112, E5628–E5637 (2015).

16. Zhao, Y. O. et al. Toxoplasma gondii and the immunity-related GTPase (IRG) resistance system in mice - A review. Mem. Inst. Oswaldo Cruz 104, 234–240 (2009).

17. Lee, Y. et al. P62 Plays a Specific Role in Interferon-γ-Induced

Presentation of a Toxoplasma Vacuolar Antigen. Cell Rep. 13, 223–233 (2015).

18. Sasai, M. et al. Essential role for GABARAP autophagy proteins in interferon-inducible GTPase-mediated host defense. Nat. Immunol. 18, (2017).

19. Choi, J. et al. The parasitophorous vacuole membrane of toxoplasma gondii is targeted for disruption by ubiquitin-like conjugation systems of autophagy. Immunity 40, 924–935 (2014).

20. Zhao, Z. et al. Autophagosome-Independent Essential Function for the Autophagy Protein Atg5 in Cellular Immunity to Intracellular Pathogens. Cell Host Microbe 4, 458–469 (2008).

21. Ohshima, J. et al. Role of Mouse and Human Autophagy Proteins in IFN-γ–Induced Cell-Autonomous Responses against Toxoplasma gondii . J. Immunol. 192, 3328–3335 (2014).

22. Bhushan, J. et al. Isg15 connects autophagy and ifn-dependent control of toxoplasma gondii infection in human cells. MBio 11, 1–19 (2020).

23. Selleck, E. M. et al. A Noncanonical Autophagy Pathway Restricts. MBio 6, 1–14 (2015).

24. Clough, B. et al. K63-Linked Ubiquitination Targets Toxoplasma gondii for Endo-lysosomal Destruction in IFNγ-Stimulated Human Cells. PLoS Pathog. 12, (2016).

25. Yamamoto, M. et al. A cluster of interferon-γ-inducible p65 gtpases plays a critical role in host defense against toxoplasma gondii. Immunity 37, 302–313 (2012).

26. Wang, L., Yan, J., Niu, H., Huang, R. & Wu, S. Autophagy and ubiquitination in Salmonella infection and the related inflammatory responses. Front. Cell. Infect. Microbiol. 8, 1–14

(2018).

27. Wu, S., Shen, Y., Zhang, S., Xiao, Y. & Shi, S. Salmonella Interacts With Autophagy to Offense or Defense. Front. Microbiol. 11, 1–13 (2020).

28. Thurston, T. L. M. The tbk1 adaptor and autophagy receptor ndp52 restricts the proliferation of ubiquitin-coated bacteria. Nat. Immunol. 10, 1215–1222 (2009).

29. Wandel, M. P. et al. Guanylate-binding proteins convert cytosolic bacteria into caspase-4 signaling platforms. Nat. Immunol. 21, 880–891 (2020).

30. Fisch, D. et al. Human GBP1 Differentially Targets Salmonella and Toxoplasma to License Recognition of Microbial Ligands and Caspase-Mediated Death. SSRN Electron. J. 1–28 (2020). doi:10.2139/ssrn.3593524